Numerical Simulation of Some Viscoelastic Fluids

Dissertation

zur Erlangung des Grades
Doktor der Naturwissenschaften
am Fachbereich Physik, Mathematik und Informatik
der Johannes Gutenberg-Universität
Mainz

vorgelegt von

Bangwei She

geboren in Anhui (China)

Jan. 2015, Mainz

1. Gutachter:
2. Gutachter:
Tag der Prüfung: 03.03.2015

Declaration

I declare that this thesis titled, "Numerical Simulation of Some Viscoelastic Fluids" and the work presented in it are my own. I confirm that:

- This work was done completely during my PhD study at the Johannes Gutenberg-University Mainz.

- Where any part of this thesis has previously been submitted for a degree or any other qualification at this University or any other institution, this has been clearly stated.

- Where I have consulted the published work of others, this is always clearly attributed.

- Where I have quoted from the work of others, the source is always given. With the exception of such quotations, this thesis is entirely my own work.

- I have acknowledged all main sources of help.

Signed:
_____

Date:
_____

Abstract

Numerical simulation of the Oldroyd-B type viscoelastic fluids is a very challenging problem. The well-known "High Weissenberg Number Problem" has haunted the mathematicians, computer scientists, and engineers over 40 years. When the Weissenberg number, which represents the ratio of elasticity to viscosity, exceeds some limits, simulations done by standard methods break down exponentially fast in time. However, some approaches, such as the logarithm transformation technique can significantly improve the limits of the Weissenberg number until which the simulations stay stable. We should point out that the global existence of weak solutions for the Oldroyd-B model is still open. Let us note that in the evolution equation of the elastic stress tensor the terms describing diffusive effects are typically neglected in the modelling due to their smallness. However, when keeping these diffusive terms in the constitutive law the global existence of weak solutions in two-space dimension can been shown.

This main part of the thesis is devoted to the stability study of the Oldroyd-B viscoelastic model. Firstly, we will show that the free energy of the diffusive Oldroyd-B model as well as its logarithm transformation are dissipative in time. Further, we will develop free energy dissipative schemes based on the characteristic finite element and finite difference framework. In addition to that, the global linear stability analysis of the diffusive Oldroyd-B model will also be discussed.

The next part of the thesis deals with the error estimates of the combined finite element and finite volume discretization of a special Oldroyd-B model which covers the limiting case of Weissenberg number going to infinity. Theoretical results are confirmed by a series of numerical experiments, which are presented in the thesis, too.

Kurzdarstellung

Numerische Simulation viskoelastischer Flüssigkeiten vom Oldroyd-B Typ ist ein sehr komplexes Problem. Tatsächlich beschäftigt das bekannte "high Weissenberg number problem" viele Mathematiker, Informatiker und Ingenieure seit längerer Zeit. Wenn die Weissenberg-Zahl, die das Verhältnis zwischen der Elastizität und der Viskosität des Fluides beschreibt, eine gewisse Schranke übersteigt, sind die Standardverfahren instabil und die Lösung exponentiell schnell in der Zeit wächst. Anderseits gibt es einige Ansätze, wie, z.B., die logarithmische Transformation, die eine deutliche Verbesserung der Stabilität des Verfahrens und die Erhöhung der Schranke der Weissenberg-Zahl, für welche die numerischen Simulationen stabil bleiben, erweisen.

Wir möchten darauf hinweisen, dass die globale Existenz schwacher Lösungen für das Oldroyd-B Modell noch immer offen bleibt. Bei der Modellierung der Zeitevolution des elastischen Spannungstensors werden typischerweise die Diffusionseffekte aufgrund ihrer Kleinheit vernachlässigt. Werden allerdings diese Diffusionsterme beibehalten, kann die globale Existenz schwacher Lösungen in zwei Raumdimension gezeigt werden.

Der Hauptteil dieser Doktorarbeit ist den Stabilitätsuntersuchungen für die viskoelastischen Flüssigkeiten vom Oldroyd-B Typ gewidmet. Als Erstes wird gezeigt, dass die freie Energie des diffusiven Oldroyd-B Modells sowie die logarithmische-Transformation dissipativ in der Zeit sind. Weiterhin entwickeln wir dissipative numerische Verfahren, die auf der charakteristischen Finiten-Elementen-Methode und Finiten-Differenzen-Methode basieren. Darüber hinaus wird die lineare Stabilitätsanalyse des diffusiven Oldroyd-B Modells diskutiert. Der nächste Teil der Arbeit befasst sich mit den Fehlerschätzungen des kombinierten Finiten-Elementen- und Finiten-Volumen-Verfahrens für ein spezielles Oldroyd-B Modell mit der undendlichen Weissenberg-Zahl. Theoretische Ergebnisse werden durch eine Reihe von numerischen Experimenten, die in der Arbeit vorgestellt sind, bestätigt.

Acknowledgements

First I would like to thank my supervisor, who has gave me the opportunity to work in the interesting research field. The thesis would not have been possible without her encouragement, guidance and help. What I learned from her is not only mathematics but also the way of arranging things in nice order. I'm grateful to all she has done for me.

I would also like to thank Prof. T and N for their scientific suppervisions during my stay at the Waseda University. In particular, it was a great pleasure to work very intensively with Prof. N. Many numerical experiments, presented in this thesis, are based on a generalization of his code for the method of characteristics.

I would like to acknowledge the German Research Foundation (DFG), in particular the "International Research Training Group 1529 Mathematical Fluid Dynamics", for the financial support of the PhD program.

I'm grateful to Prof. L, L, and T for helpful discussions and suggestions. Special thanks to Prof. Z who introduced me to the field of computational science and gave me continuous support.

I would like to express my gratitude to the secretaries for so many help. It is a pleasure to thank my office mate. I learned a lot from our discussions and cooperation. I would like to thank Dr. B, L, S, S and Y for their help in the thesis and daily life. I would also like to thank all the other members in the numerical group of the institute of mathematics.

I am grateful to all the friends I made in Mainz. They made the living in Germany much more pleasant.

I owe my deepest gratitude to my parents, sisters and wife for their understanding and endless support.

Contents

List of Figures

X

List of Tables

1 Introduction

1.1 Complex fluids, non-Newtonian fluids

Complex fluids

In the early study of Newton, he found in the one dimensional simple flow that the inertial friction force is proportional to the velocity gradient. Later on, Navier and Stokes extended the relation to multidimensional flow. They show that relationship between the shear stress $\mathbf{T}$ and strain rate $\boldsymbol{\gamma}$ is linear

$$\mathbf{T} = \eta\boldsymbol{\gamma}. \tag{1.1}$$

Here, the viscosity η which is the ratio between stress and shear rate is independent on the shear rate or its history. Fluids following this law are called Newtonian fluids for memorizing Newton's great contribution.

Nowadays, materials encountered in industry, biology and even in daily life often fall out the classical models of Newtonian fluids. They are categorized as complex fluids, showing non-linear viscous behaviours, as well as viscoelastic properties. A broad class of materials are included in this category: suspensions or solutions of macromolecules such as polymers, colloidal fluids, foams, micellar and liquid-crystal, molten materials, etc. More vivid examples are milk, yoghurt, ketchup, cosmetics, detergent, toothpaste, shampoo, paints, varnish and glaze industries, inks, adhesives, sealants as well as blood.

What makes complex fluids so popular is because of their microstructures, which exhibits interesting mechanical properties. The understanding of the rheology of complex fluids is expected to help solving challenging problems in physics, chemistry, and even medicine [6].

Non-Newtonian property

Complex fluids are non-Newtonian. The stress inside the fluids exhibits a non-linear response to the strain rate and the viscosity can even be time dependent. Most commonly, the viscosity of the non-Newtonian fluids is dependent on shear rate or shear rate history. Some non-Newtonian fluids with shear-independent viscosity, however, still exhibit normal stress-differences or other non-Newtonian behaviours. Basic types of non-Newtonian behaviours include shear thickening, shear thinning and Bingham plastic.

Shear thickening

For a shear thickening fluid, the viscosity increases when increasing the shear rate. A good example is the corn starch dissolved in water. When stirred slowly it looks milky,
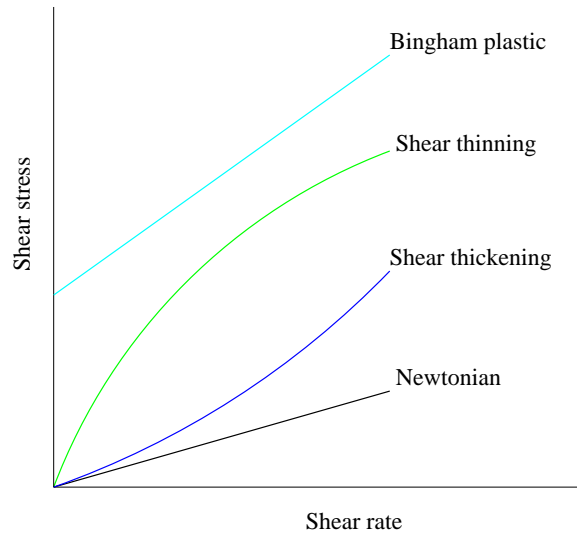
Figure 1.1: Shear stress/strain rate relationship of the different types of non-Newtonian fluids.

when stirred vigorously it becomes a very viscous liquid.

Shear thinning

For a shear thinning fluid, the viscosity decreases when increasing the shear rate. A familiar example is paint. Paint should flow readily off the brush but not drip excessively when being painted to the wall.

Bingham plastic

Bingham plastic fluids have a linear relationship of the shear stress and strain rate, but require a finite yield stress before starting to flow. Examples are clay suspensions, toothpaste, chocolate and mustard.

Figure 1.1 depicts the relationship between the shear stress and strain rate for different types of non-Newtonian fluids.

1.2 Viscoelastic fluids

Viscoelasticity is one of the most significant features arose in non-Newtonian fluids. Viscous materials resist shear flow and strain linearly in time when a stress is applied, while elastic materials quickly return to the original state once the stress is removed. Literally, viscoelastic fluids exhibit both viscous and elastic characteristics when deformed.

There are basically two approaches for the derivation of the viscoelastic fluid models. One is to propose the constitutive law which describes the relationship between the stress and strain rate. Another route starts with modelling the behaviour of the micro-structures for the feature of viscoelastic fluids. In what follows, we will give an introduction to some classic viscoelastic models originated from both sides.

1.2.1 Macro models

In classical mechanics, one describes from the macroscopic point of view the constitutive law for the viscoelastic fluid. Different models of this type can be found in literature, see for example the book by Joseph [47] and Renardy [77].

Comparing with Newtonian fluids, the constitutive law for viscoelastic fluids is rather complex. The viscosity depends not only on the current motion, but also on the history of the strain rate. Depending on this relationship is linear or not, we have linear or nonlinear models.

Linear models

When viscosity depends linearly on the strain rate history, we have linear viscoelastic models. The Boltzmann theory [15] of linear viscoelasticity gives

$$\mathbf{T}(t) = \int\limits_{-\infty}^{t} G(t - s)\boldsymbol{\gamma}(s)ds,$$

where $\boldsymbol{\gamma}(t)$ is the strain rate, $\mathbf{T}(t)$ is the resulting stress, and the viscosity is the integral of G:

$$\eta = \int\limits_{0}^{\infty} G(s)ds.$$

Maxwell's theory of linear viscoelasticity proposes an ordinary differential equation

$$\mathbf{T} + \lambda\frac{\partial\mathbf{T}}{\partial t} = \eta\boldsymbol{\gamma}, \tag{1.2}$$

where λ represents the relaxation time, which is a measure of the fluid's memory period.

Further, if we add another linear term, i.e. the time derivative of $\boldsymbol{\gamma}$, then we arrive at the Jeffrey model

$$\mathbf{T} + \lambda\frac{\partial\mathbf{T}}{\partial t} = \eta(\boldsymbol{\gamma} + \lambda_r\frac{\partial\boldsymbol{\gamma}}{\partial t}). \tag{1.3}$$

where $\lambda_r > 0$ is the retardation time.

Nonlinear models

Before going to the nonlinear viscoelastic models, we first introduce the concept of objective derivative.

$$\frac{\delta_a\mathbf{A}}{\delta t} := \frac{D\mathbf{A}}{Dt} - \mathbf{W}\cdot\mathbf{A} + \mathbf{A}\cdot\mathbf{W} - a(\mathbf{D}\cdot\mathbf{A} + \mathbf{A}\cdot\mathbf{D}), \quad -1 \le a \le 1, \tag{1.4}$$

where

$$\frac{D\mathbf{A}}{Dt} = \frac{\partial\mathbf{A}}{\partial t} + \mathbf{u}\cdot\nabla\mathbf{A} \tag{1.5}$$

is the material derivative. The rest terms on the right hand side are due to the rheology. $\mathbf{W} = \frac{\nabla\mathbf{u} - \nabla\mathbf{u}^T}{2}$ is the anti-symmetric part of the velocity gradient. The symmetric part

of the velocity gradient $\mathbf{D} = \frac{\nabla\mathbf{u}+\nabla\mathbf{u}^T}{2}$ is the so-called rate of deformation. Start from here, the shear rate of the fluids will be represented by the rate of deformation $\boldsymbol{\gamma} = \nabla\mathbf{u} + \nabla\mathbf{u}^T = 2\mathbf{D}$.

By choosing $a = 1$, -1 or 0, the objective derivative (1.4) becomes the upper convected derivative (1.6a), lower convected derivative (1.6b), or co-rotational derivative (1.6c). One can refer to Joseph [47] or Bird [14] for their derivations.

$$\overset{\nabla}{\mathbf{A}} := \frac{D\mathbf{A}}{Dt} - \nabla\mathbf{u}\cdot\mathbf{A} - \mathbf{A}\cdot\nabla\mathbf{u}^T, \tag{1.6a}$$

$$\overset{\triangle}{\mathbf{A}} := \frac{D\mathbf{A}}{Dt} + \nabla\mathbf{u}^T\cdot\mathbf{A} + \mathbf{A}\cdot\nabla\mathbf{u}, \tag{1.6b}$$

$$\overset{\circ}{\mathbf{A}} := \frac{D\mathbf{A}}{Dt} - \mathbf{W}\cdot\mathbf{A} + \mathbf{A}\cdot\mathbf{W}. \tag{1.6c}$$

Replacing the time derivative in Maxwell model (1.2) with the upper convected derivative (1.6a), we get the Upper-convected model (UCM)

$$\mathbf{T} + \lambda\overset{\nabla}{\mathbf{T}} = 2\eta\mathbf{D}. \tag{1.7}$$

Similarly, the lower-convected (1.6b) and co-rotational (1.6c) derivatives lead to the Lower-convected and the Co-rotational Maxwell model, respectively.

Adding some additional terms to the UCM model, we will arrive at some other popular models. For example, adding a term proportional to $\mathbf{T}^2$ leads to the Giesekus model [37, 36]

$$\mathbf{T} + \lambda\overset{\nabla}{\mathbf{T}} + \frac{1}{2G}\mathbf{T}^2 = 2\eta\mathbf{D}. \tag{1.8}$$

Another example is the Phan-Thien-Tanner (PTT) model [72], which can be derived by adding a term proportional to $f(\mathrm{tr}\mathbf{T})\mathbf{T}$ based on the UCM model:

$$\mathbf{T} + \lambda\overset{\nabla}{\mathbf{T}} + f(\mathrm{tr}\mathbf{T})\mathbf{T} = 2\eta\mathbf{D}. \tag{1.9}$$

We can also obtain the Johnson-Segalman model [46] by adding a term proportional to $\mathbf{TD} + \mathbf{DT}$, i.e.

$$\mathbf{T} + \lambda\overset{\nabla}{\mathbf{T}} + \xi(\mathbf{TD} + \mathbf{DT}) = 2\eta\mathbf{D}. \tag{1.10}$$

Starting from the Jeffrey model (1.3) and replacing the time derivative with the objective derivative (1.4), we have

$$\mathbf{T} + \lambda\frac{\delta_a\mathbf{T}}{\delta t} = 2\eta(\mathbf{D} + \lambda_r\frac{\delta_a\mathbf{D}}{\delta t}). \tag{1.11}$$

Depending on how we choose the parameters a, we may cover a wide range of viscoelastic models. By choosing $a = 1$ which means the upper-convected derivative (1.6a), we arrive at the Oldroyd-B model,

$$\mathbf{T} + \lambda\overset{\nabla}{\mathbf{T}} = 2\eta(\mathbf{D} + \lambda_r\overset{\nabla}{\mathbf{D}}). \tag{1.12}$$

Applying the lower convected (1.6b) and co-rotational (1.6c) derivatives lead to the

Oldroyd-A and co-rotational Oldroyd model, respectively.

1.2.2 Kinetic models

Instead of using the macro constitutive law, there are also theories which describe the molecular property or micro-structures of the viscoelastic fluids, cf. the contributions by Öttinger [69], by Bird et al. [14], by Renardy [77] and etc. For such approaches, the stress tensor can be obtained as a function of the configurations of the micro-structures, of which additional variables are required for the description, and thus leads to higher dimensional systems.

The dilute solution theory is one of the well-known molecular theories for viscoelastic fluids. In this theory the polymer molecules are treated individually and do not meet each other. Moreover, each molecule is treated as a chain of beads and springs or beads and rods. The simplest model is the dumbbell model consisting of two beads connected by a spring. Considering the linear Hooke law for the spring force

$$\mathbf{f} = H\mathbf{R}, \tag{1.13}$$

where $\mathbf{R}$ is the orientation vector of the dumbbell, one can obtain the Hookean-dumbbell viscoelastic model, which further leads to the UCM and Oldroyd-B model [54, 77]. For the nonlinear force, i.e.

$$\mathbf{f} = \gamma(|\mathbf{R}|^2)\mathbf{R}, \tag{1.14}$$

one can derive the finitely extensible nonlinear elastic (FENE) model, cf. [9, 54, 77] and etc.

There are also other type of molecular theories, such as the network theories and the reptation theories. In the network theories polymers are considered as a network of springs linked at junction points. The PTT model was originally derived using the network theories in the paper by Phan-Thien and Tanner [72]. The reptation theories is a middle ground between the two above extremes where the polymer molecules are treated individually, but constrained by a "tube" formed by other molecules. Example is the Doi-Edwards model [28].

1.3 Literature overview

In this thesis we will focus on the Oldroyd-B type viscoelastic fluids. First of all, we will give a review of the literature from both the analytical and numerical aspects.

1.3.1 Existence and uniqueness results

The early study of the existence results for viscoelastic flow can be found in [76] by Renardy, which covers the case of Oldroyd-B model. We refer the readers to Guillopé and Saut [38] for the local existence, uniqueness, and the global existence for small data, see also Fernández-Cara, Guillén and Ortega [35], Lin, Liu and Zhang [60] and references therein. Let us mention Constantin and Sun [23] for the global existence and uniqueness of weak solution for small data. See also Arada and Sequeira [5] for the global existence

and uniqueness of small and suitably regular data in bounded domain. For the theoretical study on the global strong solutions in exterior domain, we refer to the result of Hieber, Naito and Shibata [41].

The first global in time existence result was contribution by Lions and Masmoudi [61]. They consider the co-rotational Oldroyd model and show the global existence for two and three dimensional flow, where the co-rotational derivative (1.6c) is taken into account.

In the recent work of Barrett and Boyaval [8] the so-called diffusive Oldroyd-B model was studied from both numerical as well as analytical point of view. The global existence of weak solution has been presented for two dimensional space. The diffusive Oldroyd-B model has also been studied by Constantin and Kliegl in [22] and the global regularity in two dimensional space has been proven. Indeed, the diffusive term do exist in the physical modelling [9]. The neglect of the diffusion term in relative models is due to the smallness of the diffusion coefficient, as pointed out in [10, 11, 79, 27]. We would like to emphasize that the diffusive term is not a regularization but an inherent mechanism.

1.3.2 Numerical methods

The earlier work on numerical simulations of the Oldroy-B and relative viscoelastic models were realized mostly by using the standard finite difference (FD), finite volume (FV) or finite element (FE) method. Examples are contribution by Keunings, Crochet and their cooperators [25, 48, 51, 49, 63] (FE), Wapperom, Keunings and Legat [85] (backward-tracking Lagrangian particle method), Crochet, Davies and Walters [24] (FD-FE scheme), Wapperom and Webster [86, 87], Aboubacar, Matallah and Webster [1], Nadau and Sequeira [65] (hybrid FV-FE scheme), Phillips and Williams[73] (semi-Lagrangian finite volume), Xue, Phan-Thien and Tanner [88] (FV) and etc. Without exception, all these methods break down at a moderate high Weissenberg number. This interesting phenomenon is named as "High Weissenberg Number Problem (HWNP)". Although it has been reported since the earlier 1980s, the mechanism has not been fully understood [49, 50, 84].

Up to now no approach has been found to solve this problem. Nevertheless, some approaches significantly improved the stability, especially the logarithm conformation transformation approach proposed by Fattal and Kupfermann [33, 34]. They reformulate the constitutive law with the logarithm of the conformation tensor based on the knowledge that the numerical method established on polynomials can not catch the exponential growth of the conformation tensor. Further, this approach has been implemented by themselves [34, 44], Turek et al. [26, 70], Alves et al. [2], Pan and Hao [40, 71] and etc in different framework.

Recently, Balci et al. developed the square-root transformation approach by reformulate the constitutive law with the square root of the conformation tensor [7]. Both of the above two methods naturally preserve in the discrete level the positivity of the conformation tensor. The above approaches are further concluded as the kernel-conformation transformation by Alfonso et al. [3]. These stabilization approaches have been compared by Chen et al. [19] in the FV framework. There are also other types of positivity preserving approaches such as methods applying the direct discretization of the objective derivative, cf. [56, 57, 58, 83].

1.4 Overview of the thesis

The thesis deals with numerical study of some viscoelastic fluids. It is a well-known fact, that the classical, the so-called Oldroyd-B viscoelastic model yields many open problems both from analytical as well as numerical point of view. We do not have global existence of solutions and can not solve numerically the Oldroyd-B equations for arbitrary Weissenberg numbers. The aim of this thesis is to analyze the reasons and propose some solutions to stabilize numerical simulations.

The thesis is organized as follows: In Chapter 2 we describe the Oldroyd-B model and propose three types of numerical methods for their approximation. In particular, there are the characteristic finite element, combined finite difference-finite volume and characteristic finite difference methods. We will study entropy stability for the diffusive Oldroyd-B model. Furthermore, in Chapter 3 we analyze the entropy stability of the proposed numerical schemes. We will be able to prove that the characteristic finite element scheme and the characteristic finite difference scheme are indeed entropy stable for diffusive models with arbitrary Weissenberg numbers. Except of entropy stability, which is a suitable tool for nonlinear analysis, we also shortly present global linear stability method and apply it to the Oldroyd-B equations, cf. Section 3.1. At the end of Chapter 3, cf. Section 3.4, we present experimental results using the characteristic finite element scheme and characteristic finite difference scheme.

Finally, the Chapter 4 is devoted to a numerical study of a special nonlinear viscoelastic model that has been studied in [60, 52]. This chapter presents and summarizes the results that have been published in [62].

The thesis concludes with short summary and open questions presented in Chapter 5.

2 Oldroyd-B type models and their numerical approximations

In this chapter, we will present the Oldroyd-B type viscoelastic models. First we will give a detailed description of the Oldroyd-B model. In additional to that the diffusive models will be introduced. The second part is devoted to introducing some stabilization techniques, especially the logarithm transformation approach [33, 34]. Further, we extend the diffusive model to the logarithm reformulation. Moreover, we study the energy stability of the model and propose our numerical schemes for the related models.

2.1 Oldroyd-B viscoelastic model

Modelling of the viscoelastic fluids starts with the mass and momentum conservation law for the incompressible fluids:

$$\rho(\frac{\partial \mathbf{u}}{\partial t} + \mathbf{u} \cdot \nabla \mathbf{u}) = -\nabla p + \nabla \cdot \mathbf{T}, \tag{2.1a}$$

$$\nabla \cdot \mathbf{u} = 0, \tag{2.1b}$$

where ρ is the fluid density, $\mathbf{u}$ is the velocity, p is pressure, the stress tensor $\mathbf{T}$ is a function of the rate of deformation tensor $\mathbf{D}$, where $\mathbf{D}(\mathbf{u}) = (\nabla \mathbf{u} + \nabla \mathbf{u}^T)/2$. For Newtonian fluids the relationship is a linear constitutive law

$$\mathbf{T} = 2\mu_0 \mathbf{D}.$$

For the viscoelastic Oldroyd-B fluids, the constitutive law follows (1.12)

$$\mathbf{T} + \lambda \overset{\triangledown}{\mathbf{T}} = 2\mu_0 (\mathbf{D} + \lambda_r \overset{\triangledown}{\mathbf{D}}). \tag{2.1c}$$

Now we decompose the stress tensor $\mathbf{T}$ into two parts. They are the purely viscous component $2\mu_0 \alpha \mathbf{D}$ with $\alpha = \frac{\lambda_r}{\lambda}$, and the so-called extra stress $\boldsymbol{\tau}$, which contributes to some elastic properties,

$$\mathbf{T} = \boldsymbol{\tau} + 2\mu_0 \alpha \mathbf{D}. \tag{2.2}$$

According to this decomposition, we can simplify the equation (2.1c) or (1.12) to its elastic part

$$\lambda \overset{\triangledown}{\boldsymbol{\tau}} + \boldsymbol{\tau} = 2\mu_0 (1 - \alpha) D, \tag{2.3}$$

and rewrite the momentum equation (2.1a) as

$$\rho(\frac{\partial \mathbf{u}}{\partial t} + \mathbf{u} \cdot \nabla \mathbf{u}) = -\nabla p + \mu_0 \alpha \Delta \mathbf{u} + \nabla \cdot \boldsymbol{\tau}. \tag{2.4}$$

The combined system (2.1b), (2.3) and (2.4) is called the Oldroyd-B model for the incompressible fluids.

2.1.1 Dimensionless equations

Let L, T be the characteristic length and time of the flow. The characteristic velocity is straightforward $U = \frac{L}{T}$. The Weissenberg number is defined as the ratio of relaxation time and the characteristic flow time $We = \frac{\lambda}{T} = \frac{\lambda U}{L}$, where the relaxation time λ is a kind of characteristic time property of the viscoelasticity. Now we use " $\sim$ " to express the dimensionless variables [65],

$$\widetilde{\mathbf{x}} = \frac{\mathbf{x}}{L}, \widetilde{t} = \frac{t}{T} = \frac{tU}{L}, \widetilde{\mathbf{u}} = \frac{\mathbf{u}}{U}, \tag{2.5}$$

Viscosity is already dimensionless $\widetilde{\mu} = \mu_0$. The Reynolds number is given as $Re = \rho\frac{UL}{\mu_0}$. The characteristic value for pressure and stress is $S = \frac{\mu_0 U}{L}$, thus we have

$$\widetilde{p} = \frac{p}{S} = \frac{Lp}{\mu_0 U}, \widetilde{\boldsymbol{\tau}} = \frac{\boldsymbol{\tau}}{S} = \frac{L\boldsymbol{\tau}}{\mu_0 U}. \tag{2.6}$$

Substituting the dimensionless variables into the Oldroyd-B model, we obtain

$$\begin{cases} \frac{\rho U^2}{L}(\frac{\partial \widetilde{\mathbf{u}}}{\partial \widetilde{t}} + \widetilde{\mathbf{u}} \cdot \nabla \widetilde{\mathbf{u}}) = \frac{\mu_0 U}{L^2}(\nabla \widetilde{p} + \alpha \Delta \widetilde{\mathbf{u}}) + \frac{\mu_0 U}{L^2} \nabla \cdot \widetilde{\boldsymbol{\tau}}, \\ U \nabla \cdot \widetilde{\mathbf{u}} = 0, \\ (TWe)\frac{\mu_0 U^2}{L^2}\big(\frac{\partial \widetilde{\boldsymbol{\tau}}}{\partial \widetilde{t}} + \widetilde{\mathbf{u}} \cdot \nabla \widetilde{\boldsymbol{\tau}} - \nabla \widetilde{\mathbf{u}} \cdot \widetilde{\boldsymbol{\tau}} - \widetilde{\boldsymbol{\tau}} \cdot (\nabla \widetilde{\mathbf{u}})^T\big) + \frac{\mu_0 U}{L}\widetilde{\boldsymbol{\tau}} = 2(1-\alpha)\frac{\mu_0 U}{L}\widetilde{\mathbf{D}}. \end{cases}$$

Simplifying the above system and omitting " $\sim$ ", we derive the dimensionless system for the Oldroyd-B model

$$Re(\frac{\partial \mathbf{u}}{\partial t} + \mathbf{u} \cdot \nabla \mathbf{u}) = -\nabla p + \alpha \Delta \mathbf{u} + \nabla \cdot \boldsymbol{\tau}, \tag{2.7a}$$

$$\nabla \cdot \mathbf{u} = 0, \tag{2.7b}$$

$$We\big(\frac{\partial \boldsymbol{\tau}}{\partial t} + (\mathbf{u} \cdot \nabla)\boldsymbol{\tau} - \nabla \mathbf{u} \cdot \boldsymbol{\tau} - \boldsymbol{\tau} \cdot (\nabla \mathbf{u})^T\big) + \boldsymbol{\tau} = 2(1-\alpha)\mathbf{D}. \tag{2.7c}$$

Now, we introduce the conformation tensor $\boldsymbol{\sigma}$ as

$$\boldsymbol{\sigma} = \frac{We}{1-\alpha}\boldsymbol{\tau} + \mathbf{I}. \tag{2.8}$$

Substituting (2.8) into (2.7c) and using the fact that $\overset{\triangledown}{\mathbf{I}} = -2\mathbf{D}$, we can rewrite the constitutive equation in terms of conformation tensor $\boldsymbol{\sigma}$:

$$\frac{\partial \boldsymbol{\sigma}}{\partial t} + (\mathbf{u} \cdot \nabla)\boldsymbol{\sigma} - \nabla \mathbf{u} \cdot \boldsymbol{\sigma} - \boldsymbol{\sigma} \cdot (\nabla \mathbf{u})^T = \frac{1}{We}(\mathbf{I} - \boldsymbol{\sigma}). \qquad (2.9)$$

The conformation tensor $\boldsymbol{\sigma}$ is symmetric positive definite (SPD), while the extra stress tensor $\boldsymbol{\tau}$ is only symmetric. One can refer to [18, 43] for the proof of the positivity of the conformation tensor. In what follows we will concentrate on the conformation tensor variable $\boldsymbol{\sigma}$ for the Oldroyd-B system as we want to benefit from the positivity property. Switching to the conformation tensor variable, the Oldroyd-B model (2.7) becomes

$$Re(\frac{\partial \mathbf{u}}{\partial t} + \mathbf{u} \cdot \nabla \mathbf{u}) = -\nabla p + \alpha \Delta \mathbf{u} + \frac{1-\alpha}{We}\nabla \cdot (\boldsymbol{\sigma} - \mathbf{I}), \qquad (2.10\text{a})$$

$$\nabla \cdot \mathbf{u} = 0, \qquad (2.10\text{b})$$

$$\frac{\partial \boldsymbol{\sigma}}{\partial t} + (\mathbf{u} \cdot \nabla)\boldsymbol{\sigma} - \nabla \mathbf{u} \cdot \boldsymbol{\sigma} - \boldsymbol{\sigma} \cdot (\nabla \mathbf{u})^T = \frac{1}{We}(\mathbf{I} - \boldsymbol{\sigma}). \qquad (2.10\text{c})$$

As mentioned in the previous chapter, the global existence of the weak solutions for the Oldroyd-B model has not been proven. However, the global existence results have been proved for the relative diffusive model [8], where an additional diffusive term is added in the constitutive law (2.10c). It is further showing by Barrett and Süli [12] that the diffusive term is not a regularizing term but an outcome of the physical modelling. The diffusive Oldroyd-B model reads

$$Re(\frac{\partial \mathbf{u}}{\partial t} + \mathbf{u} \cdot \nabla \mathbf{u}) = -\nabla p + \alpha \Delta \mathbf{u} + \frac{1-\alpha}{We}\nabla \cdot (\boldsymbol{\sigma} - \mathbf{I}), \qquad (2.11\text{a})$$

$$\nabla \cdot \mathbf{u} = 0, \qquad (2.11\text{b})$$

$$\frac{\partial \boldsymbol{\sigma}}{\partial t} + (\mathbf{u} \cdot \nabla)\boldsymbol{\sigma} - \nabla \mathbf{u} \cdot \boldsymbol{\sigma} - \boldsymbol{\sigma} \cdot (\nabla \mathbf{u})^T = \frac{1}{We}(\mathbf{I} - \boldsymbol{\sigma}) + \varepsilon \Delta \boldsymbol{\sigma}. \qquad (2.11\text{c})$$

2.2 Logarithm transformation

As already pointed out in the previous section the Oldroyd-B model is very challenging particularly in the high Weissenberg case. To overcome this problem several approaches have been studied in the literature. We should point out that up to now no simulation technique has been found to solve this problem. Nevertheless, some approaches significantly improved and stabilized the numerical simulations. In what follows we describe the logarithm conformation representation (LCR) approach proposed by Fattal and Kupfermann[33, 34] avoid the numerical blowup in the case of high We. The main idea of this approach is to replace the conformation tensor by a new variable $\boldsymbol{\psi}(x,t) = \ln \boldsymbol{\sigma}(x,t)$ through eigenvalue computations ($\ln \mathbf{A} = \mathbf{R} \ln \boldsymbol{\Lambda} \mathbf{R}^T$).

The reformulation starts with rotating the conformation tensor $\boldsymbol{\sigma}$ into its main principle axis

$$\mathbf{R}^T \boldsymbol{\sigma} \mathbf{R} = \text{diag}\{\lambda_i\}, \qquad (2.12)$$

where λ_i, $i = 1, \cdots, d$, is an eigenvalue, $d = 2, 3$ is the dimension, $\mathbf{R}$ is the eigenvector

matrix, which is orthogonal. The goal is to design a symmetric matrix $\mathbf{B}$ which commutes with the conformation tensor $\boldsymbol{\sigma}$, a pure rotation matrix $\boldsymbol{\Omega}$ and an additional dummy part $\mathbf{N}\boldsymbol{\sigma}^{-1}$ where $\mathbf{N}, \boldsymbol{\Omega}$ are anti-symmetric matrices in terms of the velocity gradient

$$\nabla\mathbf{u} = \mathbf{B} + \boldsymbol{\Omega} + \mathbf{N}\boldsymbol{\sigma}^{-1}. \tag{2.13}$$

Subsequently, we will present how to get this decomposition in two dimensions. If $\boldsymbol{\sigma}$ is proportional to the unit tensor,

$$\mathbf{B} = \mathbf{D}(\mathbf{u}), \quad \boldsymbol{\Omega} = \mathbf{0}, \quad \mathbf{N} = (\nabla\mathbf{u} - \mathbf{D}(\mathbf{u}))\mathrm{tr}\boldsymbol{\sigma}/2. \tag{2.14}$$

Otherwise, we get the decomposition in the following steps:
Step-1, diagonalizing the conformation tensor,

$$\begin{pmatrix} \lambda_1 & 0 \\ 0 & \lambda_2 \end{pmatrix} = \mathbf{R}^T \boldsymbol{\sigma} \mathbf{R}. \tag{2.15}$$

Step-2, calculating an intermediate matrix

$$\begin{pmatrix} m_{11} & m_{12} \\ m_{21} & m_{22} \end{pmatrix} = \mathbf{R}^T (\nabla\mathbf{u}) \mathbf{R}.$$

Step-3,

$$\mathbf{N} = R \begin{pmatrix} 0 & n \\ -n & 0 \end{pmatrix} R^T, \ \mathbf{B} = \mathbf{R} \begin{pmatrix} m_{11} & 0 \\ 0 & m_{22} \end{pmatrix} \mathbf{R}^T, \ \boldsymbol{\Omega} = \mathbf{R} \begin{pmatrix} 0 & \omega \\ -\omega & 0 \end{pmatrix} \mathbf{R}^T, \tag{2.16}$$

where $n = (m_{12} + m_{21})/(\lambda_2^{-1} - \lambda_1^{-1})$, and $\omega = (\lambda_2 m_{12} + \lambda_1 m_{21})/(\lambda_2 - \lambda_1)$. Substituting the decomposition (2.13) into the constitutive equation (2.9),

$$
\begin{aligned}
\nabla\mathbf{u} \cdot \boldsymbol{\sigma} + \boldsymbol{\sigma} \cdot (\nabla\mathbf{u})^T &= (\mathbf{B} + \boldsymbol{\Omega} + \mathbf{N}\boldsymbol{\sigma}^{-1})\boldsymbol{\sigma} + \boldsymbol{\sigma}(\mathbf{B} + \boldsymbol{\Omega} + \mathbf{N}\boldsymbol{\sigma}^{-1})^T \\
&= \mathbf{B}\boldsymbol{\sigma} + \boldsymbol{\Omega}\boldsymbol{\sigma} + \mathbf{N} + \boldsymbol{\sigma}\mathbf{B} + \boldsymbol{\sigma}\boldsymbol{\Omega}^T + \boldsymbol{\sigma}(\mathbf{N}\boldsymbol{\sigma}^{-1})^T \\
&= \mathbf{B}\boldsymbol{\sigma} + \boldsymbol{\Omega}\boldsymbol{\sigma} + \mathbf{N} + \mathbf{B}\boldsymbol{\sigma} - \boldsymbol{\sigma}\boldsymbol{\Omega} - \boldsymbol{\sigma}((\boldsymbol{\sigma}^{-1})^T\mathbf{N}) \\
&= 2\mathbf{B}\boldsymbol{\sigma} + \boldsymbol{\Omega}\boldsymbol{\sigma} - \boldsymbol{\sigma}\boldsymbol{\Omega},
\end{aligned}
$$

then we get the following reformulation of the constitutive law

$$\frac{\partial\boldsymbol{\sigma}}{\partial t} + (\mathbf{u} \cdot \nabla)\boldsymbol{\sigma} - (\boldsymbol{\Omega}\boldsymbol{\sigma} - \boldsymbol{\sigma}\boldsymbol{\Omega}) - 2\mathbf{B}\boldsymbol{\sigma} = \frac{1}{We}(\mathbf{I} - \boldsymbol{\sigma}). \tag{2.17}$$

2.2.1 Constitutive equation for the logarithm formulation

As our goal is to get the evolution equation for $\boldsymbol{\psi}$, we decompose the equation (2.17) into four parts according to reference [33]:
(1) Advection:

$$\frac{\partial\boldsymbol{\sigma}}{\partial t} + (\mathbf{u} \cdot \nabla)\boldsymbol{\sigma} = 0 \ \text{ implies } \ \frac{\partial\boldsymbol{\psi}}{\partial t} + (\mathbf{u} \cdot \nabla)\boldsymbol{\psi} = 0.$$

(2) Rotation:
$$\frac{\partial \boldsymbol{\sigma}}{\partial t} = \boldsymbol{\Omega}\boldsymbol{\sigma} - \boldsymbol{\sigma}\boldsymbol{\Omega} \quad \text{implies} \quad \frac{\partial \boldsymbol{\psi}}{\partial t} = \boldsymbol{\Omega}\boldsymbol{\psi} - \boldsymbol{\psi}\boldsymbol{\Omega}.$$

Indeed, the solution for $\boldsymbol{\sigma}(t)$ is $\boldsymbol{\sigma}(t) = e^{\boldsymbol{\Omega}t}\boldsymbol{\sigma}_0 e^{-\boldsymbol{\Omega}t}$. Let $\mathbf{S} = e^{\boldsymbol{\Omega}t}$. Its transpose matrix is $\mathbf{S}^T = e^{(\boldsymbol{\Omega}t)^T} = e^{-\boldsymbol{\Omega}t}$. As $\boldsymbol{\Omega}$ is skew-symmetric, its exponential matrix is orthogonal. Thus we have $\mathbf{S}^T = \mathbf{S}^{-1}$.

Let $\boldsymbol{\psi}_0 = \ln \boldsymbol{\sigma}_0 = \mathbf{R} \ln \boldsymbol{\Lambda}_0 \mathbf{R}^T$ and $\mathbf{V} = \mathbf{S}\mathbf{R}$, where $\boldsymbol{\Lambda}_0 = \text{diag}\{\lambda_i(t=0)\}$ the eigenmatrix. The matrix $\mathbf{R}$ is orthogonal, thus $\mathbf{V}$ is also orthogonal and $\mathbf{V}^{-1} = \mathbf{V}^T$. Then we have
$$\boldsymbol{\sigma}(t) = \mathbf{S}\boldsymbol{\sigma}_0 \mathbf{S}^T = \mathbf{S}\mathbf{R}\boldsymbol{\Lambda}_0 \mathbf{R}^T \mathbf{S}^T = \mathbf{V}\boldsymbol{\Lambda}_0 \mathbf{V}^T,$$

and

$$\boldsymbol{\psi}(t) = \ln(\boldsymbol{\sigma}(t)) = \ln(\mathbf{V}\boldsymbol{\Lambda}_0 \mathbf{V}^T) = \mathbf{V} \ln \boldsymbol{\Lambda}_0 \mathbf{V}^T = \mathbf{S}\mathbf{R} \ln \boldsymbol{\Lambda}_0 \mathbf{R}^T \mathbf{S}^T = \mathbf{S}\boldsymbol{\psi}_0 \mathbf{S}^T = e^{\boldsymbol{\Omega}t}\boldsymbol{\psi}_0 e^{-\boldsymbol{\Omega}t},$$

which means

$$\frac{\partial \boldsymbol{\psi}}{\partial t} = \boldsymbol{\Omega}\boldsymbol{\psi} - \boldsymbol{\psi}\boldsymbol{\Omega}.$$

(3) Extension:
$$\frac{\partial \boldsymbol{\sigma}}{\partial t} = 2\mathbf{B}\boldsymbol{\sigma} \quad \text{implies} \quad \frac{\partial \boldsymbol{\psi}}{\partial t} = 2\mathbf{B}.$$

It is easy to find that the solution for $\boldsymbol{\sigma}(t)$ is $\boldsymbol{\sigma}(t) = e^{2\mathbf{B}t}\boldsymbol{\sigma}_0$. Let $\boldsymbol{\psi}_0 = \ln \boldsymbol{\sigma}_0$. From the fact that $\mathbf{B}$ commutes with $\boldsymbol{\sigma}_0$ we have also that $2\mathbf{B}t$ commutes with $\boldsymbol{\psi}_0$. Thus $e^{2\mathbf{B}t}e^{\boldsymbol{\psi}_0} = e^{2\mathbf{B}t+\boldsymbol{\psi}_0}$, and $\boldsymbol{\psi}(t) = \ln(\boldsymbol{\sigma}(t)) = \ln(e^{2\mathbf{B}t+\boldsymbol{\psi}_0}) = 2\mathbf{B}t+\boldsymbol{\psi}_0$, which means $\frac{\partial \boldsymbol{\psi}}{\partial t} = 2\mathbf{B}$.

(4) Sources:
$$\frac{\partial \boldsymbol{\sigma}}{\partial t} = \frac{1}{We}(\mathbf{I} - \boldsymbol{\sigma}) \quad \text{implies} \quad \frac{\partial \boldsymbol{\psi}}{\partial t} = \frac{1}{We}(\boldsymbol{\sigma}^{-1} - \mathbf{I}) = \frac{1}{We}(e^{-\boldsymbol{\psi}} - \mathbf{I}).$$

From the above four steps we can derive the following transformation of the constitutive law,

$$\frac{\partial \boldsymbol{\psi}}{\partial t} + (\mathbf{u} \cdot \nabla)\boldsymbol{\psi} - (\boldsymbol{\Omega}\boldsymbol{\psi} - \boldsymbol{\psi}\boldsymbol{\Omega}) - 2\mathbf{B} = \frac{1}{We}(e^{-\boldsymbol{\psi}} - \mathbf{I}). \tag{2.18}$$

We have the whole system reformulated using the logarithm transformation

$$\begin{cases} Re(\frac{\partial \mathbf{u}}{\partial t} + \mathbf{u} \cdot \nabla \mathbf{u}) = -\Delta p + \alpha \Delta \mathbf{u} + \frac{\beta}{We}\nabla \cdot (e^{\boldsymbol{\psi}} - \mathbf{I}), \\ \nabla \cdot \mathbf{u} = 0, \\ \frac{\partial \boldsymbol{\psi}}{\partial t} + (\mathbf{u} \cdot \nabla)\boldsymbol{\psi} - (\boldsymbol{\Omega}\boldsymbol{\psi} - \boldsymbol{\psi}\boldsymbol{\Omega}) - 2\mathbf{B} = \frac{1}{We}(e^{-\boldsymbol{\psi}} - \mathbf{I}), \end{cases} \tag{2.19}$$

where $\beta = 1 - \alpha$. In (2.11) we have presented the diffusive Oldroyd-B model. It should be noted that the logarithm transformation of the diffusive term is not straightforward,

and for this reason we propose a new diffusive logarithmic model.

$$Re(\frac{\partial \mathbf{u}}{\partial t} + \mathbf{u} \cdot \nabla \mathbf{u}) = -\Delta p + \alpha \Delta \mathbf{u} + \frac{\beta}{We} \nabla \cdot (e^{\psi} - \mathbf{I}), \qquad (2.20a)$$

$$\nabla \cdot \mathbf{u} = 0, \qquad (2.20b)$$

$$\frac{\partial \boldsymbol{\psi}}{\partial t} + (\mathbf{u} \cdot \nabla)\boldsymbol{\psi} - (\boldsymbol{\Omega}\boldsymbol{\psi} - \boldsymbol{\psi}\boldsymbol{\Omega}) - 2\mathbf{B} = \frac{1}{We}(e^{-\psi} - \mathbf{I}) + \varepsilon \Delta \boldsymbol{\psi}. \qquad (2.20c)$$

In particular we show later its stability and in some cases even experimental convergence.

2.2.2 Remarks on the stability analysis

When one tries to solve the Oldroyd-B system numerically, using any standard stable method, the solution diverges exponentially fast in time, even at moderately large values of We. The conformation tensor has been observed to grow unbounded exponentially fast. In order to analyze the reasons of arising instability we will perform stability analysis for a simplified toy model. In the next part we follow Fattal and Kupfermann [34] and consider one-dimensional linear equation for $\phi = \phi(x,t), x \in [0,1]$,

$$\frac{\partial \phi}{\partial t} + a(x)\frac{\partial \phi}{\partial x} - b(x)\phi = -\frac{1}{We}\phi, \qquad (2.21)$$

with $a(x), b(x) > 0$ and boundary condition $\phi(0,t) = 1$, and steady state

$$\phi(x) = \int_0^x \exp\left(\frac{b(x') - We^{-1}}{a(x')}\right) dx'. \qquad (2.22)$$

This equation represents a field $\phi(x,t)$ that is convected to the right with velocity $a(x)$ and grows exponentially at a rate $b(x) - We^{-1}$. With reference to Oldroyd-B model, $a(x)$ plays the role of velocity field $\mathbf{u}(x,t)$, and $b(x)$ plays the role of the deformation rate $\nabla \mathbf{u}(x,t)$.

Suppose we solve (2.21) numerically using, for example, a first order upwind scheme,

$$\phi_j^{k+1} = \phi_j^k - \frac{a_j \Delta t}{\Delta x}(\phi_j^k - \phi_{j-1}^k) + \Delta t(b_j - \frac{1}{We})\phi_j^k, \qquad (2.23)$$

where $a_j = a(x_j), b_j = b(x_j)$. Rewrite the equation in the following form:

$$\phi_j^{k+1} = [1 - \frac{a_j \Delta t}{\Delta x} + \Delta t(b_j - \frac{1}{We})]\phi_j^k + \frac{a_j \Delta t}{\Delta x}\phi_{j-1}^k.$$

Then it is at least necessary to have the following inequality

$$1 - \frac{a_j \Delta t}{\Delta x} + \Delta t \left(b_j - \frac{1}{We}\right) \leq 1, \qquad (2.24)$$

which implies that the Weissenberg number should be rather small $We \leq 1/b_j$, or

$$We > 1/b_j, \text{ with } \Delta x \leq \frac{a_j}{b_j - We^{-1}}. \qquad (2.25)$$

This condition has to hold at all mesh points. It is not a CFL condition on time step, but a restriction on the spacial mesh size. This stability criterion has the following interpretation: the spatial profile of $\phi(x,t)$ is exponential, therefore any standard scheme which is based on a polynomial reconstruction of fluxes underestimates the flux at the right edge of every computational cell. Thus, the rate at which the field ϕ is removed from a computational cell fails to balance its multiplicative growth rate, resulting in a numerical blowup. This scenario remains unchanged if the first order upwind scheme is replaced by a higher-order method; a higher-order scheme increases the critical mesh size by, at most, an order of one factor. The use of implicit schemes does not help either.

To generalize the above analysis to viscoelastic flows, assume a fixed velocity field $\mathbf{u}(x)$ (as would be obtained by a stable steady state), and consider the Oldroyd-B model, reference [34] gives a stability condition

$$\Delta x \leq \frac{|\mathbf{u}|}{2\sqrt{-\det(\nabla \mathbf{u})} - We^{-1}}.$$

We revert our attention to the scalar equation (2.21). The restriction on the mesh size is removed at once by a change of variables $\psi = \ln \phi$, in which case ψ satisfies the equation

$$\frac{\partial \psi}{\partial t} + a(x)\frac{\partial \psi}{\partial x} - b(x) = -\frac{1}{We}, \tag{2.26}$$

with boundary condition $\psi(0,t) = 0$. Now even a first-order upwind scheme

$$\psi_j^{k+1} = \psi_j^k - \frac{a_j \Delta t}{\Delta x}(\psi_j^k - \psi_{j-1}^k) + \Delta t(b_j - \frac{1}{We}), \tag{2.27}$$

no longer imposes restrictions on the size of Δx! While this stable behavior may be attributed to the transformation of multiplicative growth into additive growth. The reason for the stability is also connected to the improved treatment of the convection term. To see this, exponentiate equation (2.27) to regain the equation for ϕ_j^k

$$\phi_j^{k+1} = (\phi_j^k)^{(1 - a_j \Delta t/\Delta x)}(\phi_{j-1}^k)^{a_j \Delta t/\Delta x}e^{\Delta t(b_j - We^{-1})}, \tag{2.28}$$

and expand the multiplicative source $\exp(b\Delta t) \sim 1 + b\Delta t$. We get first order in space and time

$$\phi_j^{k+1} = (\phi_j^k)^{(1 - a_j \Delta t/\Delta x)}(\phi_{j-1}^k)^{a_j \Delta t/\Delta x} + \Delta t(b_j - We^{-1})\phi_j^k, \tag{2.29}$$

still there is no restriction on Δx.

2.2.3 Kernel-conformation representation

There are also other kinds of conformation transformation representation, such as kernel-conformation [3] and the square-root [7] transformation. The kernel-conformation transformation is givens as

$$\boldsymbol{\psi} = \log_a \boldsymbol{\sigma}, \ a > 0, \ \text{and} \ \boldsymbol{\psi} = \boldsymbol{\sigma}^{\frac{1}{k}}. \tag{2.30}$$

In the former case, the transformation is expressed as

$$\frac{\partial \boldsymbol{\psi}}{\partial t} + (\mathbf{u} \cdot \nabla)\boldsymbol{\psi} = \boldsymbol{\Omega}\boldsymbol{\psi} - \boldsymbol{\psi}\boldsymbol{\Omega} + \frac{2}{\ln a}\mathbf{B} + \frac{1}{\ln aWe}(\boldsymbol{\psi}^{-k} - \mathbf{I}). \tag{2.31}$$

This transformation is equivalent to the log-transformation when $a = e$.

In the latter case the transformation is expressed as

$$\frac{\partial \boldsymbol{\psi}}{\partial t} + (\mathbf{u} \cdot \nabla)\boldsymbol{\psi} = \boldsymbol{\Omega}\boldsymbol{\psi} - \boldsymbol{\psi}\boldsymbol{\Omega} + \frac{2}{k}\mathbf{B}\boldsymbol{\psi} + \frac{1}{kWe}(\boldsymbol{\psi}^{1-k} - \boldsymbol{\psi}). \tag{2.32}$$

It leads to the square-root transformation if $k = 2$. According to reference [3], it is better to choose $a < 10$ for the former case and $k \in [-2, -16]$ for the latter case.

Comparing the with log-transformation, we need to take care of the restriction of space interval Δx for the square-root transformation. Our extensive numerical experiments indicate that the log-transformation yields more stable results than square-root transformation.

2.3 Entropy stability analysis of the diffusive Oldroyd-B models

In this section we introduce a free energy for the viscoealastic models. The free energy consists of kinetic and elastic energy. The elastic energy is shown to be the entropy of the polymers in the fluid, cf. [42]. The entropy stability we are studying here is actually the stability of the free energy.

For the Oldroyd-B model, the free energy on bounded domain $\mathcal{T}$ reads,

$$F(\mathbf{u}, \boldsymbol{\sigma}) = \frac{Re}{2}\int_{\mathcal{T}}|\mathbf{u}|^2 + \frac{\beta}{2We}\int_{\mathcal{T}} \text{tr}(\boldsymbol{\sigma} - \ln\boldsymbol{\sigma} - \mathbf{I}). \tag{2.33}$$

On the other hand for the log-formulation (2.19), it is given as follows

$$F(\mathbf{u}, e^{\boldsymbol{\psi}}) = \frac{Re}{2}\int_{\mathcal{T}}|\mathbf{u}|^2 + \frac{\beta}{2We}\int_{\mathcal{T}} \text{tr}(e^{\boldsymbol{\psi}} - \boldsymbol{\psi} - \mathbf{I}). \tag{2.34}$$

The kinetic term $\frac{Re}{2}\int_{\mathcal{T}}|\mathbf{u}|^2$ is always non-negative. As we will show later, see (2.35b), the entropy $\int_{\mathcal{T}} \text{tr}(\boldsymbol{\sigma} - \ln\boldsymbol{\sigma} - \mathbf{I})$ is also non-negative, provided $\boldsymbol{\sigma}$ is symmetric positive-definite.

It has been shown by Boyaval et al. [18] that the free energy for the Oldroyd-B model decreases in time evolution. Such models are called dissipative models. Further, they constructed energy dissipative numerical schemes. However, their numerical solutions did not converge in the sense of mesh refinement.

We extend their results to the diffusive models. First we prove that the free energy for the diffusive Oldroyd-B model decreases in time exponentially fast to zero. Then we can show that this property also applies to the diffusive model in case of logarithm transformation.

2.3.1 Some useful preliminary properties

Before studying the stability of our diffusive viscoelastic models we first summarize some useful preliminaries. The first two lemmas have been used by Boyaval et al. [18].

Lemma 2.3.1. *[18] Let $\boldsymbol{\sigma}, \boldsymbol{\tau} \in R^{d \times d}$ be two symmetric positive-definite matrices, we have:*

$$tr \ln \boldsymbol{\sigma} = \ln \det \boldsymbol{\sigma}, \quad (2.35a)$$

$$\boldsymbol{\sigma} - \ln \boldsymbol{\sigma} - \mathbf{I} \text{ is symmetric positive semi-definite and } tr(\boldsymbol{\sigma} - \ln \boldsymbol{\sigma} - \mathbf{I}) \geq 0, \quad (2.35b)$$

$$\boldsymbol{\sigma} + \boldsymbol{\sigma}^{-1} - 2\mathbf{I} \text{ is symmetric positive semi-definite and } tr(\boldsymbol{\sigma} + \boldsymbol{\sigma}^{-1} - 2\mathbf{I}) \geq 0, \quad (2.35c)$$

$$tr(\boldsymbol{\sigma}\boldsymbol{\tau}) = tr(\boldsymbol{\tau}\boldsymbol{\sigma}) \geq 0, \quad (2.35d)$$

$$tr((\boldsymbol{\tau} - \boldsymbol{\sigma})\boldsymbol{\sigma}^{-1}) = tr(\boldsymbol{\tau}\boldsymbol{\sigma}^{-1} - \mathbf{I}) \geq \ln \det(\boldsymbol{\tau}\boldsymbol{\sigma}^{-1}) = tr(\ln \boldsymbol{\tau} - \ln \boldsymbol{\sigma}), \quad (2.35e)$$

$$tr((\ln \boldsymbol{\tau} - \ln \boldsymbol{\sigma})\boldsymbol{\tau}) \geq tr(\boldsymbol{\tau} - \boldsymbol{\sigma}). \quad (2.35f)$$

Proof. We start the proof with eigen-decomposition. As $\boldsymbol{\sigma}$ and $\boldsymbol{\tau}$ are symmetric positive-definite matrices, we have $\boldsymbol{\sigma} = \mathbf{R}_1 \boldsymbol{\Lambda} \mathbf{R}_1^T$ and $\boldsymbol{\tau} = \mathbf{R}_2 \boldsymbol{\Gamma} \mathbf{R}_2^T$, where $\boldsymbol{\Lambda} = \text{diag}\{\lambda_i\}$, $\boldsymbol{\Gamma} = \text{diag}\{\gamma_i\}$. $\lambda_i > 0$, and $\gamma_i > 0, i = 1, \dots, d$ are eigenvalues of $\boldsymbol{\sigma}$ and $\boldsymbol{\tau}$, respectively. We have denoted by d the number of all eigenvalues. Let $\mathbf{Q} = \sqrt{\boldsymbol{\Lambda}} \mathbf{R}_1^T$, then we have

$$\boldsymbol{\sigma} = \mathbf{Q}^T \mathbf{Q}. \quad (2.36)$$

By using the fact that the eigenvalues of $\ln \boldsymbol{\sigma}$ are $\ln \lambda_i$, we get immediately (2.35a), i.e.

$$\text{tr} \ln \boldsymbol{\sigma} = \sum_i \ln \lambda_i = \ln \prod_i \lambda_i = \ln \det \boldsymbol{\sigma}.$$

Let us note that both the summation as well as the product are realized for all $i = 1, \dots d$.

The proofs of (2.35b) and (2.35c) are almost the same. Obviously, $\boldsymbol{\sigma} - \ln \boldsymbol{\sigma} - \mathbf{I}$ and $\boldsymbol{\sigma} + \boldsymbol{\sigma}^{-1} - 2\mathbf{I}$ are symmetric matrices. Their eigenvalues are $f_1(\lambda_i) = \lambda_i - \ln \lambda_i - 1$ and $f_2(\gamma_i) = \gamma_i + \gamma_i^{-1} - 2$, respectively. It is easy to check that $f_1(x) \geq f_1(1) = 0$ and $f_2(x) \geq f_2(1) = 0$ for any $x \in \mathbb{R}^+$, which means the eigenvalues of the two matrices are always non-negative. Thus the two matrices are symmetric positive semi-definite and their trace are non-negative, which accomplishes the proof of (2.35b) and (2.35c).

The proof of (2.35d) starts with the definition of trace, $\text{tr}(\boldsymbol{\sigma}\boldsymbol{\tau}) = \sum_{ij} \boldsymbol{\sigma}_{ij} \boldsymbol{\tau}_{ji}$ and $\text{tr}(\boldsymbol{\tau}\boldsymbol{\sigma}) = \sum_{ij} \boldsymbol{\tau}_{ij} \boldsymbol{\sigma}_{ji}$. As $\sum_{ij} \boldsymbol{\tau}_{ij} \boldsymbol{\sigma}_{ji} = \sum_{ij} \boldsymbol{\sigma}_{ij} \boldsymbol{\tau}_{ji}$, we obtain $\text{tr}(\boldsymbol{\tau}\boldsymbol{\sigma}) = \text{tr}(\boldsymbol{\sigma}\boldsymbol{\tau})$. Consequently, by using equation (2.36) we get

$$\text{tr}(\boldsymbol{\tau}\boldsymbol{\sigma}) = \text{tr}(\boldsymbol{\sigma}\boldsymbol{\tau}) = \text{tr}(\mathbf{Q}^T \mathbf{Q}\boldsymbol{\tau}) = \text{tr}(\mathbf{Q}\boldsymbol{\tau}\mathbf{Q}^T). \quad (2.37)$$

Let $\mathbf{x}$ be any non-zero vector and $\mathbf{y} = \mathbf{Q}^T \mathbf{x} = \mathbf{R}_1 \sqrt{\boldsymbol{\Lambda}} \mathbf{x}$. As $\boldsymbol{\Lambda} > 0$, we have

$$|\mathbf{y}|^2 = \mathbf{y}^T \mathbf{y} = (\mathbf{R}_1 \sqrt{\boldsymbol{\Lambda}} \mathbf{x})^T \mathbf{R}_1 \sqrt{\boldsymbol{\Lambda}} \mathbf{x} = \mathbf{x}^T \sqrt{\boldsymbol{\Lambda}} \mathbf{R}_1^T \mathbf{R}_1 \sqrt{\boldsymbol{\Lambda}} \mathbf{x} = \mathbf{x}^T \boldsymbol{\Lambda} \mathbf{x} > 0.$$

This means $\mathbf{y}$ is non-zero. Noticing that $\boldsymbol{\tau}$ is positive-definite we get

$$\mathbf{x}^T (\mathbf{Q}\boldsymbol{\tau}\mathbf{Q}^T)\mathbf{x} = (\mathbf{Q}^T \mathbf{x})^T \boldsymbol{\tau}\mathbf{Q}^T \mathbf{x} = \mathbf{y}^T \boldsymbol{\tau}\mathbf{y} > 0.$$

Thus $\mathbf{Q}\boldsymbol{\tau}\mathbf{Q}^T$ is symmetric positive-definite, and $\text{tr}(\mathbf{Q}\boldsymbol{\tau}\mathbf{Q}^T) > 0$. Combining with equation (2.37) we obtain (2.35d), i.e.

$$\text{tr}(\boldsymbol{\tau}\boldsymbol{\sigma}) = \text{tr}(\boldsymbol{\sigma}\boldsymbol{\tau}) = \text{tr}(\mathbf{Q}\boldsymbol{\tau}\mathbf{Q}^T) = \text{tr}(\mathbf{Q}\boldsymbol{\tau}\mathbf{Q}^T) > 0.$$

Equation (2.35e) is an extension of equation (2.35d).

Let $\mathbf{A} = \mathbf{Q}\boldsymbol{\tau}^{-1}\mathbf{Q}^T$. According to the proof of (2.35d), we get $\text{tr}(\boldsymbol{\sigma}\boldsymbol{\tau}^{-1}) = \text{tr}\mathbf{A}$ and $\mathbf{A}$ is symmetric positive-definite .

Then the proof of (2.35e) is equivalent to show $\text{tr}(\mathbf{A} - \mathbf{I}) \geq \ln \det \mathbf{A}$ for any symmetric positive-definite matrix $\mathbf{A}$, which derives from (2.35a) and (2.35b).

Let $\mathbf{O} = \mathbf{R}_2\mathbf{R}_1^T$. Obviously $\mathbf{O}$ is orthonormal as $\mathbf{R}_1$ and $\mathbf{R}_2$ are orthonormal. Thus we have $\sum_j(\mathbf{O}_{ij})^2 = 1$ for all $i, i = 1, 2, 3$. Thanks to this property, we can show the derivation of (2.35f) as follows,

$$\text{tr}((\ln \boldsymbol{\sigma} - \ln \boldsymbol{\tau})\boldsymbol{\sigma} - (\boldsymbol{\sigma} - \boldsymbol{\tau})) = \sum_i(\lambda_i \ln \lambda_i - \lambda_i) + \sum_j \gamma_j - \sum_{i,j}(\mathbf{O}_{ij})^2 \lambda_i \ln \gamma_j$$

$$= \sum_i \left((\lambda_i \ln \lambda_i - \lambda_i)\sum_j(\mathbf{O}_{ij})^2\right) + \sum_j \left(\gamma_j \sum_i(\mathbf{O}_{ij})^2\right) - \sum_{i,j}(\mathbf{O}_{ij})^2 \lambda_i \ln \gamma_j$$

$$= \sum_{i,j}(\mathbf{O}_{ij})^2 \left((\gamma_j - \lambda_i) - \lambda_i(\ln \gamma_j - \ln \lambda_i)\right).$$

Since $x - y \geq y(\ln x - \ln y)$ for all $x, y > 0$, we obtain (2.35f), i.e.

$$\text{tr}((\ln \boldsymbol{\sigma} - \ln \boldsymbol{\tau})\boldsymbol{\sigma} - (\boldsymbol{\sigma} - \boldsymbol{\tau})) \geq 0,$$

which concludes the proof. $\square$

Lemma 2.3.2. *[18] For any symmetric positive-definite matrix $\boldsymbol{\sigma}(t) \in (C^1([0,T]))^{\frac{d(d+1)}{2}}$, we have $\forall t \in [0, T]$:*

$$(\frac{d}{dt}\boldsymbol{\sigma}) : \boldsymbol{\sigma}^{-1} = tr(\boldsymbol{\sigma}^{-1}\frac{d}{dt}\boldsymbol{\sigma}) = \frac{d}{dt}tr(\ln \boldsymbol{\sigma}), \tag{2.38}$$

$$(\frac{d}{dt}\ln \boldsymbol{\sigma}) : \boldsymbol{\sigma} = tr(\boldsymbol{\sigma}\frac{d}{dt}\ln \boldsymbol{\sigma}) = \frac{d}{dt}tr\boldsymbol{\sigma}. \tag{2.39}$$

Proof. Since $\boldsymbol{\sigma}(t) \in (C^1([0,T]))^{\frac{d(d+1)}{2}}$ is a symmetric positive-definite matrix, $\det \boldsymbol{\sigma}$ is positive and $C^1([0,T])$. Thus, we get the classical Jacobi formula (2.38), i.e.

$$\frac{d}{dt}tr(\ln \boldsymbol{\sigma}) = \frac{d}{dt}\ln(\det \boldsymbol{\sigma}) = (1/\det \boldsymbol{\sigma})\frac{d}{dt}\det \boldsymbol{\sigma} = tr(\boldsymbol{\sigma}^{-1}\frac{d}{dt}\boldsymbol{\sigma}) = (\frac{d}{dt}\boldsymbol{\sigma}) : \boldsymbol{\sigma}^{-1}.$$

For the proof of the second equation, we set $\boldsymbol{\psi} = \ln \boldsymbol{\sigma}$ and then we can show

$$(\frac{d}{dt}\ln \boldsymbol{\sigma}) : \boldsymbol{\sigma} = tr(\boldsymbol{\sigma}\frac{d}{dt}\ln \boldsymbol{\sigma}) = tr(e^{\boldsymbol{\psi}}\frac{d}{dt}\boldsymbol{\psi}) = tr(\frac{d}{dt}e^{\boldsymbol{\psi}}) = \frac{d}{dt}tr\boldsymbol{\sigma}.$$

$\square$

The following lemma will be useful in the evaluation of the diffusive terms in the energy

estimate.

Lemma 2.3.3. *Let $\boldsymbol{\sigma}, \boldsymbol{\tau} \in R^{d \times d}$ be symmetric positive-definite matrices, f_1 be an increasing function, and f_2 be a decreasing function, we have:*

$$(\boldsymbol{\sigma} - \boldsymbol{\tau}) : (f_1(\boldsymbol{\sigma}) - f_1(\boldsymbol{\tau})) \geq 0, \tag{2.40}$$

$$(\boldsymbol{\sigma} - \boldsymbol{\tau}) : (f_2(\boldsymbol{\sigma}) - f_2(\boldsymbol{\tau})) \leq 0, \tag{2.41}$$

$$\nabla \boldsymbol{\sigma} : \nabla \boldsymbol{\sigma}^{-1} \leq 0, \tag{2.42}$$

$$\nabla(\ln \boldsymbol{\sigma}) : \nabla \boldsymbol{\sigma} \geq 0. \tag{2.43}$$

Proof. Applying the eigen-decomposition to $\boldsymbol{\sigma}$ and $\boldsymbol{\tau}$ in d dimensions, we have $\boldsymbol{\sigma} = \mathbf{R}_1 \boldsymbol{\Lambda} \mathbf{R}_1^T$, $\boldsymbol{\tau} = \mathbf{R}_2 \boldsymbol{\Gamma} \mathbf{R}_2^T$. $\boldsymbol{\Lambda} = \text{diag}\{\lambda_i\}, \boldsymbol{\Gamma} = \text{diag}\{\gamma_i\}, i = 1, \cdots, d$. λ_i and γ_i are eigenvalues of $\boldsymbol{\sigma}$ and $\boldsymbol{\tau}$. $\mathbf{R}_1$ and $\mathbf{R}_2$ are orthonormal eigenvector matrices. Let $\mathbf{O} = \mathbf{R}_2^T \mathbf{R}_1$, then $\mathbf{O}$ is also orthonormal.

$$\text{tr}(\boldsymbol{\sigma} f(\boldsymbol{\tau})) = \text{tr}(\mathbf{R}_1 \boldsymbol{\Lambda} \mathbf{R}_1^T \mathbf{R}_2 f(\boldsymbol{\Gamma}) \mathbf{R}_2^T) = \text{tr}(\mathbf{R}_2^T \mathbf{R}_1 \boldsymbol{\Lambda} \mathbf{R}_1^T \mathbf{R}_2 f(\boldsymbol{\Gamma})) = \text{tr}(\mathbf{O} \boldsymbol{\Lambda} \mathbf{O}^T f(\boldsymbol{\Gamma}))$$

$$= \sum_{i,j} (\mathbf{O} \boldsymbol{\Lambda})_{ij} (\mathbf{O}^T f(\boldsymbol{\Gamma}))_{ji} = \sum_{i,j} \left((\sum_k \mathbf{O}_{ik} \boldsymbol{\Lambda}_{kj})(\sum_k \mathbf{O}_{kj} f(\Gamma)_{ki}) \right) = \sum_{i,j} \left((\mathbf{O}_{ij} \boldsymbol{\Lambda}_{jj})(\mathbf{O}_{ij} f(\Gamma)_{ii}) \right)$$

$$= \sum_{i,j} \left(\mathbf{O}_{ij}^2 \lambda_j f(\gamma_i) \right).$$

Similarly, we have

$$\text{tr}(\boldsymbol{\tau} f(\boldsymbol{\sigma})) = \sum_{i,j} (\mathbf{O}_{ij}^2 f(\lambda_j) \gamma_i).$$

As $\mathbf{O}$ is orthonormal, $\sum_i \mathbf{O}_{ij}^2 = 1$ for any j, $j = 1, \cdots d$.

$$\text{tr}(\boldsymbol{\sigma} f(\boldsymbol{\sigma})) = \sum_j (\lambda_j f(\lambda_j)) = \sum_j \left(\lambda_j f(\lambda_j) \sum_i \mathbf{O}_{ij}^2 \right).$$

Similarly, we have

$$\text{tr}(\boldsymbol{\tau} f(\boldsymbol{\tau})) = \sum_i (\gamma_i f(\gamma_i)) = \sum_i \left(\gamma_i f(\gamma_i) \sum_j \mathbf{O}_{ij}^2 \right).$$

Combining the above four equations we get

$$(\boldsymbol{\sigma} - \boldsymbol{\tau}) : (f(\boldsymbol{\sigma}) - f(\boldsymbol{\tau}))$$
$$= \text{tr}((\boldsymbol{\sigma} - \boldsymbol{\tau}) \cdot (f(\boldsymbol{\sigma}) - f(\boldsymbol{\tau}))) = \text{tr}(\boldsymbol{\sigma} f(\boldsymbol{\sigma}) + \boldsymbol{\tau} f(\boldsymbol{\tau}) - \boldsymbol{\tau} f(\boldsymbol{\sigma}) - \boldsymbol{\sigma} f(\boldsymbol{\tau}))$$
$$= \sum_j \left(\lambda_j f(\lambda_j) \sum_i \mathbf{O}_{ij}^2 \right) + \sum_i \left(\gamma_i f(\gamma_i) \sum_i \mathbf{O}_{ij}^2 \right) - \sum_{i,j} \left(\mathbf{O}_{ij}^2 f(\lambda_j) \gamma_i \right) - \sum_{i,j} \left(\mathbf{O}_{ij}^2 \lambda_j f(\gamma_i) \right)$$
$$= \sum_j \lambda_j \sum_i \mathbf{O}_{ij}^2 (f(\lambda_j) - f(\gamma_i)) + \sum_i \gamma_i \sum_j \mathbf{O}_{ij}^2 (f(\gamma_i) - f(\lambda_j))$$
$$= \sum_{i,j} \mathbf{O}_{ij}^2 (f(\lambda_j) - f(\gamma_i))(\lambda_j - \gamma_i).$$

19

If f is an increasing function, we get (2.40)

$$(\boldsymbol{\sigma} - \boldsymbol{\tau}) : (f(\boldsymbol{\sigma}) - f(\boldsymbol{\tau})) \geq 0,$$

otherwise we get (2.41)

$$(\boldsymbol{\sigma} - \boldsymbol{\tau}) : (f(\boldsymbol{\sigma}) - f(\boldsymbol{\tau})) \leq 0.$$

Now we go to the derivation of (2.42) and (2.43).

$$\frac{\partial \boldsymbol{\sigma}}{\partial x} : \frac{\partial f(\boldsymbol{\sigma})}{\partial x} = \lim_{dx \to 0} \frac{\boldsymbol{\sigma}(x + dx) - \boldsymbol{\sigma}(x)}{dx} : \frac{f(\boldsymbol{\sigma}(x + dx)) - f(\boldsymbol{\sigma}(x))}{dx}.$$

For $x > 0$ we know that $f(x) = \ln(x)$ is an increasing function, and $f(x) = \frac{1}{x}$ is a decreasing function. Using (2.40) and (2.41) we get

$$\frac{\partial \boldsymbol{\sigma}}{\partial x} : \frac{\partial \ln(\boldsymbol{\sigma})}{\partial x} \geq 0, \ \frac{\partial \boldsymbol{\sigma}}{\partial x} : \frac{\partial (\boldsymbol{\sigma})^{-1}}{\partial x} \leq 0.$$

Analogously, the above inequalities also hold for other space dimension. Thus we have

$$\nabla \boldsymbol{\sigma} : \nabla \ln \boldsymbol{\sigma} \geq 0, \ \nabla \boldsymbol{\sigma} : \nabla (\boldsymbol{\sigma})^{-1} \leq 0,$$

which concludes the proof. $\qquad\qquad\qquad\qquad\qquad\qquad\qquad\qquad\qquad\qquad$ $\square$

2.3.2 Stability results

Theorem 2.3.4. *(energy estimates for the diffusive Oldroyd-B model)*
Let $(\mathbf{u}, p, \boldsymbol{\sigma})$ be a smooth solution to system (2.11), supplied with homogeneous Dirichlet boundary condition for velocity, and zero Neumann boundary condition for $\boldsymbol{\sigma}$. Further, we assume that $\boldsymbol{\sigma}$ is initially symmetric positive-definite. The free energy satisfies:

$$\frac{d}{dt} F(\mathbf{u}, \boldsymbol{\sigma}) + \alpha \int_{\mathcal{T}} |\nabla \mathbf{u}|^2 + \frac{\beta}{2We^2} \int_{\mathcal{T}} tr(\boldsymbol{\sigma} - \ln \boldsymbol{\sigma} - \mathbf{I}) \leq 0. \tag{2.44}$$

This estimate implies that $F(\mathbf{u}, \boldsymbol{\sigma})$ decreases in time exponentially fast to zero.

Proof. First we get by computing the inner product of the momentum equation (2.11a) and the velocity

$$\frac{Re}{2} \frac{d}{dt} \int_{\mathcal{T}} |\mathbf{u}|^2 + \alpha \int_{\mathcal{T}} |\nabla \mathbf{u}|^2 + \frac{\beta}{We} \int_{\mathcal{T}} \nabla \mathbf{u} : \boldsymbol{\sigma} = 0. \tag{2.45}$$

Then we take the trace of transport equation (2.11c) for the conformation tensor. This yields

$$\frac{d}{dt} \int_{\mathcal{T}} tr\boldsymbol{\sigma} = 2 \int_{\mathcal{T}} \nabla \mathbf{u} : \boldsymbol{\sigma} + \frac{1}{We} \int_{\mathcal{T}} tr(\mathbf{I} - \boldsymbol{\sigma}) + \varepsilon \int_{\mathcal{T}} \Delta \boldsymbol{\sigma} : \mathbf{I} = 2 \int_{\mathcal{T}} \nabla \mathbf{u} : \boldsymbol{\sigma} + \frac{1}{We} \int_{\mathcal{T}} tr(\mathbf{I} - \boldsymbol{\sigma}). \tag{2.46}$$

Multiplying the transport equation (2.11c) for the conformation tensor with $\boldsymbol{\sigma}^{-1}$ leads

to

$$\int_{\mathcal{T}} \frac{d\boldsymbol{\sigma}}{dt} : \boldsymbol{\sigma}^{-1} = 2\int_{\mathcal{T}} \mathrm{tr}(\nabla\mathbf{u}) + \frac{1}{We}\int_{\mathcal{T}} \mathrm{tr}(\boldsymbol{\sigma}^{-1} - \mathbf{I}) + \varepsilon\int_{\mathcal{T}} \Delta\boldsymbol{\sigma} : \boldsymbol{\sigma}^{-1}. \qquad (2.47)$$

Substituting (2.38) into (2.47), and using the fact that $\mathrm{tr}(\nabla\mathbf{u}) = \mathrm{div}\ \mathbf{u} = 0$, we have

$$\frac{d}{dt}\int_{\mathcal{T}} \mathrm{tr}(\ln\boldsymbol{\sigma}) = \frac{1}{We}\int_{\mathcal{T}} \mathrm{tr}(\boldsymbol{\sigma}^{-1} - \mathbf{I}) - \varepsilon\int_{\mathcal{T}} \nabla\boldsymbol{\sigma} : \nabla\boldsymbol{\sigma}^{-1}. \qquad (2.48)$$

Now, combing (2.45) $+ \frac{\beta}{2We}\times$ (2.46) $- \frac{\beta}{2We}\times$ (2.48) and using the inequality (2.42) implies (2.44), i.e.

$$\frac{d}{dt}\int_{\mathcal{T}} \left(\frac{Re}{2}|\mathbf{u}|^2 + \frac{\beta}{2We}\mathrm{tr}(\boldsymbol{\sigma} - \ln\boldsymbol{\sigma} - \mathbf{I})\right) + \int_{\mathcal{T}} \left(\alpha|\nabla\mathbf{u}|^2 + \frac{\beta}{2We^2}\mathrm{tr}(\boldsymbol{\sigma} + \boldsymbol{\sigma}^{-1} - 2\mathbf{I})\right)$$

$$= \frac{\varepsilon\beta}{2We}\int_{\mathcal{T}} \nabla\boldsymbol{\sigma} : \nabla\boldsymbol{\sigma}^{-1} \le 0.$$

By (2.35c) we have $\mathrm{tr}(\boldsymbol{\sigma} + \boldsymbol{\sigma}^{-1} - 2\mathbf{I}) \ge 0$, thus $F(\mathbf{u}, \boldsymbol{\sigma})$ decreases in time as $\frac{dF}{dt} \le 0$. It is easy to check that $\boldsymbol{\sigma}^{-1}$ is also a symmetric positive-definite matrix. Substituting $\boldsymbol{\sigma}^{-1}$ to (2.35b) yields

$$\mathrm{tr}(\boldsymbol{\sigma}^{-1} + \ln(\boldsymbol{\sigma}) - \mathbf{I}) \ge 0,$$

thus we obtain

$$\mathrm{tr}(\boldsymbol{\sigma} + \boldsymbol{\sigma}^{-1} - 2\mathbf{I}) = \mathrm{tr}(\boldsymbol{\sigma} - \ln\boldsymbol{\sigma} - \mathbf{I}) + \mathrm{tr}(\boldsymbol{\sigma}^{-1} + \ln(\boldsymbol{\sigma}) - \mathbf{I}) \ge \mathrm{tr}(\boldsymbol{\sigma} - \ln\boldsymbol{\sigma} - \mathbf{I}).$$

Using the Poincaré inequality, we know that there exists a constant $C_p > 0$ depending on the domain $\mathcal{T}$ such that for all $\mathbf{u} \in H_0^1(\mathcal{T})$,

$$\int_{\mathcal{T}} |\mathbf{u}|^2 \le C_p \int_{\mathcal{T}} |\nabla\mathbf{u}|^2.$$

Consequently, we have

$$\frac{d}{dt}F(\mathbf{u}, \boldsymbol{\sigma}) \le -\frac{\alpha}{C_p}\int_{\mathcal{T}} |\mathbf{u}|^2 - \frac{\beta}{2We^2}\mathrm{tr}(\boldsymbol{\sigma} - \ln\boldsymbol{\sigma} - \mathbf{I})) \le -\min\left(\frac{2\alpha}{Re\ C_p}, \frac{1}{We}\right)F(\mathbf{u}, \boldsymbol{\sigma}).$$

Now we can apply the Gronwall inequality and obtain

$$F(\mathbf{u}, \boldsymbol{\sigma}) \le F(\mathbf{u}(t = 0), \boldsymbol{\sigma}(t = 0))\exp\left(-\min\left(\frac{2\alpha}{Re\ C_p}, \frac{1}{We}\right)t\right).$$

$\square$

Theorem 2.3.5. *(energy estimates for the diffusive logarithmic Oldroyd-B model)*
Let $(\mathbf{u}, p, \boldsymbol{\psi})$ be a smooth solution to system (2.20), supplied with the homogeneous Dirichlet boundary condition for velocity, and with the zero Neumann boundary condition for $\boldsymbol{\psi}$. Further, we assume that initially e^{ψ} is a symmetric positive-definite tensor. The free

energy satisfies:

$$\frac{d}{dt}F(\mathbf{u}, e^\psi) + \alpha \int_{\mathcal{T}} |\nabla \mathbf{u}|^2 + \frac{\beta}{2We^2} \int_{\mathcal{T}} tr(e^\psi + e^{-\psi} - \mathbf{I}) \le 0. \tag{2.49}$$

From this estimate, we also obtain that $F(\mathbf{u}, e^\psi)$ decreases in time exponentially fast to zero.

Proof. Again by computing the inner product of the momentum equation and the velocity we get

$$\frac{Re}{2}\frac{d}{dt}\int_{\mathcal{T}}|\mathbf{u}|^2 + \alpha \int_{\mathcal{T}}|\nabla\mathbf{u}|^2 + \frac{\beta}{We}\int_{\mathcal{T}}\nabla\mathbf{u} : e^\psi = 0. \tag{2.50}$$

Then, multiplying the transport equation for the logarithmic conformation tensor with $e^\psi - \mathbf{I}$ implies

$$\frac{d}{dt}\int_{\mathcal{T}} tr(e^\psi - \psi) = \int_{\mathcal{T}}(\boldsymbol{\Omega}\psi - \psi\boldsymbol{\Omega} + 2\mathbf{B}) : (e^\psi - \mathbf{I}) + \frac{1}{We}tr(2\mathbf{I} - e^\psi - e^{-\psi}) + \varepsilon\int_{\mathcal{T}}\Delta\psi : (e^\psi - \mathbf{I}). \tag{2.51}$$

Let us note that

$$\int_{\mathcal{T}}(\boldsymbol{\Omega}\psi - \psi\boldsymbol{\Omega}) : (e^\psi - \mathbf{I}) = \int_{\mathcal{T}}(\boldsymbol{\Omega}\psi - \psi\boldsymbol{\Omega}) : e^\psi = 0,$$

and

$$\int_{\mathcal{T}}\mathbf{B} : (e^\psi - \mathbf{I}) = \int_{\mathcal{T}}\nabla\mathbf{u} : e^\psi - \int_{\mathcal{T}} tr\mathbf{B} = \int_{\mathcal{T}}\nabla\mathbf{u} : e^\psi.$$

For the diffusive terms, using Lemma 2.3.3 we get

$$\int_{\mathcal{T}}\Delta\psi : (e^\psi - \mathbf{I}) = -\int_{\mathcal{T}}\nabla\psi : \nabla e^\psi \le 0.$$

Then equation (2.51) can be written as

$$\frac{d}{dt}\int_{\mathcal{T}} tr(e^\psi - \psi) = 2\int_{\mathcal{T}}(\nabla\mathbf{u}) : e^\psi + \frac{1}{We}tr(2\mathbf{I} - e^\psi - e^{-\psi}) - \varepsilon\int_{\mathcal{T}}\nabla\psi : \nabla e^\psi. \tag{2.52}$$

In order to eliminate the term $\int_{\mathcal{T}}\nabla\mathbf{u} : e^\psi$, we compute $(2.50) + \frac{\beta}{2We}\times (2.52)$ and use the inequality (2.42). This yields (2.49), i.e.

$$\frac{d}{dt}\int_{\mathcal{T}}\left(\frac{Re}{2}|\mathbf{u}|^2 + \frac{\beta}{2We}tr(e^\psi - \psi - \mathbf{I})\right) + \int_{\mathcal{T}}\left(\alpha|\nabla\mathbf{u}|^2 + \frac{\beta}{2We^2}tr(e^\psi + e^{-\psi} - 2\mathbf{I})\right)$$

$$= -\frac{\varepsilon\beta}{2We}\int_{\mathcal{T}}\nabla\psi : \nabla e^\psi \le 0.$$

We now follow the proof of Theorem 2.3.4 and it is clear that $F(\mathbf{u}, e^\psi)$ decreases exponentially fast to zero in time. $\square$

2.4 Characteristic finite element method

In this section we shall present the characteristic finite element scheme for the diffusive Oldroyd-B models.

The idea of the characteristic method is to consider the trajectory of the fluid particle and discretize the material derivative $\frac{D\mathbf{u}}{Dt} = \frac{\partial \mathbf{u}}{\partial t} + \mathbf{u} \cdot \nabla \mathbf{u}$ along the characteristic path $\frac{d\mathbf{x}}{dt} = \mathbf{u}$. The advantage is that the resulting system matrix of the discrete scheme is symmetric. This is advantageous when applying the implicit time approximation since we can apply standard linear algebraic solvers for symmetric matrices. The characteristic finite element method (FEM) for Navier-Stokes equations has been studied by [31, 74, 75, 81]. The second order in time scheme has been studied by Boukir et al. [16]. In [68] Notsu and Tabata developed a single time step second-order scheme, see also [13, 78]. Further, a pressure-stabilized $\mathcal{P}^1/\mathcal{P}^1$ element approximation within characteristic FEM method is proposed by Notsu and Tabata [66, 67]. Similar results can be found in [45].

2.4.1 Weak formulation

We start with introducing suitable functional spaces and the corresponding weak formulation. Let $\mathcal{T}$ be a bounded domain in $\mathbb{R}^d$, $d = 2, 3$, $V \equiv H_0^1(\mathcal{T})^d$, $Q \equiv L_0^2(\mathcal{T})$ and $W \equiv H^1(\mathcal{T})^{d \times d}$ be the function spaces for velocity, pressure and conformation tensor. Here $H^1(\mathcal{T})$ and $H_0^1(\mathcal{T})$ are the well-known Sobolev spaces, the function space $L_0^2(\mathcal{T})$ is given as

$$L_0^2(\mathcal{T}) \equiv \{q \in L^2(\mathcal{T}); \int_{\mathcal{T}} qdx = 0\}.$$

Further, let $(\cdot, \cdot)$ denote the L^2-inner products in the vector- and matrix- function spaces. The bilinear forms are defined as follows

$$a_0(\mathbf{u}, \mathbf{v}) = 2\alpha(\mathbf{D}(\mathbf{u}), \mathbf{D}(\mathbf{v})), b(\mathbf{u}, q) = -(\nabla \cdot \mathbf{u}, q),$$
$$\mathcal{A}((\mathbf{u}, p), (\mathbf{v}, q)) = a_0(\mathbf{u}, \mathbf{v}) + b(\mathbf{u}, q) + b(\mathbf{v}, p).$$

Definition 1. *A weak solution of the problem* (2.11) *is a triple* $\{(\mathbf{u}, p, \boldsymbol{\sigma})(t)\}_{t \in (0,T)} \subset V \times Q \times W$, *such that for any test function* $(\mathbf{v}, q, \boldsymbol{\phi}) \in V \times Q \times W$ *and almost any time* $t \in (0, T)$, *we have*

$$\left(Re\frac{D\mathbf{u}}{Dt}(t), \mathbf{v}\right) + \mathcal{A}((\mathbf{u}, p)(t), (\mathbf{v}, q)) = \frac{\alpha}{We}(\boldsymbol{\sigma}(t), \nabla \mathbf{v}), \tag{2.53a}$$

$$\left(\frac{D\boldsymbol{\sigma}}{Dt}(t), \boldsymbol{\phi}\right) + \varepsilon(\nabla\boldsymbol{\sigma}(t), \nabla\boldsymbol{\phi}) = (\nabla\mathbf{u}(t)\boldsymbol{\sigma}(t) + \boldsymbol{\sigma}(t)\nabla\mathbf{u}(t)^T, \boldsymbol{\phi})$$

$$+ \frac{1}{We}(\mathbf{I} - \boldsymbol{\sigma}(t), \boldsymbol{\phi}). \tag{2.53b}$$

Definition 2. *A weak solution of problem* (2.20) *is a triple* $\{(\mathbf{u}, p, \boldsymbol{\psi})(t)\}_{t \in (0,T)} \subset V \times Q \times W$, *such that for any test function* $(\mathbf{v}, q, \boldsymbol{\phi}) \in V \times Q \times W$ *and almost any time*

$t \in (0, T)$, *we have*

$$\left(Re\frac{D\mathbf{u}}{Dt}(t), \mathbf{v}\right) + \mathcal{A}((\mathbf{u}, p)(t), (\mathbf{v}, q)) = \frac{\alpha}{We}(e^{\psi(t)}, \nabla\mathbf{v}), \tag{2.54a}$$

$$\left(\frac{D\boldsymbol{\psi}}{Dt}(t), \boldsymbol{\phi}\right) + \varepsilon(\nabla\boldsymbol{\psi}(t), \nabla\boldsymbol{\phi}) = (\boldsymbol{\Omega}(t)\boldsymbol{\psi}(t) + \boldsymbol{\psi}(t)\boldsymbol{\Omega}(t) - 2\mathbf{B}(t), \boldsymbol{\phi})$$

$$+ \frac{1}{We}(e^{-\psi(t)} - \mathbf{I}, \boldsymbol{\phi}). \tag{2.54b}$$

Here, $\boldsymbol{\Omega}$ and $\mathbf{B}$ come from the decomposition (2.13), and their value can be derived from equation (2.14), or (2.16).

The initial conditions are $\left(\mathbf{u}^0, p^0, \boldsymbol{\sigma}^0(\boldsymbol{\psi}^0 = \ln\boldsymbol{\sigma}^0)\right) \in V \times Q \times W$, where $\boldsymbol{\sigma}^0$ is a symmetric positive-definite matrix. We would like to repeat that the question on the existence of global weak solutions is still an open problem in general. The first results for (2.53) have been obtained in [8, 22].

2.4.2 Discretization schemes

In what follows we formulate the characteristic FEM.

As usual, $\mathcal{P}^1(K)$ denotes polynomial space of linear functions on a finite element $K \in \mathcal{T}_h$, $\mathcal{T}_h$ is the triangulation of $\bar{\mathcal{T}}(= \bigcup_{K \in \mathcal{T}_h} K)$, and h_K is the diameter of the element K. We assume that our triangulation is regular, cf. [21].

First, let us define some suitable function spaces $X_h, M_h, \Sigma_h, V_h, Q_h, S_h$ in the following way

$$X_h \equiv \{\mathbf{v}_h \in C^0(\bar{\mathcal{T}}_h)^d; \mathbf{v}_h|_K \in \mathcal{P}^1(K)^d, \forall K \in \mathcal{T}_h\}, V_h \equiv X_h \cap V,$$

$$M_h \equiv \{q_h \in C^0(\bar{\mathcal{T}}_h); q_h|_K \in \mathcal{P}^1(K), \forall K \in \mathcal{T}_h\}, Q_h \equiv M_h \cap Q,$$

$$\Sigma_h \equiv \{\boldsymbol{\phi}_h \in C^0(\bar{\mathcal{T}}_h)^{d \times d}; \boldsymbol{\phi}_h|_K \in \mathcal{P}^1(K)^{d \times d}, \forall K \in \mathcal{T}_h\}, W_h \equiv \Sigma_h \cap W.$$

Further, we introduce some standard interpolation operators [21]

$$\Pi_h^{(1)} : C^0(\bar{\mathcal{T}}_h)^d \to X_h, \quad \Pi_h^{(2)} : C^0(\bar{\mathcal{T}}_h) \to M_h, \quad \Pi_h^{(3)} : C^0(\bar{\mathcal{T}}_h)^{d \times d} \to \Sigma_h.$$

Let Δt denote the time step and N_T the total number of time steps. We state our characteristic finite element scheme for the diffusive Oldroyd-B model (2.11):

Find $\{(\mathbf{u}_h^{n+1}, p_h^{n+1}, \boldsymbol{\sigma}_h^{n+1})\}_{n=0}^{N_T-1} \subset V_h \times Q_h \times W_h$ such that for any test function $(\mathbf{v}_h, q_h, \boldsymbol{\phi}_h) \in V_h \times Q_h \times W_h$ and for $n = 0, \cdots, N_T - 1$ it holds

$$\left(Re\frac{\mathbf{u}_h^{n+1} - \mathbf{u}_h^n \circ \mathbf{X}^n}{\Delta t}, \mathbf{v}_h\right) + \mathcal{A}((\mathbf{u}_h^{n+1}, p_h^{n+1}), (\mathbf{v}_h, q_h)) + S_h(p_h^{n+1}, q_h) = -\frac{\alpha}{We}(\boldsymbol{\sigma}_h^{n+1}, \nabla\mathbf{v}_h),$$

$$\tag{2.55a}$$

$$\left(\frac{\boldsymbol{\sigma}_h^{n+1} - \boldsymbol{\sigma}_h^n \circ \mathbf{X}^n}{\Delta t}, \boldsymbol{\phi}_h\right) + \varepsilon(\nabla\boldsymbol{\sigma}_h^{n+1}, \nabla\boldsymbol{\phi}_h) = (\nabla\mathbf{u}_h^{n+1}\boldsymbol{\sigma}_h^{n+1} + \boldsymbol{\sigma}_h^{n+1}(\nabla\mathbf{u}_h^{n+1})^T, \boldsymbol{\phi}_h)$$

$$+ \frac{1}{We}(\mathbf{I} - \boldsymbol{\sigma}_h^{n+1}, \boldsymbol{\phi}_h). \tag{2.55b}$$

Here the function $\mathbf{X}^n(t^n) : x \in \mathcal{T} \mapsto \mathbf{X}^n(t, x) \in \mathcal{T}$ defines the characteristic

$$\begin{cases} \frac{D}{Dt}\mathbf{X}^n(t, x) = \mathbf{u}_h^n(\mathbf{X}^n(t, x)), \ \forall t \in [t^n, t^{n+1}], \\ \mathbf{X}^n(t^{n+1}, x) = x. \end{cases} \tag{2.56}$$

Furthermore, the pressure stabilization term is defined as $S_h(p, q) = -\delta \sum_{K \in \mathcal{T}_h} h_K^2 \int_K \nabla p \nabla q$ and $\delta > 0$ is a suitable parameter. For the diffusive model in the case of logarithmic transformation (2.20), the characteristic FEM reads:

Find $\{(\mathbf{u}_h^{n+1}, p_h^{n+1}, \boldsymbol{\psi}_h^{n+1})\}_{n=0}^{N_T-1} \subset V_h \times Q_h \times W_h$ such that for any test function $(\mathbf{v}_h, q_h, \boldsymbol{\phi}_h) \in V_h \times Q_h \times W_h$ and for $n = 0, \cdots, N_T - 1$, we have

$$\left(Re\frac{\mathbf{u}_h^{n+1} - \mathbf{u}_h^n \circ \mathbf{X}^n)}{\Delta t}, \mathbf{v}_h\right) + \mathcal{A}((\mathbf{u}_h^{n+1}, p_h^{n+1}), (\mathbf{v}_h, q_h)) + S_h(p_h^{n+1}, q) = -\frac{\alpha}{We}(e^{\psi_h^{n+1}}, \nabla\mathbf{v}), \tag{2.57a}$$

$$\left(\frac{\boldsymbol{\psi}_h^{n+1} - \boldsymbol{\psi}_h^n \circ \mathbf{X}^n}{\Delta t}, \boldsymbol{\phi}_h\right) + \varepsilon(\nabla\boldsymbol{\psi}_h^{n+1}, \nabla\boldsymbol{\phi}_h) = (\boldsymbol{\Omega}_h^{n+1}\boldsymbol{\psi}_h^{n+1} + \boldsymbol{\psi}_h^{n+1}\boldsymbol{\Omega}_h^{n+1} - 2\mathbf{B}_h^{n+1}, \boldsymbol{\phi}_h)$$

$$+ \frac{1}{We}(e^{-\psi_h^{n+1}} - \mathbf{I}, \boldsymbol{\phi}_h), \tag{2.57b}$$

The schemes (2.55) and (2.57) are implicit in time. In order to obtain a numerical solution to such schemes we apply the fixed point iterations. Let us present the characteristic FEM for (2.55) in Algorithm 1.

Algorithm 1 Characteristic FEM for the diffusive Oldroyd-B model
---
1: Given $\mathbf{u}_h^n, p_h^n, \boldsymbol{\sigma}_h^n$, set $\mathbf{u}^{n,0} = \mathbf{u}_h^n, \boldsymbol{\sigma}_h^{n,0} = \boldsymbol{\sigma}_h^n, p_h^{n,0} = p_h^n$.
2: **for** $\ell = 0, 1, \cdots$ **do**
3:     solve the equation (2.55) with explicit RHS:

$$\left(Re\frac{\mathbf{u}_h^{n,\ell+1} - \mathbf{u}_h^n \circ \mathbf{X}^n)}{\Delta t}, \mathbf{v}_h\right) + \mathcal{A}((\mathbf{u}_h^{n,\ell+1}, p_h^{n,\ell+1}), (\mathbf{v}_h, q_h)) + S_h(p_h^{n,\ell+1}, q_h)$$

$$= -\frac{\alpha}{We}(\boldsymbol{\sigma}_h^{n,\ell}, \nabla\mathbf{v}_h),$$

$$\left(\frac{\boldsymbol{\sigma}_h^{n,\ell+1} - \boldsymbol{\sigma}_h^n \circ \mathbf{X}^n}{\Delta t}, \boldsymbol{\phi}_h\right) + \varepsilon(\nabla\boldsymbol{\sigma}_h^{n,\ell+1}, \nabla\boldsymbol{\phi}_h) + \frac{1}{We}(\boldsymbol{\sigma}^{n,\ell+1}, \boldsymbol{\phi}_h)$$

$$= (\nabla\mathbf{u}_h^{n,\ell}\boldsymbol{\sigma}_h^{n,\ell} + \boldsymbol{\sigma}_h^{n,\ell}(\nabla\mathbf{u}_h^{n,\ell})^T, \boldsymbol{\phi}_h) + \frac{1}{We}(\mathbf{I}, \boldsymbol{\phi}_h).$$

4:     **if** $(\|\mathbf{w}^{n,\ell+1} - \mathbf{w}^{n,\ell}\| \leq \xi\|\mathbf{w}^{n,\ell}\|$ for $\mathbf{w} \in \{\mathbf{u}, p, \boldsymbol{\sigma}\}$ and ξ is small enough) **then**
5:         break
6:     **end if**
7: **end for**
8: Update solution: $\mathbf{u}^{n+1} = \mathbf{u}^{n,\ell+1}, p^{n+1} = p^{n,\ell+1}, \boldsymbol{\sigma}^{n+1} = \boldsymbol{\sigma}^{n,\ell+1}$.

An analogous algorithm can be written for the characteristic FEM (2.57), cf. Algorithm 2.

Algorithm 2 Characteristic FEM for the diffusive Oldroyd-B model using log-transformation

---

1: Given $\mathbf{u}_h^n, p_h^n, \boldsymbol{\psi}_h^n$, set $\mathbf{u}^{n,0} = \mathbf{u}_h^n, \boldsymbol{\psi}_h^{n,0} = \boldsymbol{\psi}_h^n, p_h^{n,0} = p_h^n$.
2: **for** $\ell = 0, 1, \cdots$ **do**
3:    solve the equation (2.57) with explicit RHS:

$$\left(Re \frac{\mathbf{u}_h^{n,\ell+1} - \mathbf{u}_h^n \circ \mathbf{X}^n)}{\Delta t}, \mathbf{v}_h \right) + \mathcal{A}((\mathbf{u}_h^{n,\ell+1}, p_h^{n,\ell+1}), (\mathbf{v}_h, q_h)) + S_h(p_h^{n,\ell+1}, q_h)$$

$$= \frac{\alpha}{We}(e^{\psi_h^{n,\ell}}, \nabla \mathbf{v}_h),$$

$$\left(\frac{\boldsymbol{\psi}_h^{n,\ell+1} - \boldsymbol{\psi}_h^n \circ \mathbf{X}^n}{\Delta t}, \boldsymbol{\phi}_h \right) + \varepsilon(\nabla \boldsymbol{\psi}_h^{n,\ell+1}, \nabla \boldsymbol{\phi}_h) = (\boldsymbol{\Omega}_h^{n,\ell} \boldsymbol{\psi}_h^{n,\ell} + \boldsymbol{\psi}_h^{n,\ell} \boldsymbol{\Omega}_h^{n,\ell} - 2\mathbf{B}_h^{n,\ell}, \boldsymbol{\phi}_h)$$

$$+ \frac{1}{We}(e^{-\psi_h^{n,\ell}} - \mathbf{I}, \boldsymbol{\phi}_h).$$

4:    **if** $(\|\mathbf{w}^{n,\ell+1} - \mathbf{w}^{n,\ell}\| \le \xi \|\mathbf{w}^{n,\ell}\|$ for $\mathbf{w} \in \{\mathbf{u}, p, e^{\psi}\}$ and ξ is small enough) **then**
5:       break
6:    **end if**
7: **end for**
8: Update solution: $\mathbf{u}^{n+1} = \mathbf{u}^{n,\ell+1}, p^{n+1} = p^{n,\ell+1}, \boldsymbol{\psi}^{n+1} = \boldsymbol{\psi}^{n,\ell+1}$.

2.5 Combined finite difference-finite volume scheme

The aim of this section is to propose another numerical scheme for the logarithm transformation of the diffusive Oldroyd-B model (2.20), the so-called combined finite difference-finite volume (FD-FV) scheme. In the following, we describe more details about the space and time discretization.

We first discretize the domain $\mathcal{T}_h$ by dividing it into $M \times N$ regular rectangular mesh cells. Let $K_{i,j}$, $i = 1, \cdots, M, j = 1, \cdots, N$, denote an arbitrary cell, h_x be the mesh size in x-direction, and analogously h_y be the mesh size in y-direction. Then the so-called staggered approximation is applied for the fluid flow field. It means that the discretization nodes for velocity component U and V are the midpoints of edges in $x-$ or $y-$direction, respectively, where U, V denote the x and y components of the velocity, cf. Figure 2.1. Furthermore, nodes for pressure p and logarithm of the conformation tensor $\boldsymbol{\psi}$ are at the cell centers.
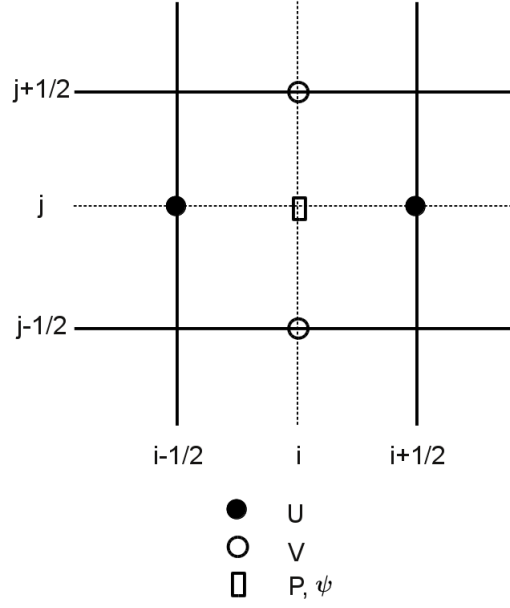
Figure 2.1: Discretization of the staggered mesh.

2.5.1 Discretization scheme

Assume we have the velocity field $\mathbf{u}^n = (U^n, V^n)$, pressure p^n and log-conformation tensor $\boldsymbol{\psi}^n$ at n-th time step t_n. In order to obtain stable results at next time step t_{n+1}, a fully implicit time discretization will be implemented. In the following, we will split our numerical simulation of the system (2.20) in two halves.

In the first part we apply the FV method for the transport equation of the log-transformation of the conformation tensor (2.20c). Specifically, we have

$$
\begin{aligned}
\frac{(\boldsymbol{\psi}^{n+1} - \boldsymbol{\psi}^n)_{i,j}}{\Delta t} = &- \frac{1}{|K_{i,j}|} \sum_{s_k} \mathbf{n}(s_k) \cdot \mathbf{u}^{n+1}(s_k) H(\boldsymbol{\psi}_{i,j}^{n+1}, \boldsymbol{\psi}_{i_k,j_k}^{n+1}) |s_k| + \varepsilon \Delta_h \boldsymbol{\psi}_{i,j}^{n+1} \\
&+ (\boldsymbol{\Omega}^{n+1} \boldsymbol{\psi}^{n+1} - \boldsymbol{\psi}^{n+1} \boldsymbol{\Omega}^{n+1} + 2\mathbf{B}^{n+1})_{i,j} + \frac{1}{We}(e^{-\boldsymbol{\psi}^{n+1}} - \mathbf{I})_{i,j},
\end{aligned}
\tag{2.58}
$$

where Δt is the time step, $|K_{i,j}|$ is the volume of mesh cell $K_{i,j}$, $K_{i_k,j_k}(k = 1, 2, 3, 4)$ are the neighbors of cell $K_{i,j}$, s_k is the interface between the cell $K_{i,j}$ and K_{i_k,j_k}, $|s_k|$ is its length, $\mathbf{n}(s_k)$ and $\mathbf{u}(s_k)$ are the outer normal and velocity of cell $K_{i,j}$ at the interface s_k. $\boldsymbol{\Omega}_{i,j}$ and $\mathbf{B}_{i,j}$ are calculated due to the decomposition of velocity gradient $\nabla_h \mathbf{u}_{i,j}$ described in Section 2.2, see formulas (2.14)–(2.16). The discrete gradient operator for velocity is defined as

$$
\nabla_h \mathbf{u}_{i,j} = \begin{pmatrix} \delta_x U_{i,j} & \delta_y U_{i,j} \\ \delta_x V_{i,j} & \delta_y V_{i,j} \end{pmatrix}.
\tag{2.59a}
$$

where

$$(\delta_x U)_{i,j} := \frac{U_{i+1/2,j} - U_{i-1/2,j}}{h_x}, \quad (\delta_y V)_{i,j} := \frac{V_{i,j+1/2} - V_{i,j-1/2}}{h_y},$$

$$(\delta_y U)_{i,j} := \frac{U_{i+1/2,j+1} + U_{i-1/2,j+1} - U_{i+1/2,j-1} - U_{i-1/2,j-1}}{4h_y}, \quad \text{(2.59b)}$$

$$(\delta_x V)_{i,j} := \frac{V_{i+1,j-1/2} + V_{i+1,j+1/2} - V_{i-1,j-1/2} - V_{i-1,j+1/2}}{4h_x},$$

The discrete Laplace operator for $\boldsymbol{\psi}$ is defined as

$$\Delta_h \boldsymbol{\psi}_{i,j} := \frac{1}{h_x^2}(\boldsymbol{\psi}_{i+1,j} - 2\boldsymbol{\psi}_{i,j} + \boldsymbol{\psi}_{i-1,j}) + \frac{1}{h_y^2}(\boldsymbol{\psi}_{i,j+1} - 2\boldsymbol{\psi}_{i,j} + \boldsymbol{\psi}_{i,j-1}). \quad \text{(2.60)}$$

Moreover, $H(\boldsymbol{\psi}_{i,j}, \boldsymbol{\psi}_{i_k,j_k})$ is the upwind value that is used in the approximation of the integral of the convection term $\int_{K_{i,j}} (\mathbf{u}^{n+1} \cdot \nabla_h \boldsymbol{\psi}^{n+1})_{K_{i,j}}$:

$$H(\boldsymbol{\psi}_{i,j}, \boldsymbol{\psi}_{i_k,j_k}) = \begin{cases} \boldsymbol{\psi}_{i,j} & \text{if } \mathbf{n}(s_k) \cdot \mathbf{u}(s_k) \geq 0, \\ \boldsymbol{\psi}_{i_k,j_k} & \text{if } \mathbf{n}(s_k) \cdot \mathbf{u}(s_k) < 0. \end{cases} \quad \text{(2.61)}$$

In the second part, we apply a suitable FD approximation for the flow equations (2.20a) and (2.20b). The idea of this part follows the lecture notes of Seibold [80]. The convection terms $\mathbf{u} \cdot \nabla \mathbf{u}$ are approximated as $\nabla \cdot (\mathbf{u} \otimes \mathbf{u})$, and the pressure terms are treated implicitly by using the Chorin projection. For more details, the FD approximation reads,

$$Re\frac{(U^{n+1} - U^n)_{i+1/2,j}}{\Delta t} = - Re\delta_x(U^{n+1})^2_{i+1/2,j} - Re\delta_y(U^{n+1}V^{n+1})_{i+1/2,j} - (\delta_x p^{n+1})_{i+1/2,j}$$
$$+ \alpha \Delta_h U^{n+1}_{i+1/2,j} + (\delta_x \sigma_{11}^{n+1})_{i+1/2,j} + (\delta_y \sigma_{12}^{n+1})_{i+1/2,j}, \quad \text{(2.62a)}$$

$$Re\frac{(V^{n+1} - V^n)_{i,j+1/2}}{\Delta t} = - Re\delta_x(U^{n+1}V^{n+1})_{i+1/2,j} - Re\delta_y(V^{n+1})^2_{i+1/2,j} - (\delta_y p^{n+1})_{i,j+1/2}$$
$$+ \alpha \Delta_h V^{n+1}_{i,j+1/2} + (\delta_x \sigma_{21}^{n+1})_{i,j+1/2} + (\delta_y \sigma_{22}^{n+1})_{i,j+1/2}, \quad \text{(2.62b)}$$

$$\nabla_h \cdot \mathbf{u}^{n+1}_{i,j} := \delta_x U^{n+1}_{i,j} + \delta_y V^{n+1}_{i,j} = 0. \quad \text{(2.62c)}$$

Here the discrete difference operators for the convection terms are defined as follows

$$(\delta_x U^2)_{i+1/2,j} := \frac{\left((\bar{U}^h)^2 - \gamma|\bar{U}^h|\widetilde{U}^h\right)_{i+1,j} - \left((\bar{U}^h)^2 - \gamma|\bar{U}^h|\widetilde{U}^h\right)_{i,j}}{h_x},$$

$$(\delta_y (UV))_{i+1/2,j} := \frac{(\bar{U}^v\bar{V}^h - \gamma|\bar{V}^h|\widetilde{U}^v)_{i+1/2,j+1/2} - (\bar{U}^v\bar{V}^h - \gamma|\bar{V}^h|\widetilde{U}^v)_{i+1/2,j-1/2}}{h_y},$$

$$(\delta_x (UV))_{i,j+1/2} := \frac{(\bar{U}^v\bar{V}^h - \gamma|\bar{U}^v|\widetilde{V}^h)_{i+1/2,j+1/2} - (\bar{U}^v\bar{V}^h - \gamma|\bar{U}^v|\widetilde{V}^h)_{i-1/2,j+1/2}}{h_x}, \quad \text{(2.63)}$$

$$(\delta_y V^2)_{i,j+1/2} := \frac{\left((\bar{V}^v)^2 - \gamma|\bar{V}^v|\widetilde{V}^v\right)_{i,j+1} - \left((\bar{V}^v)^2 - \gamma|\bar{V}^v|\widetilde{V}^v\right)_{i,j}}{h_y},$$

where

$$(\bar{U}^h)_{i,j} := \frac{U_{i-1/2,j} + U_{i+1/2,j}}{2}, (\widetilde{U}^h)_{i,j} := \frac{U_{i+1/2,j} - U_{i-1/2,j}}{2},$$

$$(\bar{U}^v)_{i+1/2,j+1/2} := \frac{U_{i+1/2,j} + U_{i+1/2,j+1}}{2}, (\widetilde{U}^v)_{i+1/2,j+1/2} := \frac{U_{i+1/2,j+1} - U_{i+1/2,j}}{2},$$

$$(\bar{V}^h)_{i+1/2,j+1/2} := \frac{V_{i+1,j+1/2} + V_{i,j+1/2}}{2}, (\widetilde{V}^h)_{i+1/2,j+1/2} := \frac{V_{i+1,j+1/2} - V_{i,j+1/2}}{2}, \quad (2.64)$$

$$(\bar{V}^v)_{i,j} := \frac{V_{i,j+1/2} + V_{i,j-1/2}}{2}, (\widetilde{V}^v)_{i,j} := \frac{V_{i,j+1/2} - V_{i,j-1/2}}{2},$$

$$\gamma = \min(1.2\Delta t \cdot \max(\max |U_{i+1/2,j}|, \max |V_{i,j+1/2}|), 1).$$

The approximation of convection terms becomes averaged central difference for $\gamma = 0$, and conservative upwind for $\gamma = 1$.

The Laplace operator Δ_h for the discrete velocity components is given as

$$\Delta_h U_{i+1/2,j} := \delta_x^2 U_{i+1/2,j} + \delta_y^2 U_{i+1/2,j}, \qquad \Delta_h V_{i,j+1/2} := \delta_x^2 V_{i,j+1/2} + \delta_y^2 V_{i,j+1/2}, \quad (2.65)$$

where

$$\delta_x^2 U_{i+1/2,j} := \frac{U_{i-1/2,j} - 2U_{i+1/2,j} + U_{i+3/2,j}}{h_x^2}, \delta_x^2 V_{i,j+1/2} := \frac{V_{i+1,j+1/2} - 2V_{i,j+1/2} + V_{i-1,j+1/2}}{h_x^2},$$

$$\delta_y^2 U_{i+1/2,j} := \frac{U_{i+1/2,j+1} - 2U_{i+1/2,j} + U_{i+1/2,j-1}}{h_y^2}, \delta_y^2 V_{i,j+1/2} := \frac{V_{i,j-1/2} - 2V_{i,j+1/2} + V_{i,j+3/2}}{h_y^2}.$$
$$(2.66)$$

The discrete difference operators for the conformation tensor components are defined as follows

$$\delta_x(\sigma_{11})_{i+1/2,j} := \frac{(\sigma_{11})_{i+1,j} - (\sigma_{11})_{i,j}}{h_x}, \quad \delta_y(\sigma_{22})_{i,j+1/2} := \frac{(\sigma_{22})_{i,j+1} - (\sigma_{22})_{i,j}}{h_y},$$

$$\delta_y(\sigma_{12})_{i+1/2,j} := \frac{(\sigma_{12})_{i+1,j+1} + (\sigma_{12})_{i,j+1} - (\sigma_{12})_{i+1,j-1} - (\sigma_{12})_{i,j-1}}{4h_y}, \quad (2.67)$$

$$\delta_x(\sigma_{21})_{i,j+1/2} := \frac{(\sigma_{21})_{i+1,j} + (\sigma_{21})_{i+1,j+1} - (\sigma_{21})_{i-1,j} - (\sigma_{21})_{i-1,j+1}}{4h_x}.$$

The discrete difference operators for the pressure terms are defined as

$$\delta_x p_{i+1/2,j} := \frac{p_{i+1,j} - p_{i,j}}{h_x}, \ \delta_y p_{i,j+1/2} := \frac{p_{i,j+1} - p_{i,j}}{h_y}. \quad (2.68)$$

In order to solve the nonlinear system of (2.58) and (2.62) implicitly, we use the fix point iteration approach. Let ℓ represent the iteration step and $\mathbf{u}^{n,\ell}, p^{n,\ell}, \boldsymbol{\psi}^{n,\ell}$ be the solution of the ℓ-th iteration. Starting from $\ell = 0$, we get the solution of next iteration step $\ell + 1$ in the following way:

Step1: Viscoelastic part

We first approximate the viscoelastic part (2.58) in the following steps:

a) Decompose the velocity gradient $\nabla_h \mathbf{u}_{i,j}^{n,\ell}$ to obtain $\mathbf{\Omega}_{i,j}^{n,\ell}$ and $\mathbf{B}_{i,j}^{n,\ell}$ according to (2.14)–(2.16) in Section 2.2.

b) Approximate equation (2.58) in an explicit manner

$$
\begin{aligned}
\boldsymbol{\psi}_{i,j}^{n,\ell+1} - \varepsilon \Delta t \Delta_h \boldsymbol{\psi}_{i,j}^{n,\ell+1} =&\ \boldsymbol{\psi}_{i,j}^n - \frac{\Delta t}{|K_{i,j}|} \sum_{s_k} \mathbf{n}(s_k) \cdot \mathbf{u}(s_k) H(\boldsymbol{\psi}_{i,j}^{n,\ell}, \boldsymbol{\psi}_{i_k,j_k}^{n,\ell}) |s_k| \\
&+ \Delta t (\mathbf{\Omega}_{i,j}^{n,\ell} \boldsymbol{\psi}_{i,j}^{n,\ell} - \boldsymbol{\psi}_{i,j}^{n,\ell} \mathbf{\Omega}_{i,j}^{n,\ell} + 2\mathbf{B}_{i,j}^{n,\ell}) + \frac{\Delta t}{We}(e^{-\boldsymbol{\psi}_{i,j}^{n,\ell}} - \mathbf{I}),
\end{aligned}
\tag{2.69}
$$

c) Update the conformation tensor

$$
\boldsymbol{\sigma}_{i,j}^{n,\ell+1} = e^{\boldsymbol{\psi}_{i,j}^{n,\ell+1}}.
\tag{2.70}
$$

Step2: Navier-Stokes part

Approximation of the fluid part (2.62) is realized by the Chorin projection method in two steps.

a) We first neglect the influence of pressure and solve the following part

$$
\mathbf{u}_t - \alpha \Delta \mathbf{u} = -\mathbf{u} \cdot \nabla \mathbf{u} + \nabla \cdot \boldsymbol{\sigma}.
$$

More precisely, it reads

$$
\begin{aligned}
\left(\frac{1}{\Delta t} - \alpha \Delta_h\right) U_{i+1/2,j}^* =&\ \frac{1}{\Delta t} U_{i+1/2,j}^n - \delta_x(U^{n,\ell})_{i+1/2,j}^2 - \delta_y(U^{n,\ell} V^{n,\ell})_{i+1/2,j} \\
&+ \frac{1-\alpha}{We}\Big(\delta_x(\sigma_{11}^{n,\ell+1})_{i+1/2,j} + \delta_y(\sigma_{12}^{n,\ell+1})_{i+1/2,j}\Big), \\
\left(\frac{1}{\Delta t} - \alpha \Delta_h\right) V_{i,j+1/2}^* =&\ \frac{1}{\Delta t} V_{i,j+1/2}^n - \delta_x(U^{n,\ell} V^{n,\ell})_{i,j+1/2} - \delta_y(V^{n,\ell})_{i,j+1/2}^2 \\
&+ \frac{1-\alpha}{We}\Big(\delta_x(\sigma_{21}^{n,\ell+1})_{i,j+1/2} + \delta_y(\sigma_{22}^{n,\ell+1})_{i,j+1/2}\Big).
\end{aligned}
\tag{2.71}
$$

b) In the next step we need to approximate the pressure terms $\mathbf{u}_t = \nabla p$, i.e.,

$$
\frac{U_{i+1/2,j}^{n,\ell+1} - U_{i+1/2,j}^*}{\Delta t} = -\delta_x p_{i+1/2,j}^{n,\ell+1}, \quad \frac{V_{i,j+1/2}^{n,\ell+1} - V_{i,j+1/2}^*}{\Delta t} = -\delta_y p_{i,j+1/2}^{n,\ell+1}.
\tag{2.72}
$$

This is realized by the following pressure projection step:

b_1) Compute $F_{i,j} = \nabla_h \cdot \mathbf{u}_{i,j}^*$.

b_2) Solve Poisson equation $-\Delta_h p_{i,j}^{n,\ell+1} = -\frac{1}{\Delta t} F_{i,j}$ to get $p_{i,j}^{n,\ell+1}$.

b_3) Update velocity field $\mathbf{u}_{i,j}^{n,\ell+1} = \mathbf{u}_{i,j}^* - \Delta t \nabla_h p_{i,j}^{n,\ell+1}$, which is divided in two parts:
$U_{i+1/2,j}^{n,\ell+1} = U_{i+1/2,j}^* - \Delta t \delta_x p_{i+1/2,j}^{n,\ell+1}$, and $V_{i,j+1/2}^{n,\ell+1} = V_{i,j+1/2}^* - \Delta t \delta_y p_{i,j+1/2}^{n,\ell+1}$.

Here, the discrete difference operators are defined as follows

$$\nabla_h \cdot \mathbf{u}_{i,j} := \delta_x U_{i,j} + \delta_y V_{i,j}, \Delta_h p_{i,j} := \delta_x^2 p_{i,j} + \delta_y^2 p_{i,j},$$
$$\delta_x^2 p_{i,j} := \frac{p_{i-1,j} - 2p_{i,j} + p_{i+1,j}}{h_x^2}, \delta_y^2 p_{i,j} := \frac{p_{i,j-1} - 2p_{i,j} + p_{i,j+1}}{h_y^2}, \tag{2.73}$$

where $\delta_x U_{i,j}$ and $\delta_y V_{i,j}$ are computed using (2.59).
The incompressibility condition (2.20b) is naturally satisfied. Indeed, we have

$$\nabla_h \cdot \mathbf{u}_{i,j}^{n,\ell+1} = \nabla_h \cdot \mathbf{u}_{i,j}^* - \Delta t \nabla_h \cdot (\nabla_h P_{i,j}^{n,\ell+1}) = F_{i,j} - \Delta t \Delta_h P_{i,j}^{n,\ell+1} = 0.$$

Finally, we state the algorithm for the combined scheme (2.58) and (2.62) as:

Algorithm 3 Combined FD-FV scheme

1: Given $\mathbf{u}^n, p^n, \boldsymbol{\psi}^n$, set $\mathbf{u}^{n,0} = \mathbf{u}^n, \boldsymbol{\psi}^{n,0} = \boldsymbol{\psi}^n, p^{n,0} = p^n$.
2: **for** $\ell = 0, 1, \cdots$ **do**
3:     solve the viscoelastic equation (2.69)
4:     update the conformation tensor with equation (2.70)
5:     solve the Navier-Stokes part (2.71) and (2.72)
6:     **if** $(\|\mathbf{v}^{n,\ell+1} - \mathbf{v}^{n,\ell}\| \leq \xi \|\mathbf{v}^{n,\ell}\|$ for $\mathbf{v} \in \{\mathbf{u}, p, \boldsymbol{\sigma}(= e^\psi)\}$ and ξ is small enough) **then**
7:        break
8:     **end if**
9: **end for**
10: Update solution: $\mathbf{u}^{n+1} = \mathbf{u}^{n,\ell+1}, p^{n+1} = p^{n,\ell+1}, \boldsymbol{\psi}^{n+1} = \boldsymbol{\psi}^{n,\ell+1}$.

2.6 Characteristic finite-difference method

In the next chapter we want to investigate the nonlinear stability of the numerical schemes. Although we will be able to show that the discrete entropy is decreasing in time for the characteristic FEM schemes, it was not possible to show the same entropy stability result for the combined FD-FV method. The reason is that in the combined FD-FV method we cannot control the sign of the convective terms. However in the characteristic method we can assume that due to conservatism

$$\int_{\mathcal{T}_h} \psi_h^n = \int_{\mathcal{T}_h} \psi_h^n \circ \mathbf{X}^n(t_n), \tag{2.74}$$

for ψ to be the elastic stress tensor, similarly to that in [18]. Thus we have decided to apply characteristic FD method to the Oldroyd-B model (2.20). The characteristic FD method is similar to the combined FD-FV method. The only difference is that the time derivative and the convective terms in the evolution equation of the stress tensor are

realized by the characteristic approach. More precisely, we have instead of (2.58)

$$\frac{(\boldsymbol{\psi}^{n+1} - \boldsymbol{\psi}^n \circ \mathbf{X}^n)_{i,j}}{\Delta t} = (\boldsymbol{\Omega}^{n+1}\boldsymbol{\psi}^{n+1} - \boldsymbol{\psi}^{n+1}\boldsymbol{\Omega}^{n+1} + 2\mathbf{B}^{n+1})_{i,j} \\ + \frac{1}{We}(e^{-\boldsymbol{\psi}_{i,j}^{n+1}} - \mathbf{I}) + \varepsilon\Delta_h\boldsymbol{\psi}_{i,j}^{n+1}. \tag{2.75}$$

Analogously, we replace (2.69), which is the fix point iteration of (2.58), by

$$\boldsymbol{\psi}_{i,j}^{n,\ell+1} - \varepsilon\Delta t\Delta_h\boldsymbol{\psi}_{i,j}^{n,\ell+1} = \boldsymbol{\psi}_{i,j}^n \circ \mathbf{X}^n + \Delta t(\boldsymbol{\Omega}_{i,j}^{n,\ell}\boldsymbol{\psi}_{i,j}^{n,\ell} - \boldsymbol{\psi}_{i,j}^{n,\ell}\boldsymbol{\Omega}_{i,j}^{n,\ell} + 2\mathbf{B}_{i,j}^{n,\ell}) \\ + \frac{\Delta t}{We}(e^{-\boldsymbol{\psi}_{i,j}^{n,\ell}} - \mathbf{I}). \tag{2.76}$$

In what follows we introduce the algorithm about how to evaluate the old time step value $\boldsymbol{\psi}_{i,j}^n \circ \mathbf{X}^n$ for the particle which is currently located at i,j-th cell center. The current position of the particle is

$$\mathbf{x}(i,j) = (x_i, y_j) = \Big((i - 1/2)h_x, \ (j - 1/2)h_y\Big). \tag{2.77}$$

Now we approximate the position of the particle at the previous time step according to the trajectory (2.56)

$$\mathbf{x}'(i,j) = (x_{i'}, y_{j'}) = \Big(x_i - (\bar{U}^h)_{i,j}^n\Delta t, \ y_j - (\bar{V}^v)_{i,j}^n\Delta t\Big), \tag{2.78}$$

where $\bar{U}_{i,j}^h$ and $\bar{V}_{i,j}^v$ are computed using (2.64).

Let $i' = x'/h_x + 0.5$, $j' = y'/h_y + 0.5$ and $i_L = \lfloor i' \rfloor$, $i_R = i_L + 1$, $j_L = \lfloor j' \rfloor$, $j_R = j_L + 1$, where $\lfloor x \rfloor$ returns the largest integer not greater than x. Suppose that $\mathbf{x}'$ is surrounded by the points $\{P_k, k = 1, 2, 3, 4\}$ (see Figure 2.2), where

$$\mathbf{x}(P_k) = \mathbf{x}(i_{P_k}, j_{P_k}). \tag{2.79}$$

It is obvious that $i_{P_1} = i_{P_3} = i_L$, $i_{P_2} = i_{P_4} = i_R$, $j_{P_1} = j_{P_2} = j_L$, $j_{P_3} = j_{P_4} = j_R$. We approximate the old time step value at old position $\mathbf{x}' = (x_{i'}, y_{j'})$ in the following way:

$$\boldsymbol{\psi}_{i,j}^n \circ \mathbf{X}^n = \sum_{k=1}^{4} w_k\boldsymbol{\psi}^n(P_k) \tag{2.80}$$

where $w_k = (1 - i_{P_k} + i')(1 - j_{P_k} + j')$ represents the weight of $k - th$ point, see Figure 2.2.
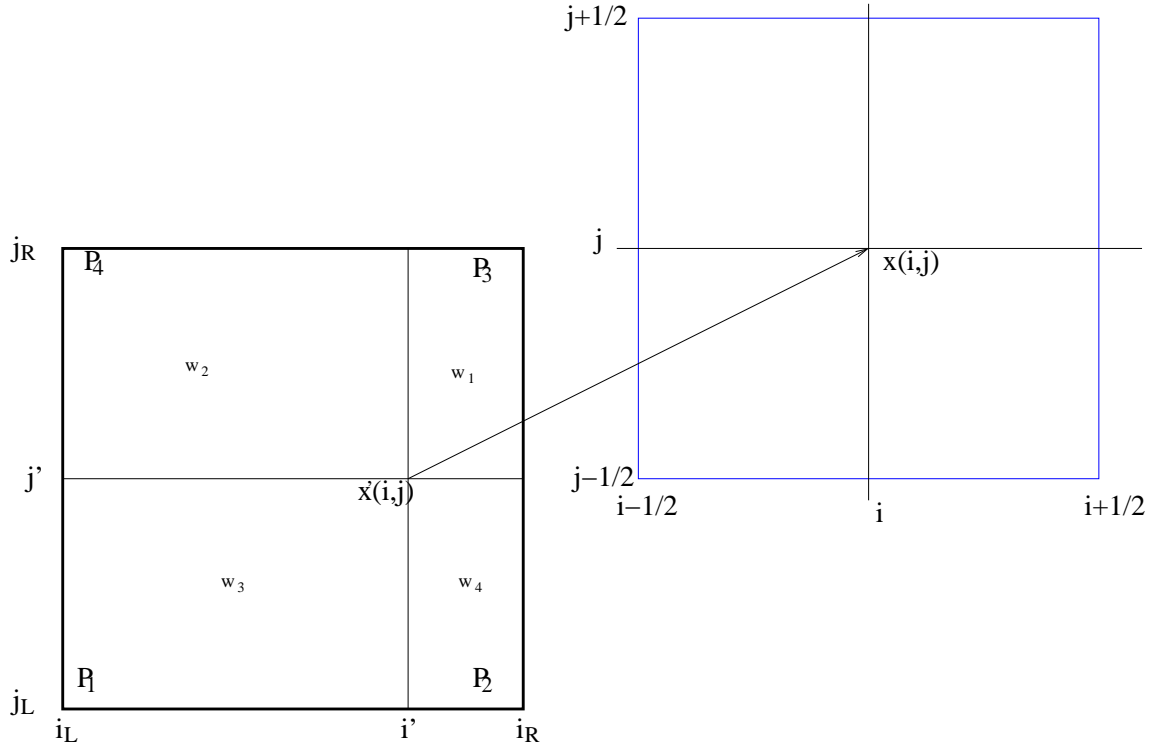
Figure 2.2: Characteristic position.

We conclude the implicit discretization of the characteristic FD method as a combination of (2.62) and (2.75). Further, we state the characteristic FD scheme as:

Algorithm 4 Characteristic FD scheme

1: Given $\mathbf{u}^n, p^n, \boldsymbol{\psi}^n$, set $\mathbf{u}^{n,0} = \mathbf{u}^n, \boldsymbol{\psi}^{n,0} = \boldsymbol{\psi}^n, p^{n,0} = p^n$.
2: **for** $\ell = 0, 1, \cdots$ **do**
3:    solve the viscoelastic equation (2.76)
4:    update the conformation tensor with equation (2.70)
5:    solve the Navier-Stokes part (2.71) and (2.72)
6:    **if** $(\|\mathbf{v}^{n,\ell+1} - \mathbf{v}^{n,\ell}\| \le \xi \|\mathbf{v}^{n,\ell}\|$ for $\mathbf{v} \in \{\mathbf{u}, p, \boldsymbol{\sigma}\}$ and ξ is small enough) **then**
7:       break
8:    **end if**
9: **end for**
10: Update solution: $\mathbf{u}^{n+1} = \mathbf{u}^{n,\ell+1}, p^{n+1} = p^{n,\ell+1}, \boldsymbol{\psi}^{n+1} = \boldsymbol{\psi}^{n,\ell+1}$.

---

3 Stability analysis of the numerical schemes for the Oldroyd-B type fluids

In this chapter, we first study the stability of the diffusive Oldroyd-B type fluids (2.11) using the linear stability analysis model. According to our simulations, we found that employing diffusive model for the transport equation of the conformation tensor helps to obtain stable results. Furthermore, we have investigated nonlinear stability by applying the energy dissipative method and have demonstrated how to control discrete entropy of our characteristic FEM. The energy stability has been studied by Boyaval et al. [18, 17] for the Oldroyd-B model(2.10), and the log-transformation of the Oldroyd-B model (2.19). Herein, we have incorporated the results to the relative diffusive models (2.11), (2.20). Finally, we study the entropy stability of the characteristic FD scheme for the system (2.20).

3.1 Global linear stability

In the research of the stability analysis for ODEs, the linear stability approach plays an important role. The main idea is to linearise the problem at a stationary point. The solution to the linearised system is just a perturbation of this stationary solution. Then the stability of the stationary state is reduced to the question: if the perturbed solution will decrease or increase in time, which is controlled by the eigenvalues of the corresponding linear system cf., e.g., [82].

3.1.1 Arnoldi algorithm

In this subsection we will give an introduction to the approximation of the eigenvalues of the matrix A for a linear system of ordinary differential equations

$$\frac{\partial \mathbf{v}}{\partial t} = A\mathbf{v}, \mathbf{v}(0) = \mathbf{v}_0. \tag{3.1}$$

The solution to the linear problem (3.1) at time T is

$$\mathbf{v}(T) = B\mathbf{v}(0),$$

where $B = e^{AT}$ [77].

Let λ^A, λ^B and $\boldsymbol{\phi}^A, \boldsymbol{\phi}^B$ be the eigenvalues and corresponding eigenvector of matrix A

and B, respectively, i.e.

$$A\phi^A = \lambda^A \phi^A, \ B\phi^B = \lambda^B \phi^B.$$

Then we have

$$B\phi^A = \exp(AT)\phi^A = \sum_{n=0}^{\infty} \frac{(AT)^n}{n!}\phi^A = \sum_{n=0}^{\infty} \frac{(\lambda^A T)^n}{n!}\phi^A = \exp(\lambda^A T)\phi^A.$$

This indicates that the eigenvector of A is also the eigenvector of B, and the relationship between eigenvalues is

$$\lambda^B = \exp(\lambda^A T),$$

which can also be written as

$$\lambda^A = \{\log |\lambda^B| + i \arg \lambda^B\}/T.$$

The approximate eigensystem of B can be expressed by a Krylov subspace $\kappa_M = \{\zeta_1, \zeta_2, \cdots, \zeta_M\}$, where $\{\zeta_i, i = 1, \cdots M\}$ is the orthogonal basis vector of the subspace κ_M.

Given a random initial vector ζ we normalize it to get $\zeta_1 = \zeta/\|\zeta\|_2$. Substituting ζ_1 into the linear system (3.1) as the initial value, we derive the solution at time T: $\mathbf{v}(T) = B\zeta_1$. Then $B\zeta_1$ can be decomposed as the linear combination of ζ_1 and ζ_2

$$B\zeta_1 = h_{1,1}\zeta_1 + h_{2,1}\zeta_2,$$

where $h_{1,1} = B\zeta_1 \cdot \zeta_1$, $h_{2,1} = \|B\zeta_1 - h_{1,1}\zeta_1\|_2$, and $\zeta_2 = (B\zeta_1 - h_{1,1}\zeta_1)/h_{2,1}$ is perpendicular to ζ_1.

Similarly, given $\zeta_1, \cdots, \zeta_i$, we could get $h_{j,i}, j = 1, \cdots i+1$ and ζ_{i+1} in the following steps: solve the linear system and get $B\zeta_i$. Decompose it as $B\zeta_i = \sum_{j=1}^{i} h_{j,i}\zeta_j + h_{i+1,i}\zeta_{i+1}$ with $h_{j,i} = B\zeta_i \cdot \zeta_j$. Let $r = B\zeta_i - \sum_{j=1}^{i} h_{j,i}\zeta_j$, then we have $h_{i+1,i} = \|r\|_2$ and $\zeta_{i+1} = r/h_{i+1,i}$. We should point out that $\|\zeta_j, j = 1, \cdots, M+1\| = 1$.

Repeat until $i = M$. In the case that M is large index and $h_{M+1,M}$ is small, we obtain

$$B\zeta_i = \sum_{j=1}^{M} h_{j,M}\zeta_j + h_{M+1,M}\zeta_{M+1} \cong \sum_{j=1}^{M} h_{j,M}\zeta_j.$$

Altogether, we have

$$B\left[\zeta_1, \cdots, \zeta_M\right] = \left[\zeta_1, \cdots, \zeta_M\right] H,$$

where

$$H = \begin{bmatrix} h_{1,1} & h_{1,2} & \cdots & h_{1,M} \\ h_{2,1} & h_{2,2} & & h_{2,M} \\ & \ddots & \ddots & \vdots \\ & & h_{M,M-1} & h_{M,M} \end{bmatrix}.$$

Let λ^H and ϕ^H be the eigenvalue and eigenvector of H, i.e., $H\phi^H = \lambda^H \phi^H$, we obtain

$$B\left[\zeta_1, \cdots, \zeta_M\right]\phi^H = \left[\zeta_1, \cdots, \zeta_M\right] H\phi^H = \left[\zeta_1, \cdots, \zeta_M\right]\lambda^H \phi^H = \lambda^H \left[\zeta_1, \cdots, \zeta_M\right]\phi^H.$$

Thus the relationship of eigenvalue and eigenvector between the matrix H and B is

$$\lambda^B = \lambda^H, \boldsymbol{\phi}^B = [\zeta_1, \cdots, \zeta_M] \, \boldsymbol{\phi}^H.$$

Now the eigenvalue problem of the linear system is reduced to solve the eigenvalue of upper Hessenberg matrix H. The eigenvalues and eigenvectors of H can be found by some standard algorithm, e.g. QR algorithm.

The real part of λ^A is important in order to study the global stability of the linear system. $Re(\lambda^A) > 0$ indicates that $|\mathbf{v}|$ increases in time, the perturbation is amplified. On the other hand, if $Re(\lambda^A) < 0$, the perturbed solution will decrease to zero. Thus the flow will approach the stable steady state. Consequently, we can use such algorithm to analyze the stability of linear ODE.

3.1.2 Linearised Oldroyd-B model

Let $\mathbf{v} = (\mathbf{u}, p, \boldsymbol{\sigma})$ be a solution of the Oldroyd-B model (2.11). Further let $\bar{\mathbf{v}} = (\bar{\mathbf{u}}, \bar{p}, \bar{\boldsymbol{\sigma}})$ be a steady state. Assume that $\mathbf{u} = \bar{\mathbf{u}} + \tilde{\mathbf{u}}, p = \bar{p} + \tilde{p}, \boldsymbol{\sigma} = \bar{\boldsymbol{\sigma}} + \tilde{\boldsymbol{\sigma}}$, where $\tilde{\mathbf{v}} = (\tilde{\mathbf{u}}, \tilde{p}, \tilde{\boldsymbol{\sigma}})$ is a small perturbation.
The steady state should satisfy the governing equations,

$$\begin{cases} Re(\frac{\partial \bar{\mathbf{u}}}{\partial t} + \bar{\mathbf{u}} \cdot \nabla \bar{\mathbf{u}}) = -\Delta \bar{p} + \alpha \Delta \bar{\mathbf{u}} + \frac{\beta}{We} \nabla \cdot (\bar{\boldsymbol{\sigma}} - \mathbf{I}) \\ \nabla \cdot \bar{\mathbf{u}} = 0 \\ \frac{\partial \bar{\boldsymbol{\sigma}}}{\partial t} + (\bar{\mathbf{u}} \cdot \nabla)\bar{\boldsymbol{\sigma}} - \nabla \bar{\mathbf{u}} \cdot \bar{\boldsymbol{\sigma}} - \bar{\boldsymbol{\sigma}} \cdot (\nabla \bar{\mathbf{u}})^T = \frac{1}{We}(\mathbf{I} - \bar{\boldsymbol{\sigma}}) + \varepsilon \Delta \bar{\boldsymbol{\sigma}} \end{cases} \quad (3.2)$$

Subtracting equation (3.2) from equation (2.11) we get the linearised system for the perturbations $\tilde{\mathbf{u}}, \tilde{p}, \tilde{\boldsymbol{\sigma}}$,

$$\begin{cases} Re(\frac{\partial \tilde{\mathbf{u}}}{\partial t} + \bar{\mathbf{u}} \cdot \nabla \tilde{\mathbf{u}}) = -\Delta \tilde{p} + \alpha \Delta \tilde{\mathbf{u}} + \frac{\beta}{We} \nabla \cdot \tilde{\boldsymbol{\sigma}} - (\tilde{\mathbf{u}} \cdot \nabla)\bar{\mathbf{u}} \\ \nabla \cdot \tilde{\mathbf{u}} = 0 \\ \frac{\partial \tilde{\boldsymbol{\sigma}}}{\partial t} + (\bar{\mathbf{u}} \cdot \nabla)\tilde{\boldsymbol{\sigma}} + (\tilde{\mathbf{u}} \cdot \nabla)\bar{\boldsymbol{\sigma}} = \nabla \bar{\mathbf{u}}\tilde{\boldsymbol{\sigma}} + \tilde{\boldsymbol{\sigma}}\nabla \bar{\mathbf{u}} + \nabla \tilde{\mathbf{u}}\bar{\boldsymbol{\sigma}} + \bar{\boldsymbol{\sigma}}\nabla \tilde{\mathbf{u}} - \frac{1}{We}\tilde{\boldsymbol{\sigma}} + \varepsilon \tilde{\boldsymbol{\sigma}} \end{cases} \quad (3.3)$$

Numerically we solve this system with the characteristic finite element method described in Section 2.4. The Algorithm 1 is applied by changing the original Oldroyd-B model with the perturbation equations (3.3). Further, the explicit time discretization is implemented by constraining the iteration step $\ell = 0$. In order to study the global linear stability, we calculate the eigenvalue of matrix A with the Arnoldi algorithm described in the Section 3.1.1.

3.1.3 Test

We consider the plane Couette flow. The stationary state for the Couette flow reads,

$$\bar{\mathbf{u}} = \begin{pmatrix} y \\ 0 \end{pmatrix}, \bar{\boldsymbol{\sigma}} = \begin{pmatrix} 1 + 2We^2 & We \\ We & 1 \end{pmatrix}.$$

In the test we set $M = 100$, $M \times M$ is the size of matrix H, and $T = 1$. We compared largest eigenvalues for different diffusive coefficients and for different meshes size h. From

Table 3.1 we observe stability when ε is of h^i, $i = 0, 1$, where ε is the diffusion coefficient, and h is the mesh size. When ε decrease to h^2, we can notice that we lose the stability again. Our results indicates that the Oldroyd-B model gets linearly unstable for very small diffusion coefficient in the transport equation for the elastic stress tensor.

1/h We	8	16	32	64	128	256
$\varepsilon = 0$						
0.5	-0.238922	-0.199503	-0.0294619	0.240331	0.355994	0.70052
1	0.0259079	0.14204	0.440585	0.743758	0.941699	1.35596
$\varepsilon = h^0$						
0.5	-0.53498	-0.587195	-0.619283	-0.636759	-0.645558	-0.650033
1	-0.126213	-0.137673	-0.147381	-0.151533	-0.154073	-0.155247
$\varepsilon = h^1$						
0.5	-0.57535	-0.614261	-0.664393	-0.704338	-0.730504	-0.75039
1	-0.204993	-0.262254	-0.322263	-0.350343	-0.377132	-0.321198
$\varepsilon = h^2$						
0.5	-0.594292	-0.426336	-0.211495	-0.109401	-0.0308632	0.262292
1	-0.288596	-0.193508	0.0688591	0.376316	0.465567	0.83494

Table 3.1: Largest real part of the eigenvalues for different diffusion coefficients.

3.2 Entropy stability for the characteristic FEM

In this section, we will show that our characteristic FEM schemes for diffusive Oldroyd-B models are energy dissipative.

3.2.1 Entropy stable characteristic FEM for the diffusive Oldroyd-B model

In this subsection, we will study the energy stability of the characteristic FEM for the diffusive Oldroyd-B model (2.11).

Lemma 3.2.1. *Let $(\mathbf{u}_h^n, p_h^n, \boldsymbol{\sigma}_h^n)_{0 \leq n \leq N_T}$ be a solution to (2.55), supplied with homogeneous Dirichlet boundary condition for velocity, and zero Neumann boundary condition for $\boldsymbol{\sigma}$. Further, we assume that $\boldsymbol{\sigma}_h$ is initially symmetric positive-definite. Then the free energy of the system (2.55)*

$$F_h^n = F(\mathbf{u}_h^n, \boldsymbol{\sigma}_h^n) = \frac{Re}{2} \int_\Omega |\mathbf{u}_h^n|^2 + \frac{\beta}{2We} \int_\Omega tr(\boldsymbol{\sigma}_h^n - \ln(\boldsymbol{\sigma}_h^n) - \mathbf{I}) \qquad (3.4)$$

satisfies

$$F_h^{n+1} - F_h^n + \int_\Omega \frac{Re}{2} |u_h^{n+1} - u_h^n|^2 + \Delta t \int_\Omega 2\alpha C_k |\nabla \mathbf{u}_h^{n+1}|^2 + \frac{\beta}{2We^2} tr(\boldsymbol{\sigma}_h^n + (\boldsymbol{\sigma}_h^n)^{-1} - \mathbf{I}) \leq 0. \qquad (3.5)$$

In particular, the sequence $(F_h^n)_{0 \leq n \leq N_T}$ is non-increasing.

Proof. We choose $\left(\mathbf{u}_h^{n+1}, -p_h^{n+1}, \frac{\beta}{2We}(\mathbf{I} - (\boldsymbol{\sigma}_h^{n+1})^{-1})\right)$ as a test function for the system (2.55), and get

$$
\begin{aligned}
0 = \int_\Omega &\left(Re\frac{\mathbf{u}_h^{n+1} - \mathbf{u}_h^n \circ X^n(t^n)}{\Delta t} \cdot \mathbf{u}_h^{n+1} + 2\alpha D(\mathbf{u}_h^{n+1}) : D(\mathbf{u}_h^{n+1}) + \frac{\beta}{We}\boldsymbol{\sigma}_h^{n+1} : \nabla\mathbf{u}_h^{n+1}\right) \\
&+ \delta \sum_{K \in \mathcal{T}_h} h_K^2 (\nabla p_h^{n+1})^2 + \frac{\beta}{2We}\int_\Omega \left(\frac{\boldsymbol{\sigma}_h^{n+1} - \boldsymbol{\sigma}_h^n \circ X^n(t^n)}{\Delta t} : (\mathbf{I} - (\boldsymbol{\sigma}_h^{n+1})^{-1}) \right. \\
&- (\nabla\mathbf{u}_h^{n+1}\boldsymbol{\sigma}_h^{n+1} + \boldsymbol{\sigma}_h^{n+1}(\nabla\mathbf{u}_h^{n+1})^T) : (\mathbf{I} - (\boldsymbol{\sigma}_h^{n+1})^{-1}) - \frac{1}{We}(\mathbf{I} - \boldsymbol{\sigma}_h^{n+1}) : (\mathbf{I} - (\boldsymbol{\sigma}_h^{n+1})^{-1}) \\
&\left. + \varepsilon\nabla\boldsymbol{\sigma}_h^{n+1} : \nabla(\mathbf{I} - (\boldsymbol{\sigma}_h^{n+1})^{-1})\right).
\end{aligned}
$$

It should be noted that due to conservatism we have assumed that [18]

$$
\int_\Omega \mathbf{u}_h^n \circ X^n(t^n) = \int_\Omega \mathbf{u}_h^n, \tag{3.6}
$$

which also holds for conformation tensor $\boldsymbol{\sigma}_h$ and its logarithm $\boldsymbol{\psi}_h$.

For the approximation of material derivative we have

$$
\begin{aligned}
\int_\Omega (\mathbf{u}_h^{n+1} - \mathbf{u}_h^n \circ X^n(t^n)) \cdot \mathbf{u}_h^{n+1} &= \int_\Omega \frac{|\mathbf{u}_h^{n+1}|^2 - |\mathbf{u}_h^n \circ X^n(t^n)|^2}{2} + \frac{(\mathbf{u}_h^{n+1} - \mathbf{u}_h^n \circ X^n(t^n))^2}{2} \\
&= \int_\Omega \frac{|\mathbf{u}_h^{n+1}|^2 - |\mathbf{u}_h^n|^2}{2} + \frac{1}{2}(\mathbf{u}_h^{n+1} - \mathbf{u}_h^n \circ X^n(t^n))^2 \geq \int_\Omega \frac{|\mathbf{u}_h^{n+1}|^2 - |\mathbf{u}_h^n|^2}{2}.
\end{aligned}
$$

Using the Korn inequality, we have

$$
\int_\Omega D(\mathbf{u}_h^{n+1}) : D(\mathbf{u}_h^{n+1}) \geq C_k \int_\Omega |\nabla\mathbf{u}_h^{n+1}|^2.
$$

Now let us go to the conformation tensor part.

$$
\begin{aligned}
\int_\Omega (\boldsymbol{\sigma}_h^{n+1} &- \boldsymbol{\sigma}_h^n \circ X^n(t^n)) : (\mathbf{I} - (\boldsymbol{\sigma}_h^{n+1})^{-1}) \\
&= \int_\Omega \text{tr}(\boldsymbol{\sigma}_h^{n+1} - \boldsymbol{\sigma}_h^n \circ X^n(t^n)) + (\boldsymbol{\sigma}_h^n \circ X^n(t^n) - \boldsymbol{\sigma}_h^{n+1}) : (\boldsymbol{\sigma}_h^{n+1})^{-1}.
\end{aligned}
$$

Using (2.35f) for $\boldsymbol{\sigma}_h^n \circ X^n(t^n)$ and $\boldsymbol{\sigma}_h^{n+1}$ we obtain

$$
\int_\Omega (\boldsymbol{\sigma}_h^n \circ X^n(t^n) - \boldsymbol{\sigma}_h^{n+1}) : (\boldsymbol{\sigma}_h^{n+1})^{-1} \geq \int_\Omega \text{tr}(\ln\boldsymbol{\sigma}_h^n \circ X^n(t^n) - \ln\boldsymbol{\sigma}_h^{n+1}).
$$

Thus we have

$$\int_\Omega (\boldsymbol{\sigma}_h^{n+1} - \boldsymbol{\sigma}_h^n \circ X^n(t^n)) : (\mathbf{I} - (\boldsymbol{\sigma}_h^{n+1})^{-1})$$

$$\geq \int_\Omega \mathrm{tr}(\boldsymbol{\sigma}_h^{n+1} - \boldsymbol{\sigma}_h^n \circ X^n(t^n)) + \mathrm{tr}(\ln \boldsymbol{\sigma}_h^n \circ X^n(t^n) - \ln \boldsymbol{\sigma}_h^{n+1})$$

$$= \int_\Omega \mathrm{tr}(\boldsymbol{\sigma}_h^{n+1} - \ln \boldsymbol{\sigma}_h^{n+1}) - \mathrm{tr}(\boldsymbol{\sigma}_h^n - \ln \boldsymbol{\sigma}_h^n),$$

where we have used the fact that $\int_\Omega \mathrm{tr}(\boldsymbol{\sigma}_h^n - \boldsymbol{\sigma}_h^n) \circ X^n(t^n) = \int_\Omega \mathrm{tr}(\boldsymbol{\sigma}_h^n - \ln \boldsymbol{\sigma}_h^n)$, cf.(3.6). Let us note that

$$(\nabla \mathbf{u}_h^{n+1} \boldsymbol{\sigma}_h^{n+1} + \boldsymbol{\sigma}_h^{n+1}(\nabla \mathbf{u}_h^{n+1})^T) : (\mathbf{I} - (\boldsymbol{\sigma}_h^{n+1})^{-1}) = 2 \int_\Omega \nabla \mathbf{u}_h^{n+1} : \boldsymbol{\sigma}_h^{n+1},$$

and

$$(\mathbf{I} - \boldsymbol{\sigma}_h^{n+1}) : (\mathbf{I} - (\boldsymbol{\sigma}_h^{n+1})^{-1}) = \mathrm{tr}(2\mathbf{I} - (\boldsymbol{\sigma}_h^{n+1})^{-1} - \boldsymbol{\sigma}_h^{n+1}).$$

Consequently, we obtain

$$F_h^{n+1} - F_h^n \leq -\int_\Omega \frac{Re}{2}|\mathbf{u}_h^{n+1} - \mathbf{u}_h^n|^2 - \Delta t \int_\Omega 2\alpha C_k |\nabla \mathbf{u}_h^{n+1}|^2 - \frac{\beta}{2We^2}\mathrm{tr}(\boldsymbol{\sigma}_h^n + (\boldsymbol{\sigma}_h^n)^{-1} - \mathbf{I}),$$

which is the inequality (3.5). Since every term on the right hand side is negative, the sequence F_h^n is non-increasing. $\qquad\square$

3.2.2 Entropy stable characteristic FEM for the diffusive Oldoroyd-B model using log-transformation

In this subsection we will study the diffusive Oldroyd-B model (2.20), where the log-transformation has been applied for the elastic stress tensor.

Lemma 3.2.2. *Let $(\mathbf{u}_h^n, p_h^n, \boldsymbol{\psi}_h^n)_{0 \leq n \leq N_T}$ be a solution to (2.57), supplied with homogeneous Dirichlet boundary condition for velocity, and with the zero Neumann boundary condition for $\boldsymbol{\psi}_h$. Further, we assume that initially $e^{\boldsymbol{\psi}_h}$ is a symmetric positive-definite tensor. Then the free energy of the system (2.57)*

$$F_h^n = F(\mathbf{u}_h^n, e^{\psi_h^n}) = \frac{Re}{2}\int_\Omega |\mathbf{u}_h^n|^2 + \frac{\beta}{2We}\int_\Omega \mathrm{tr}(e^{\psi_h^n} - \boldsymbol{\psi}_h^n - \mathbf{I}) \tag{3.7}$$

satisfies

$$F_h^{n+1} - F_h^n + \int_\Omega \frac{Re}{2}|u_h^{n+1} - u_h^n|^2 + \Delta t \int_\Omega 2\alpha C_k |\nabla \mathbf{u}_h^{n+1}|^2 + \frac{\beta}{2We^2}\mathrm{tr}(e^{\psi_h^n} + e^{-\psi_h^n} - \mathbf{I}) \leq 0. \tag{3.8}$$

In particular, the sequence $(F_h^n)_{0 \leq n \leq N_T}$ is non-increasing.

Proof. We choose $\left(\mathbf{u}_h^{n+1}, -p_h^{n+1}, \frac{\beta}{2We}(e^{\psi_h^{n+1}} - \mathbf{I})\right)$ as a test function for the system (2.57),

and get

$$0 = \int_\Omega \left(Re \frac{\mathbf{u}_h^{n+1} - \mathbf{u}_h^n \circ X^n(t^n)}{\Delta t} \cdot \mathbf{u}_h^{n+1} + 2\alpha D(\mathbf{u}_h^{n+1}) : D(\mathbf{u}_h^{n+1}) + \frac{\beta}{We} e^{\psi_h^{n+1}} : \nabla \mathbf{u}_h^{n+1} \right)$$

$$+ \sum_{K \in \mathcal{T}_h} h_K^2 \delta (\nabla p_h^{n+1})^2 + \frac{\beta}{2We} \int_\Omega \left(\frac{\psi_h^{n+1} - \psi_h^n \circ X^n(t^n)}{\Delta t} : (e^{\psi_h^{n+1}} - \mathbf{I}) \right.$$

$$- (\mathbf{\Omega}_h^{n+1} \psi_h^{n+1} - \psi_h^{n+1} \mathbf{\Omega}_h^{n+1} + 2\mathbf{B}_h^{n+1}) : (e^{\psi_h^{n+1}} - \mathbf{I}) - \frac{1}{We}(\mathbf{I} - e^{\psi_h^{n+1}}) : (e^{\psi_h^{n+1}} - \mathbf{I})$$

$$\left. + \varepsilon \nabla \psi_h^{n+1} : \nabla(e^{\psi_h^{n+1}} - \mathbf{I}) \right).$$

Similar to the proof of Lemma 3.2.1, we have

$$\int_\Omega (\mathbf{u}_h^{n+1} - \mathbf{u}_h^n \circ X^n(t^n)) \cdot \mathbf{u}_h^{n+1} \geq \int_\Omega \frac{|\mathbf{u}_h^{n+1}|^2 - |\mathbf{u}_h^n|^2}{2}, \int_\Omega D(\mathbf{u}_h^{n+1}) : D(\mathbf{u}_h^{n+1}) \geq C_k \int_\Omega |\nabla \mathbf{u}_h^{n+1}|^2.$$

Moreover, we have

$$\int_\Omega (\psi_h^{n+1} - \psi_h^n \circ X^n(t^n)) : (e^{\psi_h^{n+1}} - \mathbf{I}) = \int_\Omega (\psi_h^{n+1} - \psi_h^n \circ X^n(t^n)) : e^{\psi_h^{n+1}} - \mathrm{tr}(\psi_h^{n+1} - \psi_h^n \circ X^n(t^n)).$$

Using (2.35f) for $e^{\psi_h^{n+1}}$ and $\psi_h^n \circ X^n(t^n)$, we get

$$(\psi_h^{n+1} - \psi_h^n \circ X^n(t^n)) : e^{\psi_h^{n+1}} \geq \mathrm{tr}(e^{\psi_h^{n+1}} - e^{\psi_h^n \circ X^n(t^n)}).$$

Thus we obtain

$$\int_\Omega (\psi_h^{n+1} - \psi_h^n \circ X^n(t^n)) : (e^{\psi_h^{n+1}} - \mathbf{I}) \geq \int_\Omega \mathrm{tr}(e^{\psi_h^{n+1}} - \psi_h^{n+1}) - \int_\Omega \mathrm{tr}(e^{\psi_h^n} - \psi_h^n) \circ X^n(t^n)$$

$$= \int_\Omega \mathrm{tr}(e^{\psi_h^{n+1}} - \psi_h^{n+1}) - \int_\Omega \mathrm{tr}(e^{\psi_h^n} - \psi_h^n),$$

where we have used the fact that $\int_\Omega \mathrm{tr}(e^{\psi_h^n} - \psi_h^n) \circ X^n(t^n) = \int_\Omega \mathrm{tr}(e^{\psi_h^n} - \psi_h^n)$, cf.(3.6).
Let us note that

$$\int_\Omega (\mathbf{\Omega}_h^{n+1} \psi_h^{n+1} - \psi_h^{n+1} \mathbf{\Omega}_h^{n+1}) : (e^{\psi_h^{n+1}} - \mathbf{I}) = \int_\Omega (\mathbf{\Omega}_h^{n+1} \psi_h^{n+1} - \psi_h^{n+1} \mathbf{\Omega}_h^{n+1}) : e^{\psi_h^{n+1}} = 0,$$

$$\int_\Omega \mathbf{B}_h^{n+1} : (e^{\psi_h^{n+1}} - \mathbf{I}) = \int_\Omega \nabla \mathbf{u}_h^{n+1} : e^{\psi_h^{n+1}} - \int_\Omega \mathrm{tr} \mathbf{B}_h^{n+1} = \int_\Omega \nabla \mathbf{u}_h^{n+1} : e^{\psi_h^{n+1}},$$

and

$$(\mathbf{I} - e^{\psi_h^{n+1}}) : (e^{\psi_h^{n+1}} - \mathbf{I}) = \mathrm{tr}(e^{\psi_h^{n+1}} + e^{\psi_h^{n+1}} - 2\mathbf{I}).$$

Consequently, we obtain

$$F_h^{n+1} - F_h^n \leq - \int_\Omega \frac{Re}{2} |\mathbf{u}_h^{n+1} - \mathbf{u}_h^n|^2 - \Delta t \int_\Omega 2\alpha C_k |\nabla \mathbf{u}_h^{n+1}|^2 - \frac{\beta}{2We^2} \mathrm{tr}(e^{\psi_h^n} + e^{-\psi_h^n} - \mathbf{I}),$$

which is the equation (3.8). Since every term on the right hand side is negative, the sequence is non-increasing. $\qquad \square$

It should be pointed out that this dissipative property is a very important tool that demonstrates the nonlinear stability of our characteristic FEM for both diffusive Oldroyd-B models (2.11), (2.20).

3.3 Entropy stable characteristic FD scheme for the diffusive Oldroyd-B model using log-transformation

In this section we will show that the characteristic FD scheme also dissipates the free energy. To this end, we need to introduce some useful discrete integration by parts techniques.

3.3.1 Discrete integration by parts

Before showing the nice properties for the terms used in the characteristic finite difference scheme we firstly describe some fundamental formulas in one dimension. In this case we discretize a computational domain $\mathcal{T}$ into M cells. Let h denote a mesh size and assume that $\mathcal{T}_i$ is the $i-th$ cell, with function u sitting at vertexes, while p, ψ are at cell centers. Consequently, we have the discrete values $u_{i\pm1/2}, p_i, \psi_i, i = 1, 2, \cdots, M$.

Lemma 3.3.1. *Assume we have the zero Dirichlet boundary condition for u and the Neumann boundary condition for ψ, i.e. $u_{M+1/2} = u_{1/2} = 0$, $\psi_0 = \psi_1, \psi_{M+1} = \psi_M$. Then the following discrete integration by parts formulas hold*

$$\frac{1}{h}\sum_{i=1}^{M}(u_{i+1/2} - u_{i-1/2})p_i = -\frac{1}{h}\sum_{i=1}^{M-1}(p_{i+1} - p_i)u_{i+1/2} = -\frac{1}{h}\sum_{i=1}^{M}(p_{i+1} - p_i)u_{i+1/2}, \quad (3.9a)$$

$$\frac{1}{h}\sum_{i=1}^{M}(u_{i+1} - u_{i-1})\psi_i = -\frac{1}{h}\sum_{i=1}^{M}u_i(\psi_{i+1} - \psi_{i-1}). \quad (3.9b)$$

Proof. Let us consider the difference of the first and second terms of (3.9a). Direct computation yields

$$\frac{1}{h}\sum_{i=1}^{M}(u_{i+1/2} - u_{i-1/2})p_i + \frac{1}{h}\sum_{i=1}^{M-1}(p_{i+1} - p_i)u_{i+1/2}$$

$$= \frac{1}{h}\left(\sum_{i=1}^{M}u_{i+1/2}p_i - \sum_{i=1}^{M-1}u_{i+1/2}p_i + \sum_{i=1}^{M-1}u_{i+1/2}p_{i+1} - \sum_{i=1}^{M}u_{i-1/2}p_i\right)$$

$$= \frac{1}{h}\left(u_{M+1/2}p_M - u_{1/2}p_1\right) = 0,$$

where we have used the boundary condition $u_{M+1/2} = u_{1/2} = 0$. Moreover, since $u_{M+1/2} = 0$ we also have

$$\sum_{i=1}^{M}(p_{i+1} - p_i)u_{i+1/2} = (p_{M+1} - p_M)u_{M+1/2} + \sum_{i=1}^{M-1}(p_{i+1} - p_i)u_{i+1/2} = \sum_{i=1}^{M-1}(p_{i+1} - p_i)u_{i+1/2}.$$

The equality (3.9b) can be shown in an analogous way

$$\sum_{i=1}^{M}(u_{i+1}-u_{i-1})\psi_i + \sum_{i=1}^{M}u_i(\psi_{i+1}-\psi_{i-1}) = \sum_{i=1}^{M}(u_{i+1}\psi_i - u_i\psi_{i-1}) + \sum_{i=1}^{M}(u_i\psi_{i+1} - u_{i-1}\psi_i)$$

$$= u_{M+1}\psi_M - u_1\psi_0 + u_M\psi_{M+1} - u_0\psi_1 = (u_{M+1}+u_M)\psi_M - (u_1+u_0)\psi_1$$

$$= 2u_{M+1/2}\psi_M - 2u_{1/2}\psi_1 = 0,$$

which concludes the proof. □

Now let us consider the characteristic finite difference scheme in two-dimensional case. Accordingly, we divide the computational domain $\mathcal{T}_h$ into $M \times N$ regular rectangular mesh cells and use the same the space discretizations, cf. Figure 2.1. Assume that we have homogeneous Dirichlet boundary for velocity and Neumann boundary for every conformation tensor component σ, i.e.,

$$U_{1/2,j} = U_{M+1/2,j} = V_{i,1/2} = V_{i,N+1/2} = 0, \ \bar{U}_{i,1}^v = \bar{U}_{i,N}^v = \bar{V}_{1,j}^h = \bar{V}_{M,j}^h = 0,$$

$$\sigma_{0,j} = \sigma_{1,j}, \ \sigma_{M+1,j} = \sigma_{M,j}, \ \sigma_{i,0} = \sigma_{i,1}, \ \sigma_{i,N+1} = \sigma_{i,N}, i = 1,\cdots,M, j = 1,\cdots,N,$$

$$\tag{3.10}$$

where the superscript "$-$" represents averaging and the definition of the average operators can be found in (2.64). Recall the definition of the derivative operators (2.63), (2.65) and (2.67) used in the characteristic FD discretization (2.62), we show the following three discrete integration by parts results with the help of Lemma 3.3.1.

Lemma 3.3.2. *For the discrete difference of the transport terms* (2.63) *appearing in the momentum equation* (2.62) *the following properties hold*

$$\sum_{i=1}^{M-1}\sum_{j=1}^{N}\left(U\delta_x(U^2)\right)_{i+1/2,j} \geq \frac{1}{4}\sum_{i=1}^{M-1}\sum_{j=1}^{N}(U_{i+1/2,j})^2\left((\delta_x U)_{i+1,j} + (\delta_x U)_{i,j}\right), \tag{3.11a}$$

$$\sum_{i=1}^{M-1}\sum_{j=1}^{N}(U\delta_y(UV))_{i+1/2,j} \geq \frac{1}{4}\sum_{i=1}^{M-1}\sum_{j=1}^{N}(U_{i+1/2,j})^2\left((\delta_y V)_{i,j} + (\delta_y V)_{i+1,j}\right), \tag{3.11b}$$

$$\sum_{i=1}^{M}\sum_{j=1}^{N-1}(V\delta_x(UV))_{i,j+1/2} \geq \frac{1}{4}\sum_{i=1}^{M}\sum_{j=1}^{N-1}(V_{i,j+1/2})^2\left((\delta_x U)_{i,j+1} + (\delta_x U)_{i,j}\right), \tag{3.11c}$$

$$\sum_{i=1}^{M}\sum_{j=1}^{N-1}\left(V\delta_y(V^2)\right)_{i,j+1/2} \geq \frac{1}{4}\sum_{i=1}^{M}\sum_{j=1}^{N-1}(V_{i,j+1/2})^2\left((\delta_y V)_{i,j+1} + (\delta_y V)_{i,j}\right). \tag{3.11d}$$

Proof. The proof of (3.11a) starts with splitting the discrete derivative $\delta_x(U^2)_{i+1/2,j}$ into two parts, the part containing γ and the central difference part

$$\delta_x(U^2)_{i+1/2,j} = \delta_x^\gamma(U^2)_{i+1/2,j} + \delta_x^C(U^2)_{i+1/2,j},$$

where

$$\delta_x^\gamma(U^2) = \gamma\frac{(|\bar{U}^h|\tilde{U}^h)_{i,j} - (|\bar{U}^h|\tilde{U}^h)_{i+1,j}}{h_x}, \quad \delta_x^C(U^2) = \frac{(\bar{U}^h)_{i+1,j}^2 - (\bar{U}^h)_{i,j}^2}{h_x}.$$

Applying (3.9a) in x-direction on the "γ" term we have

$$
\begin{aligned}
\sum_{i=1}^{M-1}\sum_{j=1}^{N}\left(U\delta_x^\gamma(U^2)\right)_{i+1/2,j} &= \sum_{i=1}^{M-1}\sum_{j=1}^{N}\gamma\frac{(|\bar{U}^h|\widetilde{U}^h)_{i,j}-(|\bar{U}^h|\widetilde{U}^h)_{i+1,j}}{h_x}U_{i+1/2,j}\\
&=\frac{\gamma}{h_x}\sum_{i=1}^{M-1}\sum_{j=1}^{N}(|\bar{U}^h|\widetilde{U}^h)_{i,j}(U_{i+1/2,j}-U_{i-1/2,j})=\frac{2\gamma}{h_x}\sum_{i=1}^{M-1}\sum_{j=1}^{N}|\bar{U}_{i,j}^h|(\widetilde{U}_{i,j}^h)^2\geq 0.
\end{aligned}
\tag{3.12}
$$

Applying twice the formula (3.9a) in x-direction for the central difference part we get

$$
\begin{aligned}
&\sum_{i=1}^{M-1}\sum_{j=1}^{N}\left(U\delta_x^C(U^2)\right)_{i+1/2,j}\\
&=\sum_{j=1}^{N}\left(\frac{1}{h_x}\sum_{i=1}^{M-1}\left((\bar{U}_{i+1,j}^h)^2-(\bar{U}_{i,j}^h)^2\right)U_{i+1/2,j}\right)=\sum_{j=1}^{N}\left(-\frac{1}{h_x}\sum_{i=1}^{M}(U_{i+1/2,j}-U_{i-1/2,j})(\bar{U}_{i,j}^h)^2\right)\\
&=\sum_{j=1}^{N}\left(-\frac{1}{h_x}\sum_{i=1}^{M}(U_{i+1/2,j}-U_{i-1/2,j})\frac{U_{i+1/2,j}+U_{i-1/2,j}}{2}\bar{U}_{i,j}^h\right)\\
&=\sum_{j=1}^{N}\left(-\frac{1}{2h_x}\sum_{i=1}^{M}(U_{i+1/2,j}^2-U_{i-1/2,j}^2)\bar{U}_{i,j}^h\right)=\sum_{j=1}^{N}\left(\frac{1}{2h_x}\sum_{i=1}^{M-1}(\bar{U}_{i+1,j}^h-\bar{U}_{i,j}^h)U_{i+1/2,j}^2\right)\\
&=\sum_{j=1}^{N}\left(\frac{1}{4h_x}\sum_{i=1}^{M-1}(U_{i+3/2,j}-U_{i+1/2,j}+U_{i+1/2,j}-U_{i-1/2,j})U_{i+1/2,j}^2\right)\\
&=\frac{1}{4}\sum_{i=1}^{M-1}\sum_{j=1}^{N}U_{i+1/2,j}^2\left(\delta_x U_{i+1,j}+\delta_x U_{i,j}\right).
\end{aligned}
\tag{3.13}
$$

Summing up (3.12) and (3.13) straightly leads to (3.11a).

Analogously, the proof of (3.11b) is done by using the decomposition of the discrete derivative of UV with respect to y $\delta_y(UV)_{i+1/2,j}=\delta_y^\gamma(UV)_{i+1/2,j}+\delta_y^C(UV)_{i+1/2,j}$, where

$$
\begin{aligned}
\delta_y^\gamma(UV)_{i+1/2,j+1/2}&=\gamma\frac{(|\bar{V}^h|\widetilde{U}^v)_{i+1/2,j-1/2}-(|\bar{V}^h|\widetilde{U}^v)_{i+1/2,j+1/2}}{h_y},\\
\delta_y^C(UV)_{i+1/2,j+1/2}&=\frac{(\bar{U}^v\bar{V}^h)_{i+1/2,j+1/2}-(\bar{U}^v\bar{V}^h)_{i+1/2,j-1/2}}{h_y}.
\end{aligned}
$$

By applying the formula (3.9a) in y-direction, it is easy to show the following inequality

$$
\begin{aligned}
\sum_{i=1}^{M-1}\sum_{j=1}^{N}\left(U\delta_y^\gamma(UV)\right)_{i+1/2,j}&=\sum_{i=1}^{M-1}\sum_{j=1}^{N}\gamma\frac{(|\bar{V}^h|\widetilde{U}^v)_{i+1/2,j-1/2}-(|\bar{V}^h|\widetilde{U}^v)_{i+1/2,j+1/2}}{h_y}U_{i+1/2,j}\\
&=\frac{\gamma}{h_y}\sum_{i=1}^{M-1}\sum_{j=1}^{N}(|\bar{V}^h|\widetilde{U}^v)_{i+1/2,j+1/2}(U_{i+1/2,j+1}-U_{i+1/2,j})\\
&=\frac{2\gamma}{h_y}\sum_{i=1}^{M-1}\sum_{j=1}^{N}|\bar{V}_{i+1/2,j+1/2}^h|\left(\widetilde{U}_{i+1/2,j+1/2}^v\right)^2\geq 0.
\end{aligned}
\tag{3.14}
$$

In addition, we show the following equality as well

$$
\sum_{i=1}^{M-1}\sum_{j=1}^{N}\left(U\delta_y^C(UV)\right)_{i+1/2,j}
$$

$$
= \frac{1}{h_y}\sum_{i=1}^{M-1}\sum_{j=1}^{N}(\bar{U}^v_{i+1/2,j+1/2}\bar{V}^h_{i+1/2,j+1/2} - \bar{U}^v_{i+1/2,j-1/2}\bar{V}^h_{i+1/2,j-1/2})U_{i+1/2,j}
$$

$$
= \sum_{i=1}^{M-1}\left(-\frac{1}{h_y}\sum_{j=1}^{N-1}(U_{i+1/2,j+1} - U_{i+1/2,j})\bar{U}^v_{i+1/2,j+1/2}\bar{V}^h_{i+1/2,j+1/2}\right)
$$

$$
= -\frac{1}{2h_y}\sum_{i=1}^{M-1}\sum_{j=1}^{N-1}\left(U^2_{i+1/2,j+1} - U^2_{i+1/2,j}\right)\bar{V}^h_{i+1/2,j+1/2} \tag{3.15}
$$

$$
= \frac{1}{2h_y}\sum_{i=1}^{M-1}\sum_{j=1}^{N}\left(\bar{V}^h_{i+1/2,j+1/2} - \bar{V}^h_{i+1/2,j-1/2}\right)U^2_{i+1/2,j}
$$

$$
= \frac{1}{2h_y}\sum_{i=1}^{M-1}\sum_{j=1}^{N}U^2_{i+1/2,j}\left(\frac{V_{i,j+1/2}+V_{i+1,j+1/2}}{2} - \frac{V_{i,j-1/2}+V_{i+1,j-1/2}}{2}\right)
$$

$$
= \frac{1}{4}\sum_{i=1}^{M-1}\sum_{j=1}^{N}U^2_{i+1/2,j}\left(\delta_y V_{i,j} + \delta_y V_{i+1,j}\right).
$$

Summing up (3.14) and (3.15) together yields (3.11b).

The proof of (3.11c) is more or less similar. First step is to split the derivative $\delta_x(UV)_{i,j+1/2}$ into two parts

$$
\delta_x(UV)_{i,j+1/2} = \delta_x^\gamma(UV)_{i,j+1/2} + \delta_x^C(UV)_{i,j+1/2},
$$

where

$$
\delta_x^\gamma(UV)_{i,j+1/2} = \gamma\frac{(|\bar{U}^v|\widetilde{V}^h)_{i-1/2,j+1/2} - (|\bar{U}^v|\widetilde{V}^h)_{i+1/2,j+1/2}}{h_x},
$$

$$
\delta_x^C(UV)_{i,j+1/2} = \frac{(\bar{U}^v\bar{V}^h)_{i+1/2,j+1/2} - (\bar{U}^v\bar{V}^h)_{i-1/2,j+1/2}}{h_x}.
$$

Applying (3.9a) in x-direction for the "γ" term gives

$$
\sum_{i=1}^{M}\sum_{j=1}^{N-1}\left(V\delta_x^\gamma(UV)\right)_{i,j+1/2} = \sum_{i=1}^{M}\sum_{j=1}^{N-1}\gamma\frac{(|\bar{U}^v|\widetilde{V}^h)_{i-1/2,j+1/2} - (|\bar{U}^v|\widetilde{V}^h)_{i+1/2,j+1/2}}{h_x}V_{i,j+1/2}
$$

$$
= \frac{\gamma}{h_x}\sum_{i=1}^{M}\sum_{j=1}^{N-1}(|\bar{U}^v|\widetilde{V}^h)_{i+1/2,j+1/2}(V_{i+1,j+1/2} - V_{i,j+1/2})
$$

$$
= \frac{2\gamma}{h_x}\sum_{i=1}^{M}\sum_{j=1}^{N-1}|\bar{U}^v_{i+1/2,j+1/2}|(\widetilde{V}^h_{i+1/2,j+1/2})^2 \geq 0. \tag{3.16}
$$

45

Similarly, for the central difference part we have

$$
\sum_{i=1}^{M} \sum_{j=1}^{N-1} \left(V \delta_x (UV) \right)_{i,j+1/2}
$$

$$
= \frac{1}{h_x} \sum_{i=1}^{M} \sum_{j=1}^{N-1} \left((\bar{U}^v \bar{V}^h)_{i+1/2,j+1/2} - (\bar{U}^v \bar{V}^h)_{i-1/2,j+1/2} \right) V_{i,j+1/2}
$$

$$
= \sum_{j=1}^{N-1} \left(-\frac{1}{h_x} \sum_{i=1}^{M-1} \bar{U}^v_{i+1/2,j+1/2} \bar{V}^h_{i+1/2,j+1/2} (V_{i+1,j+1/2} - V_{i,j+1/2}) \right)
$$

$$
= \sum_{j=1}^{N-1} \left(-\frac{1}{2h_x} \sum_{i=1}^{M-1} \bar{U}^v_{i+1/2,j+1/2} \left(V^2_{i+1,j+1/2} - V^2_{i,j+1/2} \right) \right) \tag{3.17}
$$

$$
= \sum_{j=1}^{N-1} \left(\frac{1}{2h_x} \sum_{i=1}^{M} V^2_{i,j+1/2} (\bar{U}^v_{i+1/2,j+1/2} - \bar{U}^v_{i-1/2,j+1/2}) \right)
$$

$$
= \frac{1}{4h_x} \sum_{i=1}^{M} \sum_{j=1}^{N-1} V^2_{i,j+1/2} (U_{i+1/2,j+1} + U_{i+1/2,j} - U_{i-1/2,j+1} - U_{i-1/2,j})
$$

$$
= \frac{1}{4} \sum_{i=1}^{M} \sum_{j=1}^{N-1} V^2_{i,j+1/2} \left(\delta_x U_{i,j+1} + \delta_x U_{i,j} \right).
$$

Summing up (3.16) and (3.17) together represents (3.11c).

Finally, making use of (3.9a) in y-direction we obtain (3.11d) in the following way. First, we split $\delta_y(V^2)_{i,j+1/2}$ into two parts

$$
\delta_y(V^2)_{i,j+1/2} = \delta_y^{\gamma}(V^2)_{i,j+1/2} + \delta_y^C(V^2)_{i,j+1/2},
$$

where

$$
\delta_y^{\gamma}(V^2)_{i,j+1/2} = \gamma \frac{(|\bar{V}^v| \widetilde{V}^v)_{i,j} - (|\bar{V}^v| \widetilde{V}^v)_{i,j+1}}{h_y},
$$

$$
\delta_y^C(V^2)_{i,j+1/2} = \frac{(\bar{V}^v)^2_{i,j+1} - (\bar{V}^v)^2_{i,j}}{h_y}.
$$

Then it is obvious that the following inequality for the "γ" part holds true

$$
\sum_{i=1}^{M} \sum_{j=1}^{N-1} \left(V \delta_y^{\gamma}(V^2) \right)_{i,j+1/2} = \sum_{i=1}^{M} \sum_{j=1}^{N-1} \gamma \frac{(|\bar{V}^v| \widetilde{V}^v)_{i,j} - (|\bar{V}^v| \widetilde{V}^v)_{i,j+1}}{h_y} V_{i,j+1/2}
$$

$$
= \frac{\gamma}{h_y} \sum_{i=1}^{M} \sum_{j=1}^{N-1} (|\bar{V}^v| \widetilde{V}^v)_{i,j} (V_{i,j+1/2} - V_{i,j-1/2}) \tag{3.18}
$$

$$
= \frac{2\gamma}{h_y} \sum_{i=1}^{M} \sum_{j=1}^{N-1} |\bar{V}^v_{i,j}| (\widetilde{V}^v_{i,j})^2 \geq 0.
$$

For the central difference part $\delta_y(V^2)$ we have

$$\sum_{i=1}^{M}\sum_{j=1}^{N-1}\left(V\delta_y(V^2)\right)_{i,j+1/2}$$

$$=\sum_{i=1}^{M}\left(\frac{1}{h_y}\sum_{j=1}^{N-1}\left((\bar{V}_{i,j+1}^v)^2-(\bar{V}_{i,j}^v)^2\right)V_{i,j+1/2}\right)=\sum_{i=1}^{M}\left(-\frac{1}{h_y}\sum_{j=1}^{N}(V_{i,j+1/2}-V_{i,j-1/2})(\bar{V}_{i,j}^v)^2\right)$$

$$=\sum_{i=1}^{M}\left(-\frac{1}{2h_y}\sum_{j=1}^{N}(V_{i,j+1/2}^2-V_{i,j-1/2}^2)(\bar{V}_{i,j}^v)\right)=\sum_{i=1}^{M}\left(\frac{1}{2h_y}\sum_{j=1}^{N-1}(\bar{V}_{i,j+1}^v-\bar{V}_{i,j}^v)V_{i,j+1/2}^2\right)$$

$$=\sum_{i=1}^{M}\left(\frac{1}{2h_y}\sum_{j=1}^{N-1}\left(\frac{V_{j+3/2}+V_{i,j+1/2}}{2}-\frac{V_{i,j+1/2}+V_{i,j-1/2}}{2}\right)V_{i,j+1/2}^2\right)$$

$$=\frac{1}{4}\sum_{i=1}^{M}\sum_{j=1}^{N-1}V_{i,j+1/2}^2\left(\delta_yV_{i,j+1}+\delta_yV_{i,j}\right).$$

(3.19)

Combination of the (3.18) and (3.19) leads to (3.11d), which concludes the proof. □

The next lemma is to show the discrete derivative calculus for the Laplace terms defined in (2.65).

Lemma 3.3.3. *Let us define*

$$|\nabla_hU_{i+1/2,j}|^2:=\frac{1}{2}\left((\delta_xU)_{i+1,j}^2+(\delta_xU)_{i,j}^2+(\delta_yU)_{i+1/2,j+1/2}^2+(\delta_yU)_{i+1/2,j-1/2}^2\right),$$

$$|\nabla_hV_{i,j+1/2}|^2:=\frac{1}{2}\left((\delta_xV)_{i+1/2,j+1/2}^2+(\delta_xV)_{i-1/2,j+1/2}^2+(\delta_yV)_{i,j+1}^2+(\delta_yV)_{i,j}^2\right).$$

Then we have the following properties for the Laplace terms used in the momentum equations (2.62),

$$\sum_{i=1}^{M-1}\sum_{j=1}^{N}(\Delta_hU)_{i+1/2,j}\,U_{i+1/2,j}\leq-\sum_{i=1}^{M-1}\sum_{j=1}^{N}|\nabla_hU_{i+1/2,j}|^2,\qquad(3.20a)$$

$$\sum_{i=1}^{M}\sum_{j=1}^{N-1}(\Delta_hV)_{i,j+1/2}\,V_{i,j+1/2}\leq-\sum_{i=1}^{M}\sum_{j=1}^{N-1}|\nabla_hV_{i,j+1/2}|^2.\qquad(3.20b)$$

Proof. Firstly, we have by direct computation and discrete integration by parts formula (3.9a) in x-direction

$$\sum_{i=1}^{M-1}\sum_{j=1}^{N}\left(\delta_x^2U\right)_{i+1/2,j}U_{i+1/2,j}=\frac{1}{h_x^2}\sum_{i=1}^{M-1}\sum_{j=1}^{N}(U_{i+3/2,j}+U_{i-1/2,j}-2U_{i+1/2,j})U_{i+1/2,j}$$

$$=-\frac{1}{2}\frac{1}{h_x^2}\sum_{i=1}^{M-1}\sum_{j=1}^{N}\left(4U_{i+1/2,j}^2-2U_{i+3/2,j}U_{i+1/2,j}-2U_{i+1/2,j}U_{i-1/2,j}\right)$$

$$=-\frac{1}{2h_x^2}\sum_{i=1}^{M-1}\sum_{j=1}^{N}\left((U_{i+3/2,j}-U_{i+1/2,j})^2+(U_{i+1/2,j}-U_{i-1/2,j})^2\right)-\frac{1}{2h_x^2}L_1,$$

where

$$L_1 := \sum_{i=1}^{M-1}\sum_{j=1}^{N}\left(2U_{i+1/2,j}^2 - U_{i+3/2,j}^2 - U_{i-1/2,j}^2\right) = \sum_{j=1}^{N}\left(U_{3/2,j}^2 - U_{M+1/2,j}^2 + U_{M-1/2,j}^2 - U_{1/2,j}^2\right)$$

$$= \sum_{j=1}^{N}\left(U_{3/2,j}^2 + U_{M-1/2,j}^2\right) \geq 0,$$

due to boundary condition. Thus we obtain

$$\sum_{i=1}^{M-1}\sum_{j=1}^{N}\left(\delta_x^2 U\right)_{i+1/2,j}U_{i+1/2,j} \leq -\frac{1}{2h_x^2}\sum_{i=1}^{M-1}\sum_{j=1}^{N}(U_{i+3/2,j} - U_{i+1/2,j})^2 + (U_{i+1/2,j} - U_{i-1/2,j})^2$$

$$= -\frac{1}{2}\sum_{i=1}^{M-1}\sum_{j=1}^{N}(\delta_x U)_{i+1,j}^2 + (\delta_x U)_{i,j}^2.$$

(3.21)

Applying the same arguments for U in y-direction we obtain

$$\sum_{i=1}^{M-1}\sum_{j=1}^{N}\left(\delta_y^2 U\right)_{i+1/2,j}U_{i+1/2,j}$$

$$= \frac{1}{h_y^2}\sum_{i=1}^{M-1}\sum_{j=1}^{N}\left((U_{i+1/2,j+1} + U_{i+1/2,j-1} - 2U_{i+1/2,j})U_{i+1/2,j}\right)$$

$$= -\frac{1}{2}\frac{1}{h_y^2}\sum_{i=1}^{M-1}\sum_{j=1}^{N}\left(4U_{i+1/2,j}^2 - 2U_{i+1/2,j+1}U_{i+1/2,j} - 2U_{i+1/2,j-1}U_{i+1/2,j}\right)$$

$$= -\frac{1}{2h_y^2}\sum_{i=1}^{M-1}\sum_{j=1}^{N}\left((U_{i+1/2,j+1} - U_{i+1/2,j})^2 + (U_{i+1/2,j} - U_{i+1/2,j-1})^2 + L_2\right)$$

$$= -\frac{1}{2h_y^2}\sum_{i=1}^{M-1}\sum_{j=1}^{N}\left((U_{i+1/2,j+1} - U_{i+1/2,j})^2 + (U_{i+1/2,j} - U_{i+1/2,j-1})^2\right)$$

$$= -\frac{1}{2}\sum_{i=1}^{M-1}\sum_{j=1}^{N}\left((\delta_y U)_{i+1/2,j+1/2}^2 + (\delta_y U)_{i+1/2,j-1/2}^2\right),$$

(3.22)

where we have used the fact that

$$L_2 := \sum_{i=1}^{M-1}\sum_{j=1}^{N}\left(2U_{i+1/2,j}^2 - U_{i+1/2,j+1}^2 - U_{i+1/2,j-1}^2\right)$$

$$= \sum_{i=1}^{M-1}\left(U_{i+1/2,1}^2 - U_{i+1/2,N+1}^2 + U_{i+1/2,N}^2 - U_{i+1/2,0}^2\right)$$

$$= \sum_{i=1}^{M-1}\left(U_{i+1/2,1}^2 - U_{i+1/2,0}^2 + U_{i+1/2,N}^2 - U_{i+1/2,N+1}^2\right) = 0,$$

due to boundary condition.

For the completeness of the proof we also present the results for V. First we have

$$\sum_{i=1}^{M}\sum_{j=1}^{N-1}\left(\delta_x^2 V\right)_{i,j+1/2} V_{i,j+1/2}$$

$$= \frac{1}{h_x^2}\sum_{i=1}^{M}\sum_{j=1}^{N-1}\left(V_{i+1,j+1/2}+V_{i-1,j+1/2}-2V_{i,j+1/2}\right)V_{i,j+1/2}$$

$$= -\frac{1}{2}\frac{1}{h_x^2}\sum_{i=1}^{M}\sum_{j=1}^{N-1}\left(4V_{i,j+1/2}^2-2V_{i+1,j+1/2}V_{i,j+1/2}-2V_{i-1,j+1/2}V_{i,j+1/2}\right)$$

$$= -\frac{1}{2h_x^2}\sum_{i=1}^{M}\sum_{j=1}^{N-1}\left((V_{i+1,j+1/2}-V_{i,j+1/2})^2+(V_{i,j+1/2}-V_{i-1,j+1/2})^2\right)-\frac{1}{2h_x^2}L_3 \qquad (3.23)$$

$$= -\frac{1}{2h_x^2}\sum_{i=1}^{M}\sum_{j=1}^{N-1}\left((V_{i+1,j+1/2}-V_{i,j+1/2})^2+(V_{i,j+1/2}-V_{i-1,j+1/2})^2\right)$$

$$= -\frac{1}{2}\sum_{i=1}^{M}\sum_{j=1}^{N-1}\left((\delta_x V)_{i+1/2,j+1/2}^2+(\delta_x V)_{i-1/2,j+1/2}^2\right),$$

where we have used

$$L_3 := \sum_{i=1}^{M}\sum_{j=1}^{N-1}\left(2V_{i,j+1/2}^2-V_{i+1,j+1/2}^2-V_{i-1,j+1/2}^2\right)$$

$$= \sum_{j=1}^{N-1}\left(V_{1,j+1/2}^2-V_{M+1,j+1/2}^2+V_{M,j+1/2}^2-V_{0,j+1/2}^2\right)$$

$$= \sum_{j=1}^{N-1}\left(V_{1,j+1/2}^2-V_{0,j+1/2}^2+V_{M,j+1/2}^2-V_{M+1,j+1/2}^2\right)=0.$$

Similarly, we also have

$$\sum_{i=1}^{M}\sum_{j=1}^{N-1}\left(\delta_y^2 V\right)_{i,j+1/2} V_{i,j+1/2}$$

$$= \frac{1}{h_y^2}\sum_{i=1}^{M}\sum_{j=1}^{N-1}\left((V_{i,j+3/2}+V_{i,j-1/2}-2V_{i,j+1/2})V_{i,j+1/2}\right)$$

$$= -\frac{1}{2}\frac{1}{h_y^2}\sum_{i=1}^{M}\sum_{j=1}^{N-1}\left(4V_{i,j+1/2}^2-2V_{i,j+3/2}V_{i,j+1/2}-2V_{i,j-1/2}V_{i,j+1/2}\right)$$

$$= -\frac{1}{2}\frac{1}{h_y^2}\sum_{i=1}^{M}\sum_{j=1}^{N-1}\left((V_{i,j+3/2}-V_{i,j+1/2})^2+(V_{i,j+1/2}-V_{i,j-1/2})^2+L_4\right) \qquad (3.24)$$

$$\le -\frac{1}{2}\frac{1}{h_y^2}\sum_{i=1}^{M}\sum_{j=1}^{N-1}\left((V_{i,j+3/2}-V_{i,j+1/2})^2+(V_{i,j+1/2}-V_{i,j-1/2})^2\right)$$

$$= -\frac{1}{2}\sum_{i=1}^{M}\sum_{j=1}^{N-1}\left((\delta_y V)_{i,j+1}^2+(\delta_y V)_{i,j}^2\right).$$

Here we have analogously as before

$$L_4 := \sum_{i=1}^{M} \sum_{j=1}^{N-1} \left(2V_{i,j+1/2}^2 - V_{i,j-1/2}^2 - V_{i,j+3/2}^2\right) = \sum_{i=1}^{M} \left(V_{i,N-1/2}^2 - V_{i,1/2}^2 + V_{i,3/2}^2 - V_{i,N+1/2}^2\right)$$

$$= \sum_{i=1}^{M} \left(V_{i,N-1/2}^2 + V_{i,3/2}^2\right) \geq 0.$$

Combining the above equations (3.21), (3.22), (3.23) and (3.24), we conclude that (3.20a), (3.20b) hold. □

Our next goal is to demonstrate the discrete derivative calculus for the elastic stress tensor defined in (2.67) and velocity gradient defined in (2.59).

Lemma 3.3.4. *Denoting for simplicity $A = \sigma_{11}, B = \sigma_{12}, C = \sigma_{22}$ allows us to rewrite $\boldsymbol{\sigma}$ on the finite difference cell $K_{i,j}$ as*

$$\boldsymbol{\sigma}_{i,j} = \begin{pmatrix} A & B \\ B & C \end{pmatrix}_{i,j}.$$

Let

$$S_1(\boldsymbol{\sigma}, \mathbf{u}) := \sum_{i=1}^{M-1} \sum_{j=1}^{N} \left((\delta_x A + \delta_y B)U\right)_{i+1/2,j} + \sum_{i=1}^{M} \sum_{j=1}^{N-1} \left((\delta_x B + \delta_y C)V\right)_{i,j+1/2}, \quad (3.25a)$$

$$S_2(\boldsymbol{\sigma}, \mathbf{u}) := \sum_{i=1}^{M} \sum_{j=1}^{N} (\nabla \mathbf{u}_h : \boldsymbol{\sigma})_{i,j} = \sum_{i=1}^{M} \sum_{j=1}^{N} \left((\delta_x U)A + (\delta_y U)B + (\delta_x V)B + (\delta_y V)C\right)_{i,j}. \quad (3.25b)$$

Then the following identity holds

$$S_1(\boldsymbol{\sigma}, \mathbf{u}) + S_2(\boldsymbol{\sigma}, \mathbf{u}) = 0. \quad (3.26)$$

Proof. Firstly, we have by applying the formula (3.9a) on $\left((\delta_x A)U\right)_{i+1/2,j}$ that

$$\sum_{i=1}^{M-1} \sum_{j=1}^{N} \left((\delta_x A)U\right)_{i+1/2,j} = \frac{1}{h_x} \sum_{i=1}^{M-1} \sum_{j=1}^{N} (A_{i+1,j} - A_{i,j})U_{i+1/2,j}$$

$$= -\frac{1}{h_x} \sum_{i=1}^{M} \sum_{j=1}^{N} (U_{i+1/2,j} - U_{i-1/2,j})A_{i,j} = -\sum_{i=1}^{M} \sum_{j=1}^{N} \left((\delta_x U)A\right)_{i,j}, \quad (3.27)$$

and analogously for the term $\left((\delta_y C)V\right)_{i,j+1/2}$ we obtain

$$\sum_{i=1}^{M} \sum_{j=1}^{N-1} \left((\delta_y C)V\right)_{i,j+1/2} = \frac{1}{h_y} \sum_{i=1}^{M} \sum_{j=1}^{N-1} (C_{i,j+1} - C_{i,j})V_{i,j+1/2}$$

$$= -\frac{1}{h_y} \sum_{i=1}^{M} \sum_{j=1}^{N} (V_{i,j+1/2} - V_{i,j-1/2})C_{i,j} = -\sum_{i=1}^{M} \sum_{j=1}^{N} \left((\delta_y V)C\right)_{i,j}. \quad (3.28)$$

We have for the discrete y-derivative of U slightly more tedious calculation

$$\sum_{i=1}^{M-1}\sum_{j=1}^{N}\left((\delta_y B)U\right)_{i+1/2,j}$$

$$=\frac{1}{4h_y}\sum_{i=1}^{M-1}\sum_{j=1}^{N}(B_{i+1,j+1}-B_{i+1,j-1})U_{i+1/2,j}+(B_{i,j+1}-B_{i,j-1})U_{i+1/2,j}$$

$$=\frac{1}{4h_y}\sum_{i=1}^{M-1}\sum_{j=1}^{N}(B_{i,j+1}-B_{i,j-1})U_{i-1/2,j}+(B_{i,j+1}-B_{i,j-1})U_{i+1/2,j}$$

$$\quad+\frac{1}{4h_y}\sum_{j=1}^{N}\left((B_{M,j+1}-B_{M,j-1})U_{M-1/2,j}-(B_{1,j+1}-B_{1,j-1})U_{1/2,j}\right)$$

$$=\frac{1}{2h_y}\sum_{i=1}^{M-1}\sum_{j=1}^{N}(B_{i,j+1}-B_{i,j-1})\bar{U}_{i,j}^{h}+\frac{1}{4h_y}\sum_{j=1}^{N}(B_{M,j+1}-B_{M,j-1})U_{M-1/2,j}$$

$$=\frac{1}{2h_y}\sum_{i=1}^{M}\sum_{j=1}^{N}(B_{i,j+1}-B_{i,j-1})\bar{U}_{i,j}^{h}-\frac{1}{2h_y}\sum_{j=1}^{N}(B_{M,j+1}-B_{M,j-1})\bar{U}_{M,j}^{h}$$

$$\quad+\frac{1}{4h_y}\sum_{j=1}^{N}(B_{M,j+1}-B_{M,j-1})U_{M-1/2,j}=\frac{1}{2h_y}\sum_{i=1}^{M}\sum_{j=1}^{N}(B_{i,j+1}-B_{i,j-1})\bar{U}_{i,j}^{h}$$

$$=-\frac{1}{2h_y}\sum_{i=1}^{M}\sum_{j=1}^{N}(\bar{U}_{i,j+1}^{h}-\bar{U}_{i,j-1}^{h})B_{i,j}=-\sum_{i=1}^{M}\sum_{j=1}^{N}(\delta_y UB)_{i,j},$$

$$(3.29)$$

where we have applied (3.9b). Similar result holds for x-derivative of velocity V

$$\sum_{i=1}^{M}\sum_{j=1}^{N-1}\left((\delta_x B)V\right)_{i,j+1/2}$$

$$=\frac{1}{4h_x}\sum_{i=1}^{M}\sum_{j=1}^{N-1}(B_{i+1,j}-B_{i-1,j})V_{i,j-1/2}+(B_{i+1,j}-B_{i-1,j})V_{i,j+1/2}$$

$$\quad+\frac{1}{4h_x}\sum_{i=1}^{M}\left((B_{i+1,N}-B_{i-1,N})V_{i,N-1/2}-(B_{i+1,1}-B_{i-1,1})V_{i,1/2}\right)$$

$$=\frac{1}{2h_x}\sum_{i=1}^{M}\sum_{j=1}^{N-1}(B_{i+1,j}-B_{i-1,j})\bar{V}_{i,j}^{v}+\frac{1}{4h_x}\sum_{i=1}^{M}(B_{i+1,N}-B_{i-1,N})V_{i,N-1/2}$$

$$=\frac{1}{2h_x}\sum_{i=1}^{M}\sum_{j=1}^{N}(B_{i+1,j}-B_{i-1,j})\bar{V}_{i,j}^{v}-\frac{1}{2h_x}\sum_{i=1}^{M}(B_{i+1,N}-B_{i-1,N})\bar{V}_{i,N}^{v}$$

$$\quad+\frac{1}{4h_x}\sum_{i=1}^{M}(B_{i+1,N}-B_{i-1,N})V_{i,N-1/2}$$

$$=-\frac{1}{2h_x}\sum_{i=1}^{M}\sum_{j=1}^{N}(\bar{V}_{i+1,j}^{v}-\bar{V}_{i-1,j}^{v})B_{i,j}=-\sum_{i=1}^{M}\sum_{j=1}^{N}\left(\delta_x V)B\right)_{i,j}.$$

$$(3.30)$$

Combining (3.27)–(3.30) together we obtain (3.26). $\qquad\square$

3.3.2 Entropy stability

Now we will proceed with the main result of this section which demonstrates the dissipation of the free energy.

Lemma 3.3.5. *Let $(U_{i+1/2,j}^n, V_{i,j+1/2}^n, p_{i,j}^n, \boldsymbol{\sigma}_{i,j}^n)_{0 \leq n \leq N_T}$ be a solution of the discrete characteristic FD scheme, which is the combination of (2.62) and (2.75), supplied with boundary conditions (3.10). Then the free energy*

$$F_h^n = \frac{Re}{2} \left(\sum_{i=1}^{M-1} \sum_{j=1}^{N} (U_{i+1/2,j}^n)^2 + \sum_{i=1}^{M} \sum_{j=1}^{N-1} (V_{i,j+1/2}^n)^2 \right) + \frac{1-\alpha}{2We} \sum_{i=1}^{M} \sum_{j=1}^{N} tr \left(e^{\boldsymbol{\psi}^n} - \boldsymbol{\psi}^n - \mathbf{I} \right)_{i,j}$$

(3.31)

satisfies

$$F_h^{n+1} - F_h^n + \alpha \Delta t \left(\sum_{i=1}^{M-1} \sum_{j=1}^{N} |\nabla_h U_{i+1/2,j}^{n+1}|^2 + \sum_{i=1}^{M} \sum_{j=1}^{N-1} |\nabla_h V_{i,j+1/2}^{n+1}|^2 \right)$$

$$+ \frac{\Delta t (1-\alpha)}{2We^2} \sum_{i=1}^{M} \sum_{j=1}^{N} tr(e^{\boldsymbol{\psi}^{n+1}} + e^{-\boldsymbol{\psi}^{n+1}} - 2\mathbf{I})_{i,j} \leq 0.$$

(3.32)

In particular, the sequence $(F_h^n)_{0 \leq n \leq N_T}$ is non-increasing.

Proof. Let us first recall the finite difference part of the characteristic FD scheme for the momentum equation, and make the following operations: we multiply (2.62a) with $U_{i+1/2,j}$, (2.62b) with $V_{i+1/2,j}$, (2.62c) with $p_{i,j}$ and sum them together. Let

$$S := \sum_{i=1}^{M-1} \sum_{j=1}^{N} \left(Re \frac{(U^{n+1} - U^n)_{i+1/2,j}}{\Delta t} + Re \left(\delta_x (U^{n+1})^2 + \delta_y (UV)^{n+1} \right)_{i+1/2,j} \right) U_{i+1/2,j}^{n+1}$$

$$- \left(\alpha (\delta_x^2 U^{n+1} + \delta_y^2 U^{n+1}) - \delta_x p^{n+1} + \frac{1-\alpha}{We} (\delta_x \boldsymbol{\sigma}_{11}^{n+1} + \delta_y \boldsymbol{\sigma}_{12}^{n+1}) \right)_{i+1/2,j} U_{i+1/2,j}^{n+1}$$

$$+ \sum_{i=1}^{M-1} \sum_{j=1}^{N} \left(Re \frac{(V^{n+1} - V^n)_{i,j+1/2}}{\Delta t} + Re \left(\delta_x (UV)^{n+1} + \delta_y (V^{n+1})^2 \right)_{i,j+1/2} \right) V_{i,j+1/2}$$

$$- \left(\alpha (\delta_x^2 V^{n+1} + \delta_y^2 V^{n+1}) - \delta_y p^{n+1} + \frac{1-\alpha}{We} (\delta_x \boldsymbol{\sigma}_{21}^{n+1} + \delta_y \boldsymbol{\sigma}_{22}^{n+1}) \right)_{i,j+1/2} V_{i,j+1/2}$$

$$+ \sum_{i=1}^{M} \sum_{j=1}^{N} \left(\delta_x U^{n+1} + \delta_y V^{n+1} \right)_{i,j} p_{i,j}.$$

(3.33)

Obviously, we have $S = 0$. It is easy to get

$$(U_{i+1/2,j}^{n+1} - U_{i+1/2,j}^n) \cdot U_{i+1/2,j}^{n+1} = \frac{(U_{i+1/2,j}^{n+1})^2 - (U_{i+1/2,j}^n)^2}{2} + \frac{(U_{i+1/2,j}^{n+1} - U_{i+1/2,j}^n)^2}{2}$$

$$\geq \frac{(U_{i+1/2,j}^{n+1})^2 - (U_{i+1/2,j}^n)^2}{2}.$$

(3.34)

Similarly

$$(V_{i,j+1/2}^{n+1} - V_{i,j+1/2}^n) \cdot V_{i,j+1/2}^{n+1} \geq \frac{(V_{i,j+1/2}^{n+1})^2 - (V_{i,j+1/2}^n)^2}{2}. \tag{3.35}$$

Using Lemma 3.3.2 and the fact that $(\delta_x U + \delta_y V)_{i,j} = 0$ we also obtain

$$\begin{aligned}
\sum_{i=1}^{M-1}\sum_{j=1}^{N} \left(U\delta_x(U^2)\right)_{i+1/2,j} + \sum_{i=1}^{M-1}\sum_{j=1}^{N} \left(U\delta_y(UV)\right)_{i+1/2,j} &= 0, \\
\sum_{i=1}^{M}\sum_{j=1}^{N-1} \left(V\delta_x(UV)\right)_{i,j+1/2} + \sum_{i=1}^{M}\sum_{j=1}^{N-1} \left(V\delta_y(V^2)\right)_{i,j+1/2} &= 0.
\end{aligned} \tag{3.36}$$

For the pressure terms we have

$$\begin{aligned}
\sum_{i=1}^{M-1}\sum_{j=1}^{N} \left((\delta_x p)U\right)_{i+1/2,j} &= \frac{1}{h_x}\sum_{j=1}^{N}\sum_{i=1}^{M-1} (p_{i+1,j} - p_{i-1,j})U_{i+1/2,j} \\
&= -\frac{1}{h_x}\sum_{j=1}^{N}\sum_{i=1}^{M}(U_{i+1/2,j} - U_{i-1/2,j})p_{i,j} = -\sum_{i=1}^{M}\sum_{j=1}^{N} \left((\delta_x U)p\right)_{i,j},
\end{aligned}$$

and similarly,

$$\sum_{i=1}^{M}\sum_{j=1}^{N-1} \left((\delta_y p)V\right)_{i,j+1/2} = -\sum_{i=1}^{M}\sum_{j=1}^{N} \left((\delta_y V)p\right)_{i,j}.$$

Thus we have

$$\sum_{i=1}^{M-1}\sum_{j=1}^{N} \left((\delta_x p)U\right)_{i+1/2,j} + \sum_{i=1}^{M}\sum_{j=1}^{N-1} \left((\delta_y p)V\right)_{i,j+1/2} + \sum_{i=1}^{M}\sum_{j=1}^{N} \left((\delta_x U)p + (\delta_y V)p\right)_{i,j} = 0. \tag{3.37}$$

Using (3.25), (3.34), (3.35), (3.37) and Lemma 3.3.3 we derive

$$\begin{aligned}
0 = S \geq {}& \frac{\alpha - 1}{We}S_1(\boldsymbol{\sigma}, \mathbf{u}) + \sum_{i=1}^{M-1}\sum_{j=1}^{N} Re\frac{(U_{i+1/2,j}^{n+1})^2 - (U_{i+1/2,j}^n)^2}{2\Delta t} + \alpha|\nabla_h U_{i+1/2,j}^{n+1}|^2 \\
& + \sum_{i=1}^{M}\sum_{j=1}^{N-1} Re\frac{(V_{i,j+1/2}^{n+1})^2 - (V_{i,j+1/2}^n)^2}{2\Delta t} + \alpha|\nabla_h V_{i,j+1/2}^{n+1}|^2.
\end{aligned} \tag{3.38}$$

Now we consider the transport equation for the elastic stress tensor $\boldsymbol{\psi}$ and multiply (2.75) with $(e^{\psi_{i,j}^{n+1}} - \mathbf{I})$. This leads to

$$\begin{aligned}
0 = S' = {}& \sum_{i=1}^{M}\sum_{j=1}^{N} \frac{(\boldsymbol{\psi}^{n+1} - \boldsymbol{\psi}^n \circ X^n)_{i,j}}{\Delta t} : (e^{\psi^{n+1}} - \mathbf{I})_{i,j} \\
& - \left(\boldsymbol{\Omega}^{n+1}\boldsymbol{\psi}^{n+1} - \boldsymbol{\psi}^{n+1}\boldsymbol{\Omega}^{n+1} + 2\mathbf{B}^{n+1} + \frac{1}{We}(e^{-\psi^{n+1}} - \mathbf{I}) + \varepsilon\Delta_h\boldsymbol{\psi}^{n+1}\right)_{i,j} : (e^{\psi^{n+1}} - \mathbf{I})_{i,j}.
\end{aligned} \tag{3.39}$$

Similar to the proof of Lemma 3.2.2 we have

$$\sum_{i=1}^{M}\sum_{j=1}^{N}(\boldsymbol{\psi}^{n+1} - \boldsymbol{\psi}^n \circ X^n)_{i,j} : (e^{\psi_{i,j}^{n+1}} - \mathbf{I}) \geq \sum_{i=1}^{M}\sum_{j=1}^{N}\left(\mathrm{tr}(e^{\psi_{i,j}^{n+1}} - \boldsymbol{\psi}_{i,j}^{n+1}) - \mathrm{tr}(e^{\psi_{i,j}^{n}} - \boldsymbol{\psi}_{i,j}^{n})\right)$$

$$\sum_{i=1}^{M}\sum_{j=1}^{N}\left(\boldsymbol{\Omega}^{n+1}\boldsymbol{\psi}^{n+1} - \boldsymbol{\psi}^{n+1}\boldsymbol{\Omega}^{n+1} + 2\mathbf{B}^{n+1}\right) : (e^{\psi_{i,j}^{n+1}} - \mathbf{I}) = \sum_{i=1}^{M}\sum_{j=1}^{N} 2\nabla\mathbf{u}_{i,j}^{n+1} : e^{\psi_{i,j}^{n+1}}$$

$$\sum_{i=1}^{M}\sum_{j=1}^{N}(e^{-\psi_{i,j}^{n+1}} - \mathbf{I}) : (e^{\psi_{i,j}^{n+1}} - \mathbf{I}) = -\sum_{i=1}^{M}\sum_{j=1}^{N} \mathrm{tr}(e^{-\psi_{i,j}^{n+1}} + e^{\psi_{i,j}^{n+1}} - 2\mathbf{I}).$$

$$(3.40)$$

For the diffusive terms, we first obtain

$$\sum_{i=1}^{M}\sum_{j=1}^{N}\Delta_h\boldsymbol{\psi}_{i,j}^{n+1} : e^{\psi_{i,j}^{n+1}} = -\sum_{i=1}^{M}\sum_{j=1}^{N}\nabla_h\boldsymbol{\psi}_{i,j}^{n+1} : \nabla_h e^{\psi_{i,j}^{n+1}}$$

$$= -\sum_{i=1}^{M}\sum_{j=1}^{N}(\boldsymbol{\psi}_{i+1,j}^{n+1} - \boldsymbol{\psi}_{i-1,j}^{n+1}) : (e^{\psi_{i+1,j}} - e^{\psi_{i-1,j}}) \qquad (3.41)$$

$$- \sum_{i=1}^{M}\sum_{j=1}^{N}(\boldsymbol{\psi}_{i,j+1} - \boldsymbol{\psi}_{i,j-1})^{n+1} : (e^{\psi_{i,j+1}} - e^{\psi_{i,j-1}})^{n+1} \leq 0,$$

where we have used (2.40). Then it is easy to show

$$\sum_{i=1}^{M}\sum_{j=1}^{N}\Delta\boldsymbol{\psi}_{i,j}^{n+1} : \mathbf{I}$$

$$= \sum_{i=1}^{M}\sum_{j=1}^{N}\mathrm{tr}(\boldsymbol{\psi}_{i+1,j} + \boldsymbol{\psi}_{i,j+1} - 4\boldsymbol{\psi}_{i,j} + \boldsymbol{\psi}_{i-1,j} + \boldsymbol{\psi}_{i,j-1})^{n+1} \qquad (3.42)$$

$$= \sum_{i=1}^{M}\mathrm{tr}(\boldsymbol{\psi}_{i,N+1} - \boldsymbol{\psi}_{i,N} - \boldsymbol{\psi}_{i,1} + \boldsymbol{\psi}_{i,0})^{n+1} + \sum_{j=1}^{N}\mathrm{tr}(\boldsymbol{\psi}_{M+1,j} - \boldsymbol{\psi}_{M,j} - \boldsymbol{\psi}_{1,j}\boldsymbol{\psi}_{0,j})^{n+1}$$

$$= 0,$$

due to the corresponding boundary condition.
Combining (3.40), (3.41), (3.42) together yields

$$0 = S' \geq -2S_2(\boldsymbol{\sigma}, \mathbf{u})$$

$$+ \sum_{i=1}^{M}\sum_{j=1}^{N}\frac{1}{\Delta t}\mathrm{tr}\left((e^{\psi^{n+1}} - \boldsymbol{\psi}^{n+1}) - (e^{\psi^n} - \boldsymbol{\psi}^n)\right)_{i,j} + \mathrm{tr}(e^{\psi^{n+1}} + e^{-\psi^{n+1}} - 2\mathbf{I})_{i,j}.$$

$$(3.43)$$

Multiplying (3.43) with a factor $\frac{1-\alpha}{2We}$, summing with (3.38) and using (3.26) together

with Lemma 3.3.4 leads to

$$\sum_{i=1}^{M-1}\sum_{j=1}^{N} Re \frac{(U_{i+1/2,j}^{n+1})^2 - (U_{i+1/2,j}^n)^2}{2\Delta t} + \alpha|\nabla_h U_{i+1/2,j}^{n+1}|^2$$

$$+ \sum_{i=1}^{M}\sum_{j=1}^{N-1} Re \frac{(V_{i,j+1/2}^{n+1})^2 - (V_{i,j+1/2}^n)^2}{2\Delta t} + \alpha|\nabla_h V_{i,j+1/2}^{n+1}|^2$$

$$+ \sum_{i=1}^{M}\sum_{j=1}^{N} \frac{1}{\Delta t}\frac{1-\alpha}{We}\mathrm{tr}\left((e^{\boldsymbol{\psi}^{n+1}} - \boldsymbol{\psi}^{n+1}) - (e^{\boldsymbol{\psi}^n} - \boldsymbol{\psi}^n)\right)_{i,j} + \frac{1-\alpha}{2We^2}\mathrm{tr}(e^{\boldsymbol{\psi}^{n+1}} + e^{-\boldsymbol{\psi}^{n+1}} - 2\mathbf{I})_{i,j}$$

$$\leq 0. \tag{3.44}$$

Consequently, the sequence $\{F^n\}_{n=0}^{N_T}$ is non-increasing since we have

$$F^{n+1} - F^n \leq -\Delta t\bigg(\alpha\Big(\sum_{i=1}^{M-1}\sum_{j=1}^{N}|\nabla_h U_{i+1/2,j}^{n+1}|^2 + \sum_{i=1}^{M}\sum_{j=1}^{N-1}|\nabla_h V_{i,j+1/2}^{n+1}|^2\Big)$$

$$+ \frac{1-\alpha}{2We^2}\sum_{i=1}^{M}\sum_{j=1}^{N}\mathrm{tr}(e^{\boldsymbol{\psi}^{n+1}} + e^{-\boldsymbol{\psi}^{n+1}} - 2\mathbf{I})_{i,j}\bigg) \leq 0. \tag{3.45}$$

□

Using the discrete integration by parts formulas from the previous subsection we have shown that the characteristic FD method also dissipates the free energy.

3.4 Numerical results

In this section, we will test our numerical Algorithms 1, 2, 3, 4 proposed in the previous chapter with some benchmark problems. Our aim is to demonstrate the performance of these numerical methods. We first study the numerical influence of the Weissenberg number We and the diffusion coefficient ε. Furthermore, the experimental order of convergence will be studied.

The first benchmark test we will analyze is the driven cavity problem, and the second is 4:1 planar contraction channel problem.

3.4.1 Driven cavity

Our first test case is the lid-driven cavity problem. The geometry and mesh of the problem is given in Figure 3.1. The computational domain is $\mathcal{T}_h = [0,1]^2$. The initial conditions are taken to be

$$\mathbf{u} = \mathbf{0}, \boldsymbol{\sigma} = \mathbf{I}. \tag{3.46}$$

A Dirichlet boundary condition is set for velocity

$$\mathbf{u} = \begin{cases} (16x^2(1-x)^2, 0)^T, & \text{if } y = 1, x \in (0,1), \\ \mathbf{0}, & \text{else.} \end{cases} \tag{3.47}$$
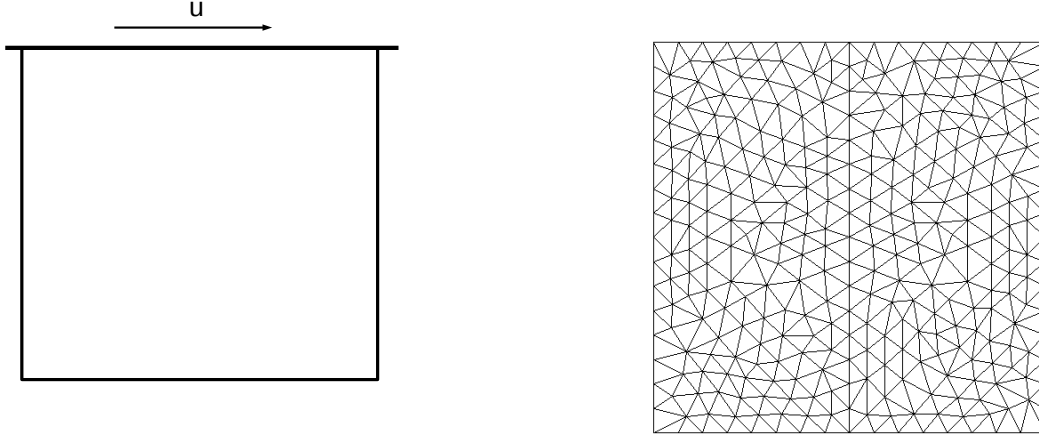
Figure 3.1: Geometry and mesh for the cavity flow problem.

Further, we choose extrapolated boundary condition for the conformation tensor and its logarithm, which means

$$\frac{\partial \boldsymbol{\sigma}}{\partial \mathbf{n}} = 0, \text{ or } \frac{\partial \boldsymbol{\psi}}{\partial \mathbf{n}} = 0, \tag{3.48}$$

where $\mathbf{n}$ is the outer normal of the boundary.

Non-diffusive Oldroyd-B model

Before presenting the results for the diffusive model, we first show some typical figure of the original Oldroyd-B model (2.19) using the log-transformation. Here we choose the combined FD-FV scheme, Algorithm 3, and set $\varepsilon = 0$. The mesh size is set to $h_x = h_y = 1/64$, and the time step size is set as $\Delta t = CFL \frac{h_x}{max(|\mathbf{u}|)}$.

In Figure 3.2 we show the streamline of different Weissenberg number $We = 0.5, 1, 3, 5$ at time 30 and $Re = 1$. The figure gives obvious vertex shifting phenomenon: the center of the vertex shifts to the left as We increases. Moreover, some vortexes origin at the right boundary for large We.

In Figure 3.3 we show the kinetic energy and the free energy defined by (2.34) . It is observed that the kinetic energy decreases for increasing the Weissenberg number We. The kinetic and free energy for $We \leq 3$ are more or less tending to a steady state, while for large $We = 5$ the energy is oscillating for long time.
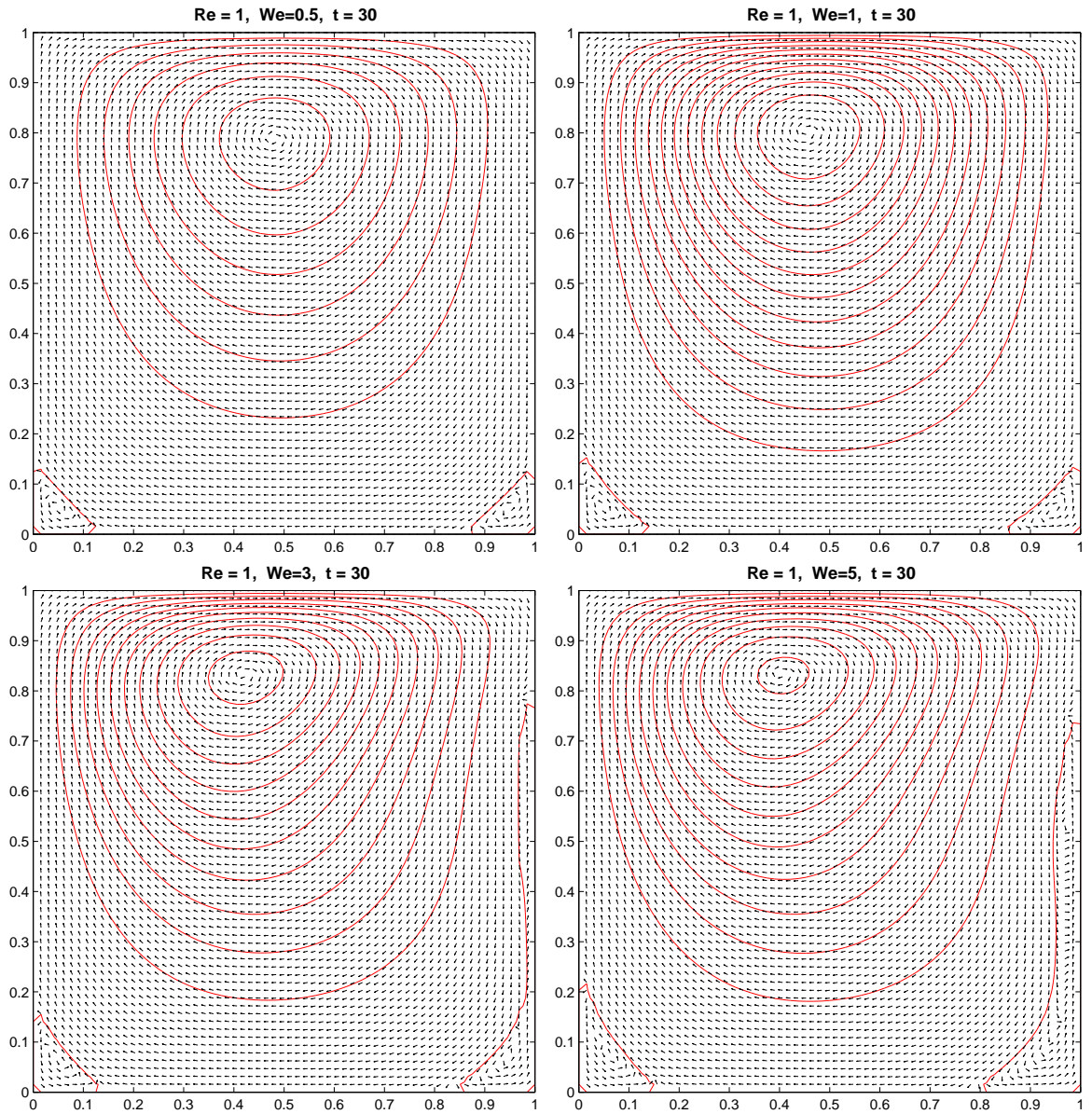
Figure 3.2: Streamline for the non-diffusive Oldroyd-B model, computed by the combined FD-FV scheme, Algorithm 3.

Table 3.2: L^2-norm error with respect to mesh refinement of the non-diffusive Oldroyd-B model for σ_{11}: $\|\sigma_{11}(h)-\sigma_{11}(h/2)\|$, computed by the combined FD-FV scheme, Algorithm 3.

mesh size h	$We = 0.5$	$We = 1$	$We = 3$
1/32	0.3502	1.5846	4.8967
1/64	0.5006	3.3141	10.8242
1/128	0.7181	5.3517	18.5389
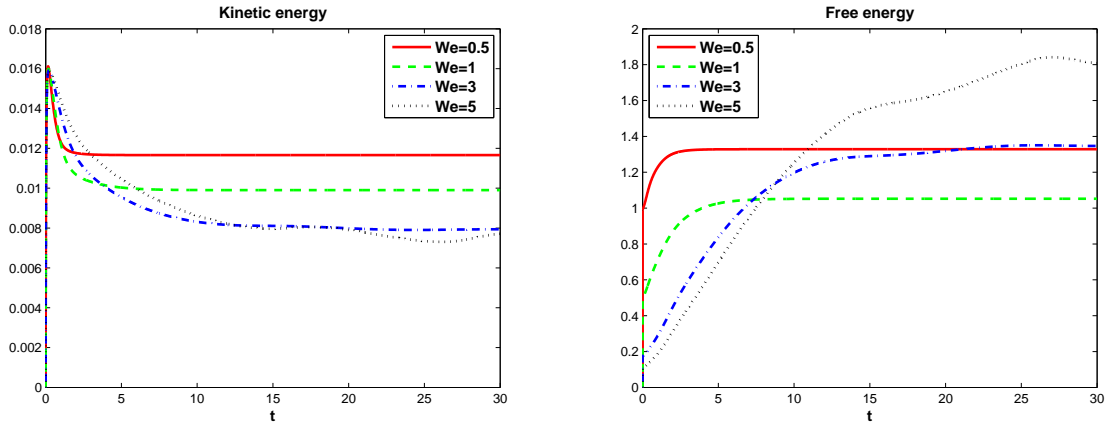
Figure 3.3: Kinetic and free energy for the non-diffusive Oldroyd-B model, computed by the combined FD-FV scheme, Algorithm 3.

(a) σ_{11}

(b) ψ_{11}
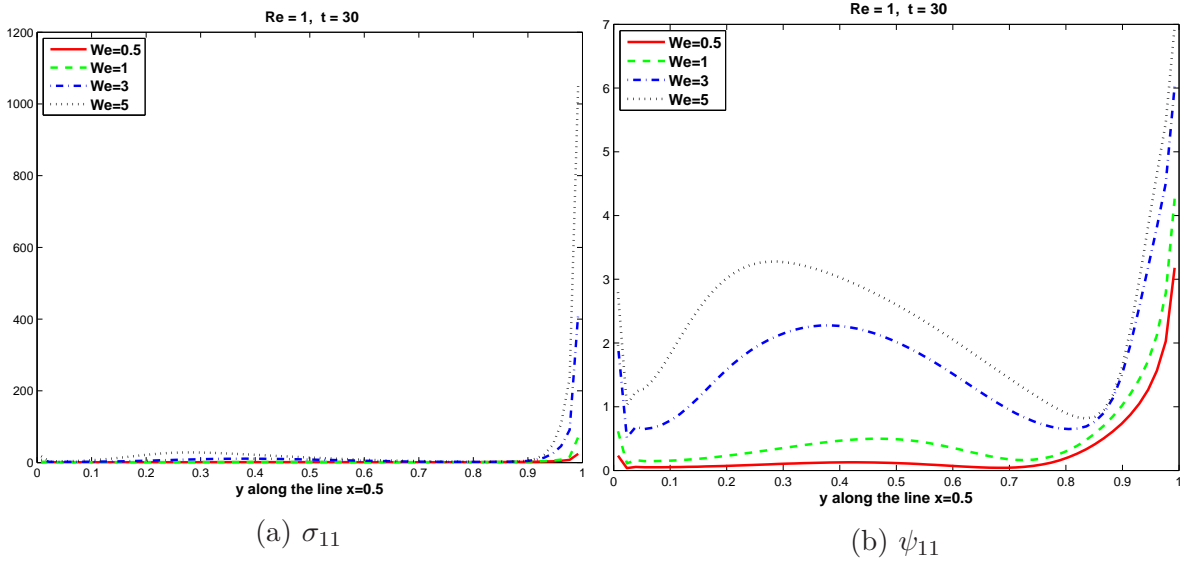
Figure 3.4: Conformation tensor component along $x = 0.5$ at $t = 30$, $Re = 1$, computed by the combined FD-FV scheme, Algorithm 3.

We show in Figure 3.4 σ_{11} and ψ_{11} along the line $x = 0.5$, which are the first component of the conformation tensor and the logarithm tensor at $t = 30$, $Re = 1$ for different We. Figure 3.4a obviously shows that σ_{11} grows exponentially large near the top boundary $y = 1$ for large We. Standard methods fail to capture the exponential profile is thought to be one of the reasons for the "HWNP". Thanks to the logarithm transformation approach, we are able to capture its logarithm, which is polynomial, see Figure 3.4b. This confirms the remark in Section 2.2.2. However, we can not say that the "HWNP" is solved as the numerical results do not converge in the sense of mesh refinement, see Table 3.2.

As mentioned before, standard methods without using log-transformation can not solve the problem for high Weissenberg number, i.e. $We > 1$. The advantage here is that the combined FD-FV scheme increases the Weissenberg limits with the help of the log-transformation.

Diffusive Oldroyd-B model

Now we switch to the diffusive Oldroyd-B model (2.20) where the log-transformation has also been applied. Solving the system with the FD-FV scheme, Algorithm 3, by setting $\varepsilon = 0.01$, we even get convergent results for $We = 1$, see Table 3.3.

Table 3.3: L^2-norm error with respect to mesh refinement and experimental order of convergence of the diffusive Oldroyd-B model for $\mathbf{u}, p, \nabla\mathbf{u}$ and $\boldsymbol{\sigma}$, computed by the combined FD-FV scheme, Algorithm 3.

mesh size h	$e(\mathbf{u}_h)$	$e(p_h)$	$e(\nabla\mathbf{u}_h)$	$e(\boldsymbol{\sigma}_h)$
1/32	1.18e-02	1.03e-03	1.40e-00	4.83e-01
1/64	3.84e-03	3.06e-04	7.38e-01	2.29e-01
1/128	8.43e-04	6.50e-05	2.62e-01	8.10e-02
EOC				
1/32	1.62	1.75	0.92	1.08
1/64	2.19	2.23	1.49	1.50

Influence of the Weissenberg number and the diffusion coefficient ε

This subsection aims to study the effects of the Weissenberg number We and the diffusion coefficient ε in the diffusive Oldroyd-B model (2.20) using the log-transformation. We will focus on the variation of the free energy components defined in the beginning of Section 2.3, which are the kinetic energy and entropy, according to the choice of parameters in the case of the driven cavity problem. The test is based on the characteristic finite element scheme, Algorithm 2, and the mesh used here is $M4$, see in Table 3.4.

For the study of the influence of the Weissenberg number, we fix the diffusion coefficient ε. By setting $\varepsilon = 1, 1e-2, 1e-3$, we present the kinetic and entropy of the diffusive Oldroyd-B model for different Weissenberg numbers $We = 0.1, 0.5, 1, 5, 50$ in Figures 3.5, 3.6 and 3.7. We can clearly see, that the kinetic energy decreases, while the entropy is increasing in time. Moreover, with increasing We, the entropy increases, while the kinetic energy behaves in a more complex way. Comparing with small diffusion coefficient $\varepsilon = 1e-3$, larger coefficient, $\varepsilon = 1e-2$ or $\varepsilon = 1$, stabilizes more the results.

Figure 3.5: Kinetic energy and entropy of the diffusive Oldroyd-B model (2.20) for different Weissenberg numbers, $\varepsilon = 1$, computed by characteristic FEM, Algorithm 2.
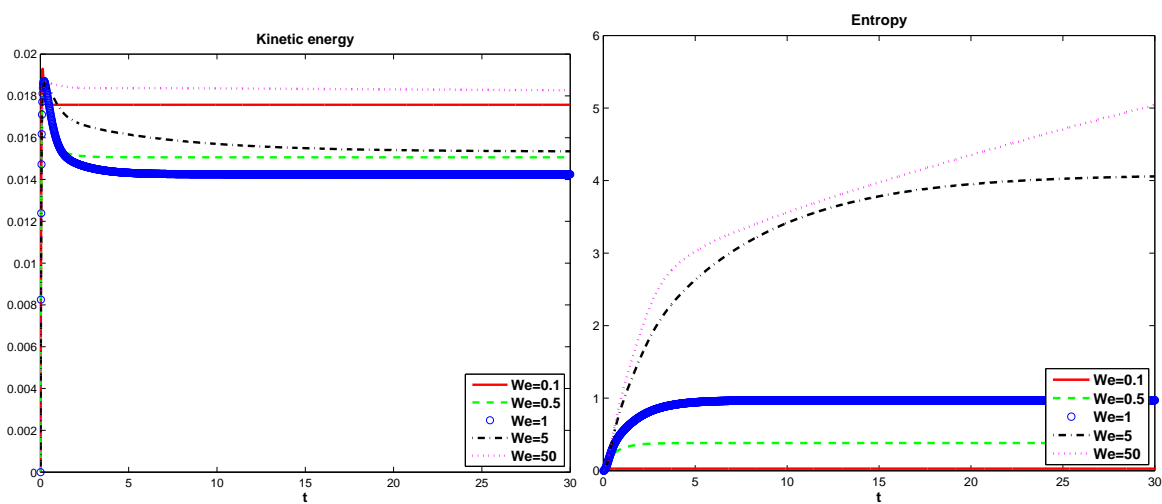
Figure 3.6: Kinetic and entropy for the diffusive Oldroyd-B model (2.20), $\varepsilon = 0.01$, computed by characteristic FEM, Algorithm 2.
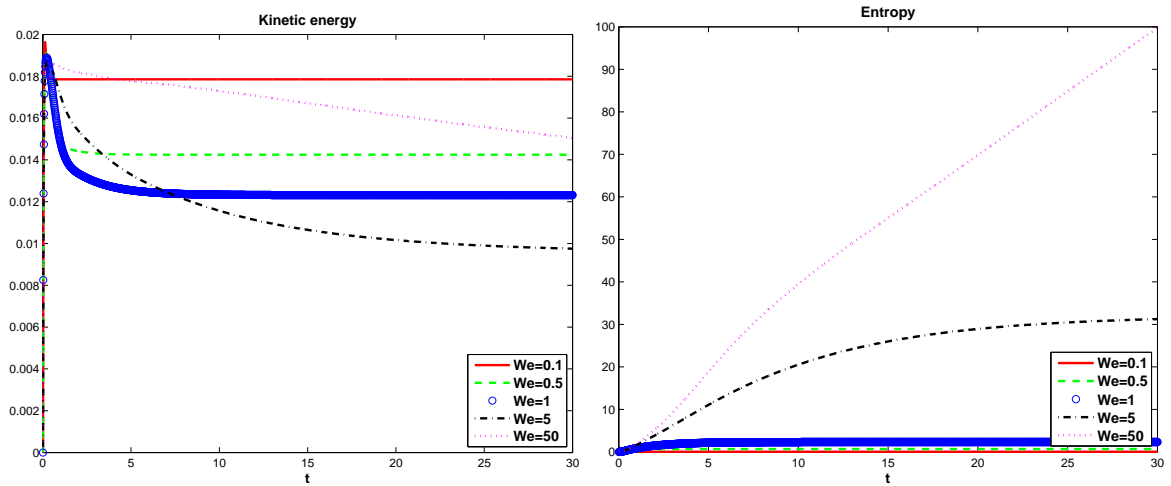
Figure 3.7: Kinetic energy and entropy of the diffusive Oldroyd-B model (2.20) for different Weissenberg numbers, $\varepsilon = 1e - 3$, computed by characteristic FEM, Algorithm 2.

In the next experiment, we fix the Weissenberg number We and study the influence of the diffusion coefficient ε. By setting $We = 0.5$ and 5, we show the results of kinetic energy and entropy for different diffusion coefficients $\varepsilon = 1e - 3, 1e - 2, 1e - 1, 1$ in Figure 3.8 and 3.9, respectively. We can notice that for higher $\varepsilon; \varepsilon \geq 1e - 2$, we have almost constant behaviour of the kinetic energy and entropy.
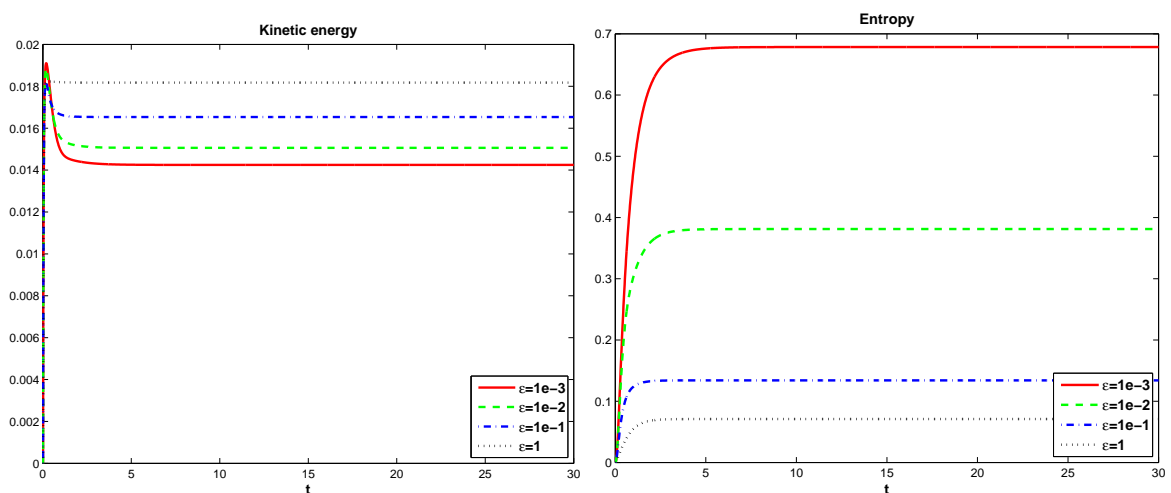
Figure 3.8: Kinetic energy and entropy of the diffusive Oldroyd-B model (2.20) for different diffusion coefficients ε at $We = 0.5$, computed by characteristic FEM, Algorithm 2.
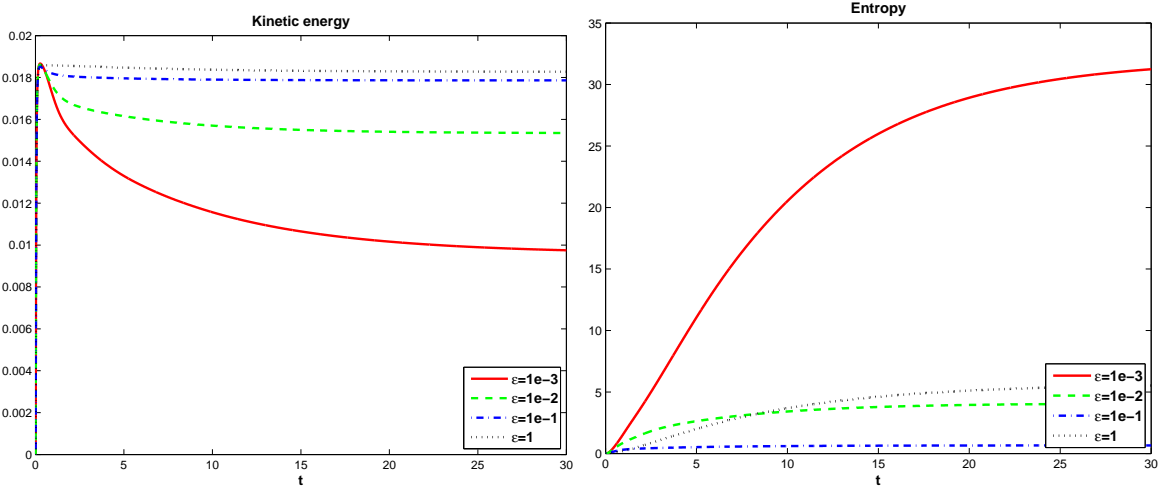
Figure 3.9: kinetic energy and entropy of the diffusive Oldroyd-B model (2.20) for different diffusion coefficients ε at $We = 5$, computed by characteristic FEM, Algorithm 2.

Comparison of different discretization schemes

In this test case we want to compare the behavior of the numerical methods: Algorithm 4 and Algorithm 2, that we have introduced and studied analytically in Sections 3.2 and 3.3, respectively, for the diffusive logarithm Oldroyd-B model (2.20).

For the characteristic FD method, we set the mesh size to be $h_x = h_y = 1/64 = 0.015625$. Time step is chosen as

$$\Delta t = \text{CFL}\frac{h_x}{\max(|U|, |V|)}, \text{ with } \mathbf{u} = (U, V), \tag{3.49}$$

where CFL is chosen as 0.6. For the characteristic FEM method, our triangular mesh information is $M4$ which is given in Table 3.4.

Table 3.4: Mesh information of the characteristic FEM.

mesh	number of mesh point	number of element	average mesh size
M1	94	154	1.27e-01
M2	330	594	6.37e-02
M3	1278	2426	3.15e-02
M4	4987	9716	1.58e-02

The mesh size of $M4$ is comparable with the above FD discretization. Now let us compare their results. First we choose a small diffusion coefficient $\varepsilon = 0.01$ and represent the kinetic energy in Figure 3.10.
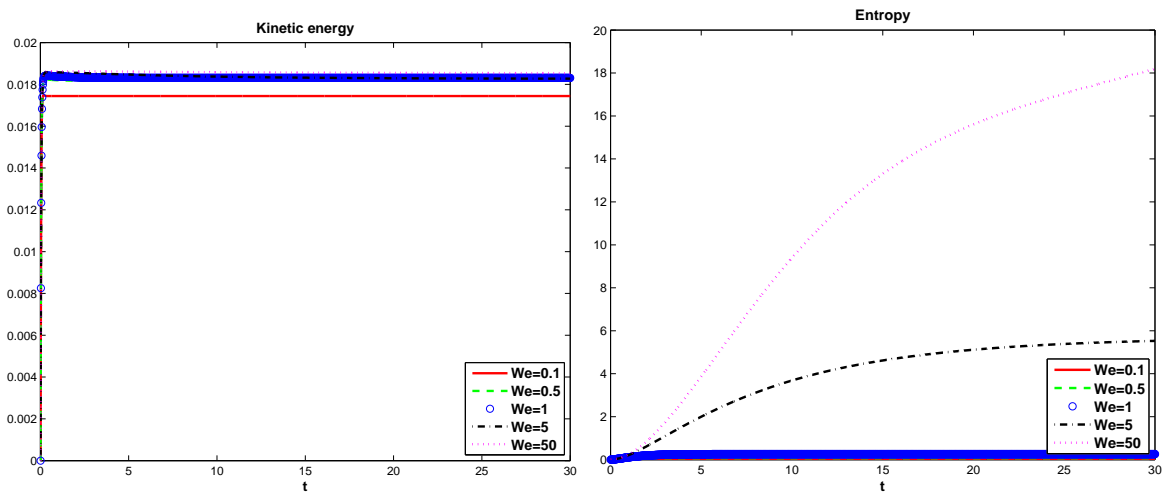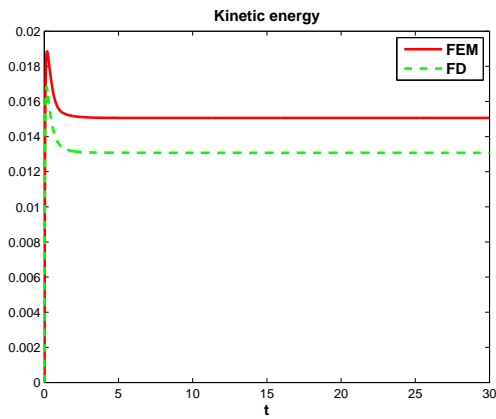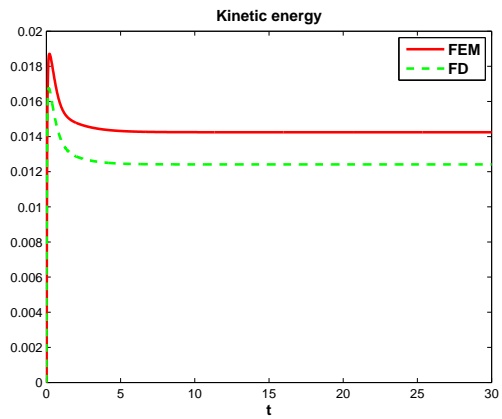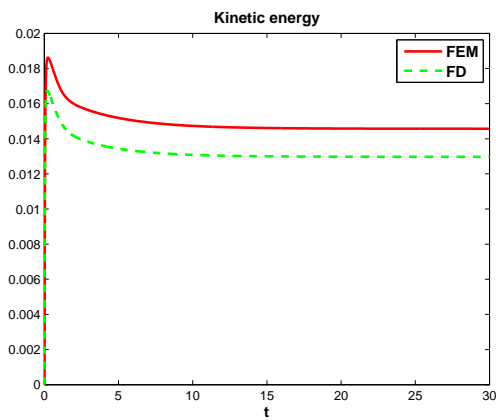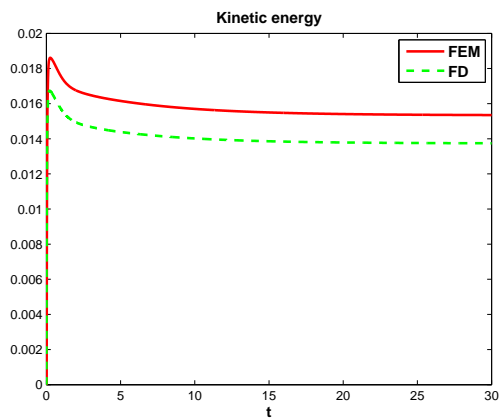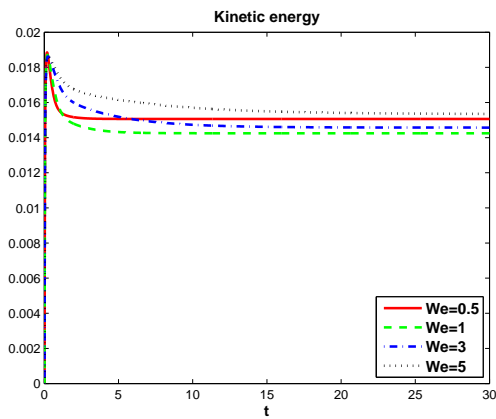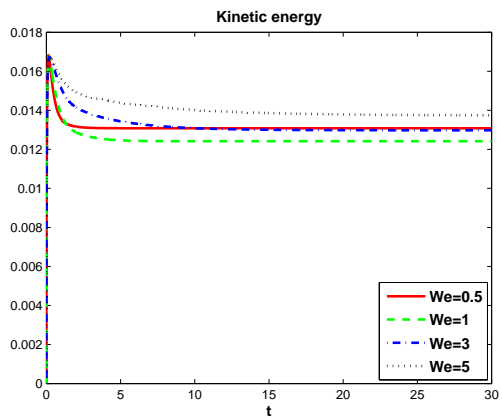
Figure 3.10: Kinetic energy of the diffusive Oldroyd-B model (2.20) for different Weissenberg numbers, computed by characteristic FEM 2 and characteristic FD 4.

We see clearly that the kinetic energy computed by the characteristic FEM is bigger than that of the characteristic FD scheme. For both scheme, the kinetic energy is decreasing in time. Moreover, if $We < 1$ the absolute value for different We are decreasing,

while if $We > 1$ the absolute values increase for increasing We, see the values of the steady state in Figure 3.10e and 3.10f.

Experimental convergence analysis

The aim of this section is to analyze the experimental order of convergence of different numerical schemes and various Weissenberg numbers for the diffusive Oldroyd-B model (2.20), where the logarithm transformation has been applied. Let ϕ_h denote the numerical solution and ϕ be the corresponding exact solution. We define the L^2-norm for the characteristic FD scheme

$$\|\phi_h\|_{L^2} = \left(\sum_{K \in \mathcal{T}_h} (\phi_h|_K)^2 |K| \right)^{1/2}, \|\phi_h\|_{H^1} = \left(\|\phi_h\|_{L^2}^2 + \sum_{K \in \mathcal{T}_h} (\nabla_h \phi_h|_K)^2 |K| \right)^{1/2}. \quad (3.50)$$

In the characteristic FEM we have used the $\mathcal{P}^1$ elements. Let $P_i, i = 1, 2, 3$, be the three nodal points of the element K and $\varphi_i \in \mathcal{P}^1(K), i = 1, 2, 3$, be the corresponding local basis functions,

$$\varphi_i(x, y) = \frac{a_i + b_i x + c_i y}{2|K|} \quad (3.51)$$

where $|K|$ is the area of element

$$|K| = \frac{1}{2} \det \begin{bmatrix} 1 & x_1 & y_1 \\ 1 & x_2 & y_2 \\ 1 & x_3 & y_3 \end{bmatrix} = \frac{1}{2}(x_2 - x_1)(y_3 - y_1) - (x_3 - x_1)(y_2 - y_1) \quad (3.52)$$

and

$$a_1 = x_2 y_3 - x_3 y_2, b_1 = y_2 - y_3, c_1 = x_3 - x_2, \quad (3.53)$$

etc., with cyclic rotation of indices 1, 2, and 3, cf. [89]. Further we have $\phi_h(x, y)|_K = \sum_{i=1}^{3} \phi_h(P_i)\varphi_i(x, y)$. Now we define the norm as

$$\|\phi_h\|_{L^2} = \left(\sum_{K \in \mathcal{T}_h} \int_K \sum_{i=1}^{3} \sum_{j=1}^{3} \phi_h(P_i)\varphi_i(x, y)\phi_h(P_j)\varphi_j(x, y) \right)^{1/2}, \quad (3.54a)$$

$$\|\phi_h\|_{H^1} = \left(\|\phi_h\|_{L^2}^2 + \sum_{K \in \mathcal{T}_h} \int_K \sum_{i=1}^{3} \sum_{j=1}^{3} \nabla_h \phi_h(P_i)\varphi_i(x, y) \cdot \nabla_h \phi_h(P_j)\varphi_j(x, y) \right)^{1/2}. \quad (3.54b)$$

Further, we denote the L^2-error as $e(\phi_h) = \|\phi_h - \phi\|_{L^2}$ and H^1-error $e_1(\phi_h) = \|\phi_h - \phi\|_{H^1}$. In our experiment the exact solution ϕ is replaced by the solution computed at a very fine mesh as the exact analytical solution is not available. The experimental order of convergence (EOC) is defined as

$$\text{EOC} = \log_2 \left(e(\phi_h)/e(\phi_{h/2}) \right). \quad (3.55)$$

Tables 3.5, 3.6, 3.7 and 3.8 illustrate the mesh convergence results of the characteristic finite element method at $t = 30$ for different Weissenberg numbers.

Table 3.9 performs the mesh convergence results for characteristic finite difference method Algorithm 4 at $t = 4$ with different Weissenberg numbers.

Table 3.5: Error norms and EOC for diffusive Oldroyd-B model (2.20), $\varepsilon = 0.01$, We=0.5, computed by characteristic FEM, Algorithm 2.

Error						
h	$e(\mathbf{u}_h)$	$e(p_h)$	$e(\boldsymbol{\sigma}_h)$	$e_1(u)$	$e_1(p_h)$	$e_1(\boldsymbol{\sigma}_h)$
1/8	1.77e-02	2.11e-01	4.46e-01	6.24e-01	6.97e-01	6.33e+00
1/16	5.32e-03	5.88e-02	1.04e-01	3.45e-01	2.32e-01	3.35e+00
1/32	1.23e-03	2.36e-02	2.87e-02	1.64e-01	8.74e-02	1.69e+00
1/64	3.41e-04	8.77e-03	8.57e-03	8.05e-02	3.90e-02	8.39e-01
1/128	8.89e-05	3.97e-03	2.37e-03	4.08e-02	1.87e-02	3.97e-01
EOC						
1/8	1.73	1.84	2.10	0.85	1.58	0.92
1/16	2.12	1.32	1.85	1.07	1.41	0.99
1/32	1.85	1.43	1.74	1.03	1.17	1.01
1/64	1.94	1.14	1.85	0.98	1.06	1.08

Table 3.6: Error norms and EOC for diffusive Oldroyd-B model (2.20), $\varepsilon = 0.01$, We=1, computed by characteristic FEM, Algorithm 2.

Error						
h	$e(\mathbf{u}_h)$	$e(p_h)$	$e(\boldsymbol{\sigma}_h)$	$e_1(u)$	$e_1(p_h)$	$e_1(\boldsymbol{\sigma}_h)$
1/8	1.84e-02	2.42e-01	1.05e+00	6.33e-01	7.55e-01	1.45e+01
1/16	5.41e-03	6.74e-02	2.29e-01	3.49e-01	2.35e-01	6.64e+00
1/32	1.26e-03	2.63e-02	6.14e-02	1.65e-01	8.91e-02	3.17e+00
1/64	3.40e-04	1.06e-02	2.19e-02	8.14e-02	3.97e-02	1.60e+00
1/128	8.46e-05	4.61e-03	7.51e-03	4.14e-02	1.90e-02	7.58e-01
EOC						
1/8	1.76	1.84	2.20	0.86	1.68	1.13
1/16	2.10	1.36	1.90	1.08	1.40	1.07
1/32	1.89	1.32	1.48	1.02	1.17	0.99
1/64	2.00	1.20	1.55	0.98	1.06	1.08

Table 3.7: Error norms and EOC for diffusive Oldroyd-B model (2.20), $\varepsilon = 0.01$, We=5, computed by characteristic FEM, Algorithm 2.

			Error			
h	$e(\mathbf{u}_h)$	$e(p_h)$	$e(\boldsymbol{\sigma}_h)$	$e_1(u)$	$e_1(p_h)$	$e_1(\boldsymbol{\sigma}_h)$
1/8	1.56e-02	1.84e-01	2.12e+00	5.85e-01	5.55e-01	3.15e+01
1/16	4.69e-03	9.74e-02	1.06e+00	3.19e-01	2.19e-01	1.86e+01
1/32	1.08e-03	3.07e-02	3.27e-01	1.51e-01	8.18e-02	8.05e+00
1/64	3.16e-04	1.21e-02	1.31e-01	7.54e-02	3.68e-02	4.12e+00
1/128	9.00e-05	4.61e-03	4.32e-02	3.85e-02	1.72e-02	1.98e+00
			EOC			
1/8	1.73	0.91	0.99	0.88	1.34	0.76
1/16	2.11	1.67	1.70	1.07	1.42	1.21
1/32	1.78	1.34	1.32	1.01	1.15	0.97
1/64	1.81	1.39	1.60	0.97	1.10	1.05

Table 3.8: Error norms and EOC for diffusive Oldroyd-B model (2.20), $\varepsilon = 0.01$, We=50, computed by characteristic FEM, Algorithm 2.

			Error			
h	$e(\mathbf{u}_h)$	$e(p_h)$	$e(\boldsymbol{\sigma}_h)$	$e_1(u)$	$e_1(p_h)$	$e_1(\boldsymbol{\sigma}_h)$
1/8	1.37e-02	1.16e-01	3.21e+00	5.52e-01	4.33e-01	3.54e+01
1/16	3.93e-03	4.99e-02	1.23e+00	2.99e-01	1.88e-01	2.09e+01
1/32	8.03e-04	1.70e-02	3.38e-01	1.39e-01	7.47e-02	8.40e+00
1/64	1.97e-04	7.01e-03	9.71e-02	7.29e-02	3.54e-02	4.23e+00
			EOC			
1/8	1.80	1.22	1.38	0.88	1.21	0.76
1/16	2.29	1.55	1.86	1.10	1.33	1.31
1/32	2.02	1.28	1.80	0.93	1.07	0.99

Table 3.9: Error norms and EOC for diffusive Oldroyd-B model (2.20), $\varepsilon = 0.01$, computed by characteristic finite difference method, Algorithm 4.

(a) We=0.5

h	$e(\mathbf{u}_h)$	$e(p_h)$	$e(\nabla\mathbf{u}_h)$	$e(\boldsymbol{\sigma}_h)$	$e_1(\mathbf{u}_h)$	$e_1(\boldsymbol{\sigma}_h)$
			Error			
1/8	2.59e-02	4.06e-04	2.15e-01	3.21e-01	2.17e-01	5.77e+00
1/16	7.87e-03	1.27e-04	7.11e-02	1.23e-01	7.16e-02	3.02e+00
1/32	1.85e-03	3.60e-05	1.95e-02	4.15e-02	1.96e-02	1.03e+00
1/64	3.44e-04	9.00e-06	4.58e-03	1.21e-02	4.59e-03	2.93e-01
			EOC			
1/8	1.72	1.68	1.60	1.38	1.60	0.93
1/16	2.09	1.82	1.87	1.57	1.87	1.55
1/32	2.43	2.00	2.09	1.78	2.09	1.82

(b) We=1

h	$e(\mathbf{u}_h)$	$e(p_h)$	$e(\nabla\mathbf{u}_h)$	$e(\boldsymbol{\sigma}_h)$	$e_1(\mathbf{u}_h)$	$e_1(\boldsymbol{\sigma}_h)$
			Error			
1/8	2.70e-02	3.30e-04	2.25e-01	7.38e-01	2.26e-01	1.06e+01
1/16	7.93e-03	9.20e-05	7.54e-02	2.44e-01	7.58e-02	5.58e+00
1/32	1.88e-03	2.50e-05	2.23e-02	7.81e-02	2.24e-02	1.91e+00
1/64	3.84e-04	7.00e-06	5.88e-03	2.39e-02	5.89e-03	5.61e-01
			EOC			
1/8	1.77	1.84	1.58	1.60	1.58	0.92
1/16	2.08	1.88	1.76	1.64	1.76	1.55
1/32	2.29	1.84	1.92	1.71	1.92	1.77

(c) We=5

h	$e(\mathbf{u}_h)$	$e(p_h)$	$e(\nabla\mathbf{u}_h)$	$e(\boldsymbol{\sigma}_h)$	$e_1(\mathbf{u}_h)$	$e_1(\boldsymbol{\sigma}_h)$
			Error			
1/8	2.50e-02	1.57e-04	2.08e-01	1.45e+00	2.10e-01	1.93e+01
1/16	7.08e-03	3.90e-05	6.31e-02	4.39e-01	6.35e-02	9.70e+00
1/32	1.69e-03	9.00e-06	1.64e-02	1.79e-01	1.65e-02	3.37e+00
1/64	3.24e-04	3.00e-06	3.67e-03	6.71e-02	3.69e-03	1.04e+00
			EOC			
1/8	1.82	2.01	1.72	1.72	1.72	0.99
1/16	2.07	2.12	1.94	1.29	1.94	1.53
1/32	2.38	1.58	2.16	1.42	2.16	1.70

3.4.2 4 to 1 contraction flow

In this test we will consider one of the most well-known benchmarks for the viscoelastic fluids, the so-called 4:1 contraction problem. Hereby, the Algorithm 2 will be studied for the diffusive Oldroyd-B model (2.20) as well as the non-diffusive model (2.19). Let us point out that the log-transformation has been applied for both models. Previous studies on the numerical simulation of this problem can be found, e.g. [1, 4, 32, 39, 59,

64, 65, 73, 85, 88]. One of the main difficulties is the singularity at the re-entrant corner due to the abrupt contraction [39, 65].
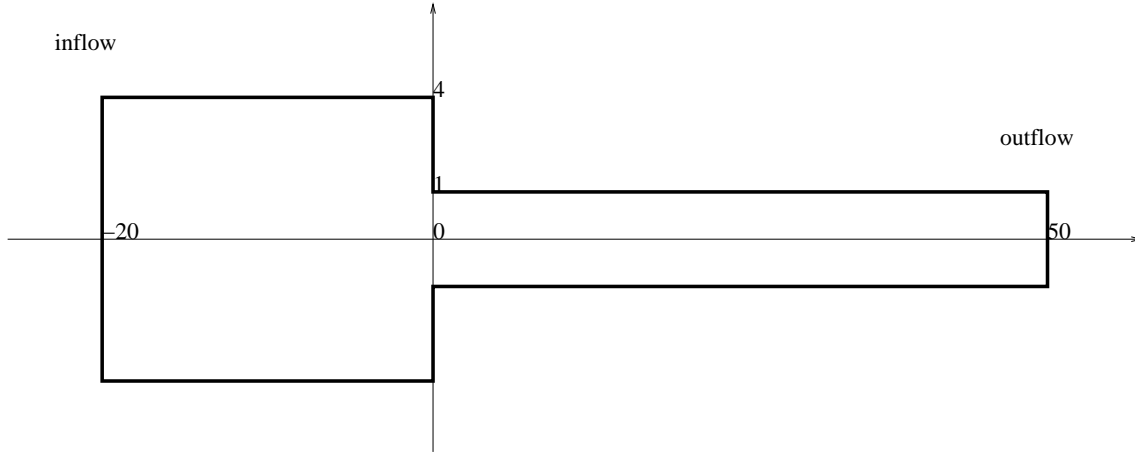
Figure 3.11: Geometry of 4:1 contraction flow.

As shown in Figure 3.11, the computational domain is taken to be from $x = -20$ to $x = 50$, the upstream has a width of 8 while downstream's width is set to be 2. Similar to [19] we use only the upper half of the computational domain as it is symmetric with respect to x axis.

We assume the flow to be fully developed at the inlet. A parabolic Dirichlet condition is used for the velocity

$$U = \frac{1}{8}(1 - y^2/16), \ V = 0, \ \text{with } \mathbf{u} = (U, V). \tag{3.56a}$$

The inflow boundary condition for the conformation tensor can be analytically derived [30, 32]

$$\boldsymbol{\sigma} = \begin{pmatrix} 1 + 2(We\frac{\partial U}{\partial y})^2 & We\frac{\partial U}{\partial y} \\ We\frac{\partial U}{\partial y} & 1 \end{pmatrix}. \tag{3.56b}$$

Analogously to many references, e.g. [59, 65], we assume that the downstream length is long enough such that the flow at outlet is also fully developed, which leads to the Dirichlet condition for the velocity at outlet

$$U = \frac{1}{2}(1 - y^2), \ V = 0. \tag{3.56c}$$

In comparison to that, the zero Neumann boundary condition is also applied at the outlet for velocity. If not specified, the boundary condition at the outlet is set according to (3.56c). Moreover, no-slip conditions are imposed on the solid walls and symmetry conditions are specified on the symmetric axis.

$$\sigma_{12}(x, 0) = V(x, 0) = 0. \tag{3.56d}$$

Other parameters are chosen similarly to the above references.

$$\alpha = 1/9, Re = 0.$$
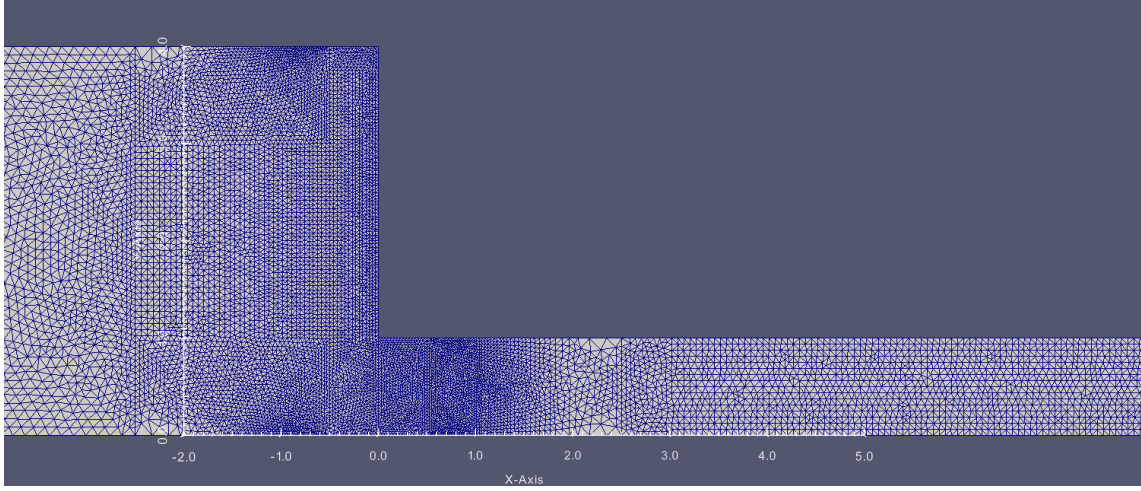
Figure 3.12: Mesh of 4:1 contraction flow, created by "FreeFEM++-cs" [55].

The center of the computational mesh for the 4:1 contraction flow is shown in Figure 3.12, with a local refinement near the abrupt contraction corner. Details of the mesh are as follows. Total number of mesh points, elements are $np = 26538$, $ne = 50874$. Maximum, minimum and mean values of the mesh diagram are $(hmax, hmin, hmean) = (2.05e - 01, 1.62e - 02, 7.29e - 02)$.

Non-diffusive Oldroyd-B model

We first present the results of the non-diffusive Oldroyd-B model (2.19). Figure 3.14 shows the results of $We = 3$ at $t = 1$. We can see a big vertex at the up corner of abrupt contraction. The pressure is decreasing along the x axis.

In Figure 3.15 we compare the results for different Weissenberg numbers. Figure 3.15a indicates that the pressure is decreasing along the x axis, with a gradual decline rate in the upstream region and a steeper rate in the downstream channel. Moreover, it can be concluded that bigger We cause to smaller pressure drop at outlet with respect to the inlet pressure. Velocities of different We are almost the same. In Figures 3.15c and 3.15d we can see that there are jumps for the conformation tensor at the contraction corner, and the jumps are larger for large We.

Diffusive Oldroyd-B model

In the following test we will present the results for the diffusive Oldroyd-B model. Figures 3.16 and 3.17 show the results of different We for $\varepsilon = 0.01$ and 1, respectively. Similar to the non-diffusive model, the pressure is decreasing along x-axis and larger We cause to smaller pressure drop. The jumps of the conformation tensor around the contraction corner are bigger for larger We. Comparing with the results of smaller diffusion

coefficients, e.g. $\varepsilon \leq 0.01$, the results of larger diffusion ($\varepsilon = 1$) are quite different. First, the value of pressure at the inlet are getting smaller. The second point is that velocity in the downstream region along the x-axis are getting larger for larger We (see Figure 3.17b), which almost does not change for small diffusion coefficients $\varepsilon \leq 0.01$ (see Figures 3.16b and 3.15b). The conformation tensor in the downstream region is also changing for different We. The values are getting smaller for larger We. The last point is that both velocity and conformation tensor have a jump of the magnitude $1e - 2$ near the outlet for $\varepsilon = 1$.

In the next experiment, we study the influence of different outlet boundary conditions for velocity. By setting $\varepsilon = 0.01, 1$ and $We = 5$ we show the results in Figure 3.18. It can be observed that, both velocity and conformation tensor at the outlet are more stable in the case of applying Dirichlet boundary condition for velocity.

In Figure 3.13 we show the results of kinetic energy and free energy for different Weissenberg numbers. With the increase of We, the kinetic energy are the same while the entropy is increasing in a short time.

(a) Kinetic energy (b) Entropy
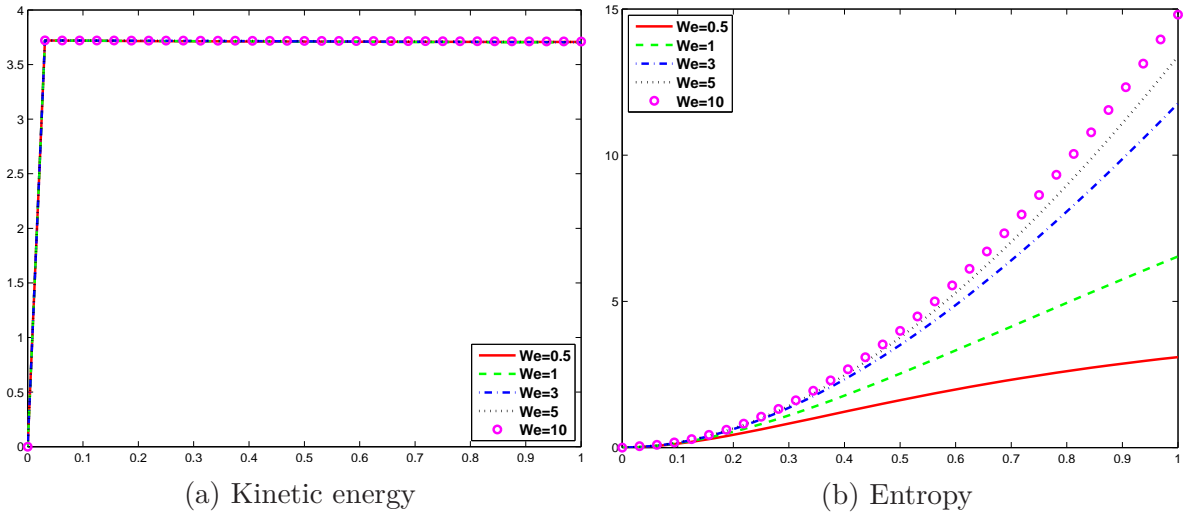
Figure 3.13: Evolution of the diffusive Oldroyd-B model, $\varepsilon = 0.01$ for different We: kinetic energy and entropy, computed by characteristic FEM, Algorithm 2.

From the above two test problems we conclude that the diffusive model is more stable. In the driven cavity test we have observed the mesh convergent results of the diffusive Oldroyd-B model even for very high Weissenberg numbers, where the logarithm transformation has been applied. Our numerical experiments demonstrate that the flow in the 4:1 contraction channel is a much severe test case. Although we were able to obtain numerically stable results for $We = 10$, the mesh convergence has not been achieved. This can be of our future research.
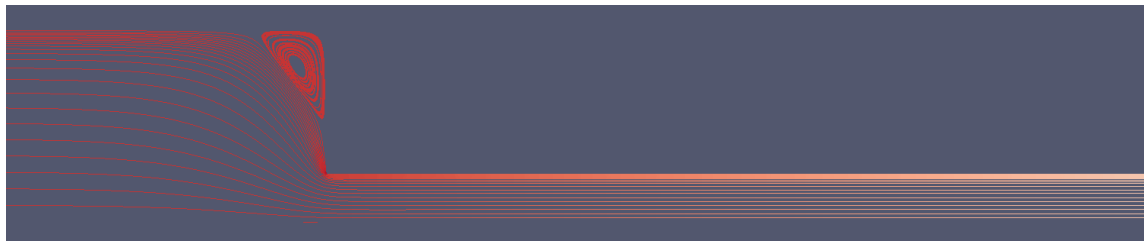
(a) Streamlines

(b) Pressure: min=0, max=19.2
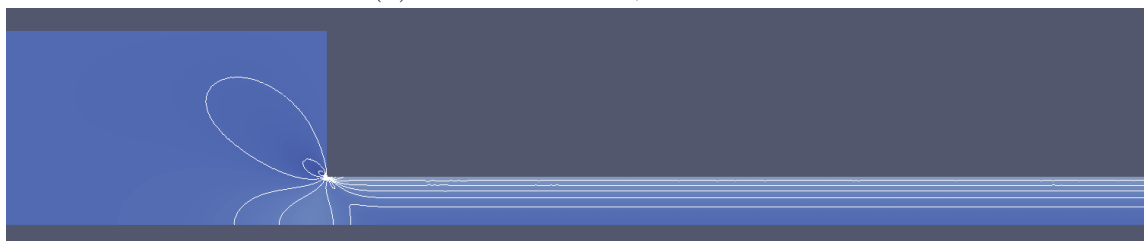
(c) Conformation tensor σ_{11}: min=0.398, max=4.54
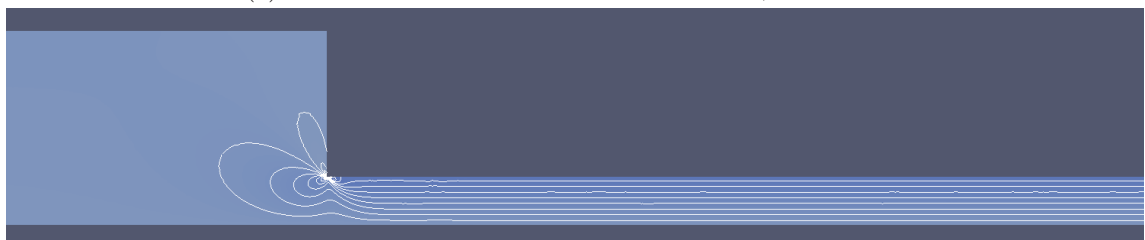
(d) Conformation tensor σ_{12}: min=-2.05, max=0.8

(e) Conformation tensor σ_{22}: min=0.745, max=2.76

Figure 3.14: Results of the non-diffusive Oldroyd-B model at $We = 3, t = 1$, from up to down are streamline, contour lines for pressure, $\boldsymbol{\sigma}_{11}$, $\boldsymbol{\sigma}_{12}$ and $\boldsymbol{\sigma}_{22}$, computed by characteristic FEM, Algorithm 2.

(a) Pressure along $y = 0$

(b) Velocity component U along $y = 0$

(c) σ_{11} along $y = 0$

(d) σ_{22} along $y = 0$

Figure 3.15: Results of the non-diffusive Oldroyd-B model at $t = 1$ along the symmetric axis $y = 0$ for different We: pressure p, velocity component U, conformation components $\boldsymbol{\sigma}_{11}$ and $\boldsymbol{\sigma}_{22}$, computed by characteristic FEM, Algorithm 2.

(a) Pressure along $y = 0$

(b) Velocity component U along $y = 0$

(c) σ_{11} along $y = 0$

(d) σ_{22} along $y = 0$

Figure 3.16: Results of the diffusive Oldroyd-B model, $\varepsilon = 0.01$, at $t = 1$ along the symmetric axis $y = 0$ for different We: pressure p, velocity component U, conformation components $\boldsymbol{\sigma}_{11}$ and $\boldsymbol{\sigma}_{22}$, computed by characteristic FEM, Algorithm 2.

(a) Pressure along $y = 0$

(b) Velocity component U along $y = 0$

(c) σ_{11} along $y = 0$

(d) σ_{22} along $y = 0$

Figure 3.17: Results of the diffusive Oldroyd-B model, $\varepsilon = 1$, at $t = 1$ along the symmetric axis $y = 0$ for different We: pressure p, velocity component U, conformation components $\boldsymbol{\sigma}_{11}$ and $\boldsymbol{\sigma}_{22}$, computed by characteristic FEM, Algorithm 2.

(a) Pressure along $y = 0$

(b) Velocity component U along $y = 0$

(c) σ_{11} along $y = 0$

(d) σ_{22} along $y = 0$
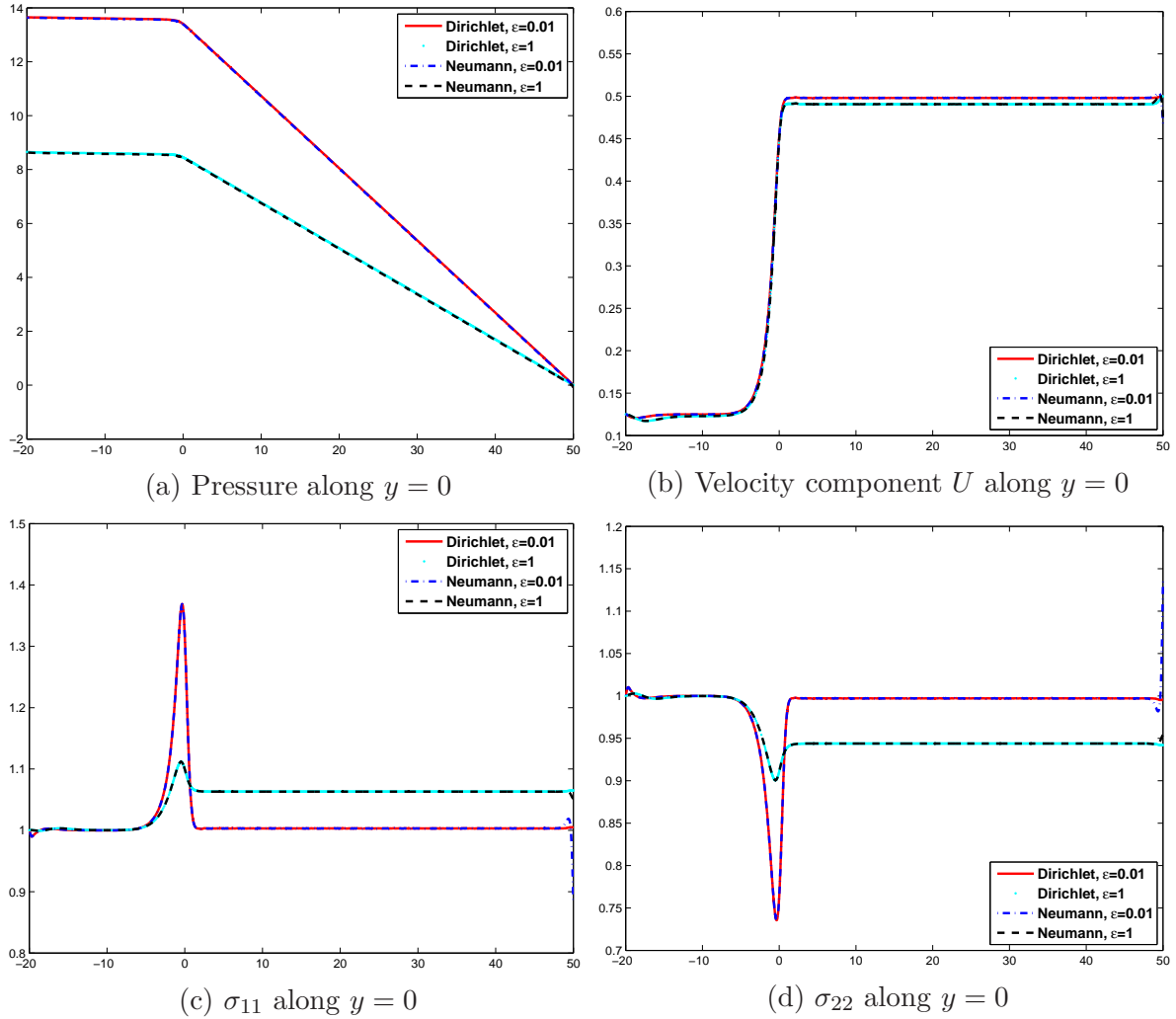
Figure 3.18: Results of the diffusive Oldroyd-B model, at $t = 1$ along the symmetric axis $y = 0$ for different ε and different outlet boundary conditions: pressure p, velocity component U, conformation components $\boldsymbol{\sigma}_{11}$ and $\boldsymbol{\sigma}_{22}$, computed by characteristic FEM, Algorithm 2.

4 Error analysis of the finite element and finite volume methods for a special Oldroyd-B model

This chapter is a part of the work [62]. We will study a variation of the classical Oldroyd-B visocelastic model (4.1), which has been theoretically studied by Lin et al. [60].

Concerning this model, we should mention that the question of global in time existence of weak solutions is still open. On the other hand, the local existence of strong solutions has been proven in [20, 53, 52], as well as in [60], where the global in time existence of regular weak solution has also been presented.
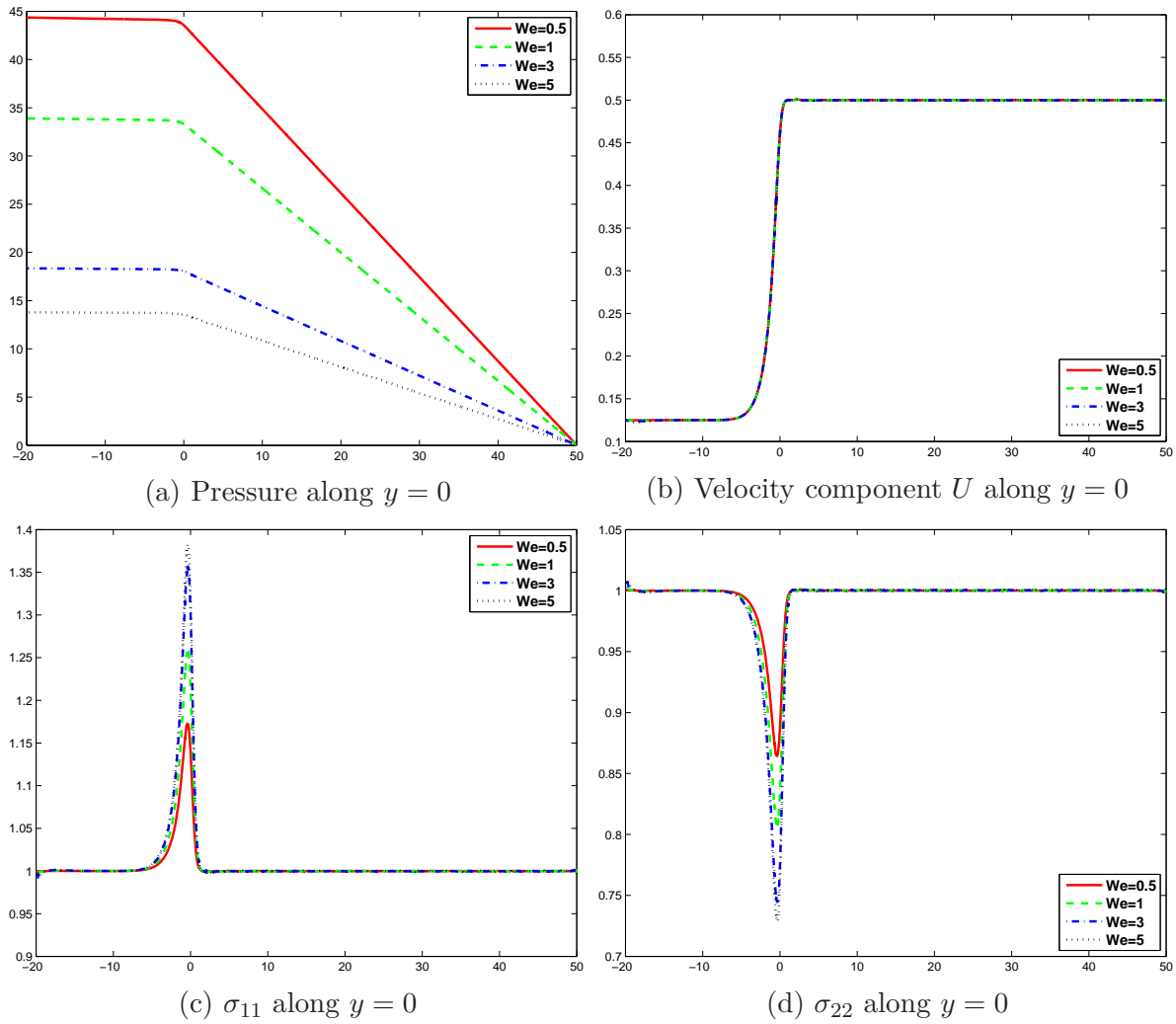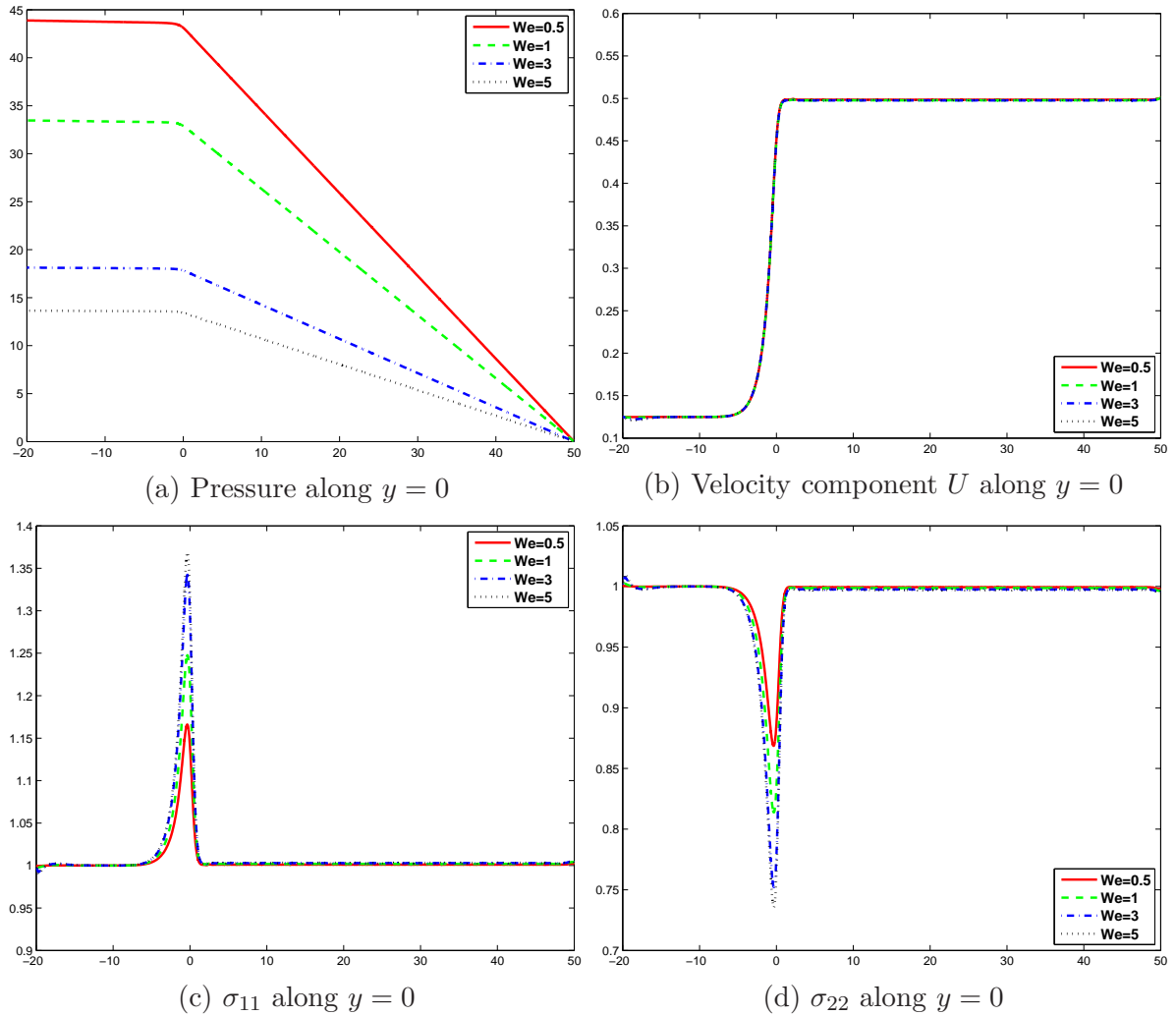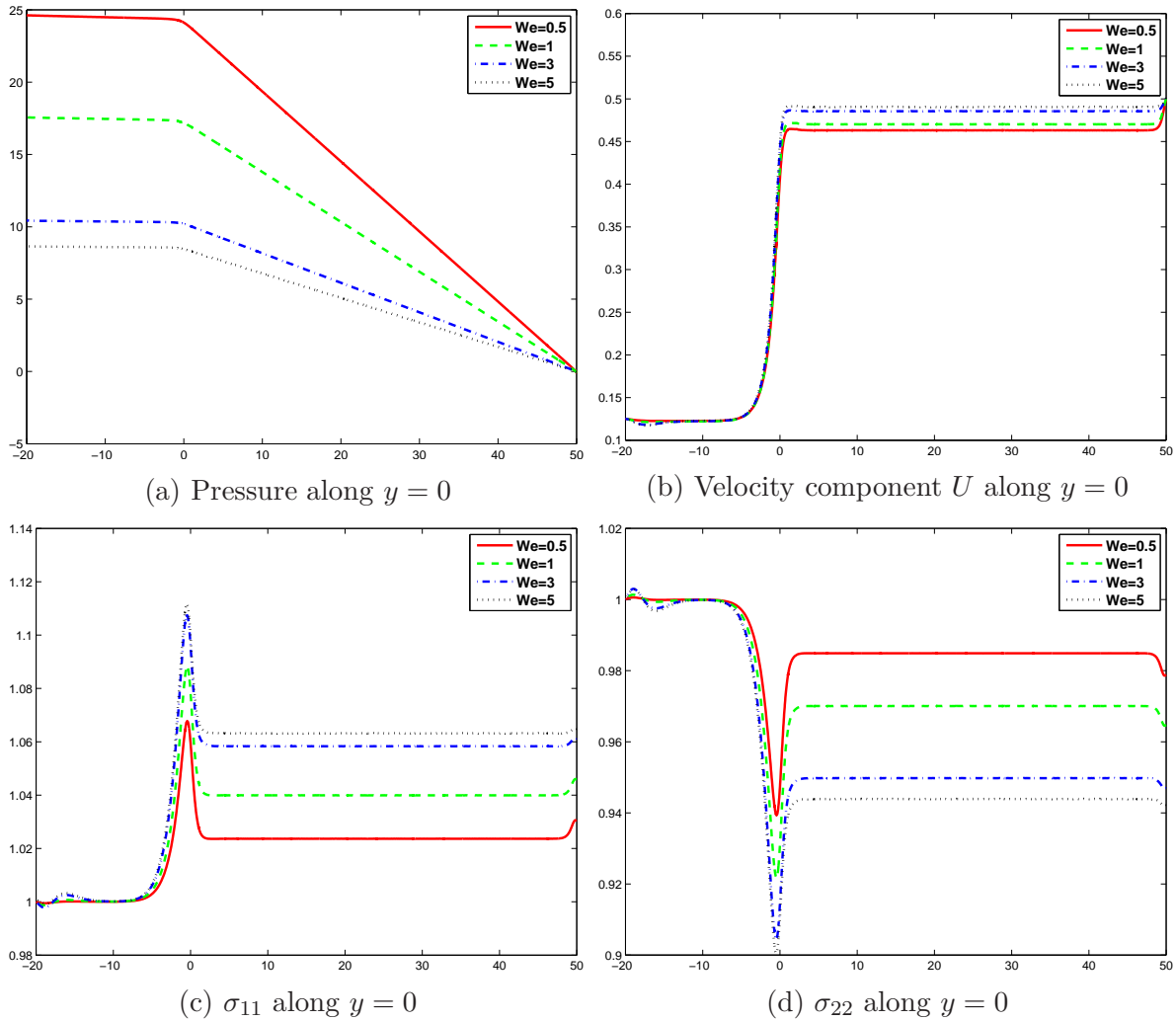
The aim of this chapter is to present the error analysis of a finite element-finite volume (FE-FV) approximation of the problem.

The chapter is organized as follows. In Section 4.1 we will introduce the model and its FE-FV approximation. The main result on the convergence rates as well as its proof will be stated in Section 4.2. In the last section we will validate theoretical error estimates by the numerical experiments.

4.1 Modelling and numerical approximations

4.1.1 Governing equations

We consider in a bounded domain $\Omega \subset \mathbb{R}^2$ the following viscoelastic model, which can be achieved as a limiting case of the Oldroyd-B model when the relaxation time goes to infinity. Note that this assumption is equivalent to the fact that the Weissenberg number We is set to infinity.

$$\partial_t \mathbf{u} + \mathbf{u} \cdot \nabla \mathbf{u} = -\nabla p + \Delta \mathbf{u} + \nabla \cdot (\mathbf{F}\mathbf{F}^T), \qquad (4.1a)$$

$$\nabla \cdot \mathbf{u} = 0, \qquad (4.1b)$$

$$\partial_t \mathbf{F} + \mathbf{u} \cdot \nabla \mathbf{F} = \nabla \mathbf{u} \mathbf{F}. \qquad (4.1c)$$

The system is closed with the no-slip boundary condition

$$\mathbf{u}|_{\partial\Omega} = 0 \qquad (4.1d)$$

and the initial condition

$$\mathbf{u}(0, \cdot) = \mathbf{u}_0, \qquad \mathbf{F}(0, \cdot) = \mathbf{F}_0. \qquad (4.1e)$$

Indeed, when setting the elastic part of the stress tensor $\boldsymbol{\tau} = \mathbf{F}\mathbf{F}^T$ we recover the Oldroyd-B model (2.7) with $We \to \infty$. This is achieved simply through multiplying

(4.1c) by $\mathbf{F}^T$ and summing the result with its transpose

$$\partial_t \boldsymbol{\tau} + \mathbf{u} \cdot \nabla \boldsymbol{\tau} - \nabla \mathbf{u} \boldsymbol{\tau} - \boldsymbol{\tau} \nabla \mathbf{u}^T = 0. \tag{4.2}$$

Assumptions on regularity of the solution to (4.1). It has been proven in [60, Theorem 2.2] that for initial data of the form

$$\mathbf{F}_0 = \nabla \times \boldsymbol{\Phi}_0, \quad \nabla \boldsymbol{\Phi}_0 \in W^{k,2}(\Omega), \ \boldsymbol{u}_0 \in W^{k,2}(\Omega), \ k \geq 2, \tag{4.3}$$

there exists a positive time T, which depends only on $\|\nabla \boldsymbol{\varphi}_0\|_{2,2}$ and $\|\boldsymbol{u}_0\|_{2,2}$, such that the system (4.1) possesses a unique solution in the time interval $[0, T]$ with

$$\begin{aligned}
\partial_t^j \nabla^\alpha \boldsymbol{u} &\in L^\infty(0, T; W^{k-2j-|\alpha|,2}(\Omega)) \cap L^2(0, T; W^{k-2j-|\alpha|+1,2}(\Omega)), \\
\partial_t^j \nabla^\alpha \mathbf{F} &\in L^\infty(0, T; W^{k-2j-|\alpha|,2}(\Omega)),
\end{aligned} \tag{4.4}$$

for all j and α satisfying $2j + |\alpha| \leq k$.

In accordance with (4.3)–(4.4), we set the following assumptions on the regularity of the exact solution $(\boldsymbol{u}, p, \mathbf{F})$

$$\begin{aligned}
\partial_t \boldsymbol{u} &\in L^\infty(0, T; L^2(\Omega)) \cap L^2(0, T; W^{1,2}(\Omega)), \\
\boldsymbol{u} &\in L^\infty(0, T; W^{2,2}(\Omega)) \cap L^2(0, T; W^{3,2}(\Omega)), \\
\partial_t \mathbf{F} &\in L^\infty(0, T; L^2(\Omega)), \\
\mathbf{F} &\in L^\infty(0, T; W^{2,2}(\Omega)).
\end{aligned} \tag{4.5}$$

From (4.1b) and (4.1c) we further obtain

$$\begin{aligned}
\nabla p &= \mathrm{div}(\mathbf{F}\mathbf{F}^\top) - \partial_t \boldsymbol{u} - \mathrm{div}(\boldsymbol{u} \otimes \boldsymbol{u}) + \Delta \boldsymbol{u} \in L^2(0, T; W^{1,2}(\Omega)), \\
\partial_t \mathbf{F} &= \nabla \boldsymbol{u} \mathbf{F} - \boldsymbol{u} \cdot \nabla \mathbf{F} \in L^\infty(0, T; W^{1,2}(\Omega)).
\end{aligned} \tag{4.6}$$

4.1.2 Approximation

Let $\{\mathcal{T}_h\}_{h>0}$ be a family of partitions of Ω into triangles and h be the largest edge in $\mathcal{T}_h$. For any $T \in \mathcal{T}_h$ and $k = 0, 1, 2, \ldots$ we denote by $\mathcal{P}^k(T)$ the space of k-th order polynomials on T. We define the spaces

$$\begin{aligned}
W_h &:= \{\boldsymbol{v} \in W_0^{1,2}(\Omega; \mathbb{R}^2); \ \forall T \in \mathcal{T}_h : \ \boldsymbol{v}|_T \in \mathcal{P}^2(T)^2\}, \\
L_h &:= \{q \in L_0^2(\Omega) \cap C(\overline{\Omega}); \ \forall T \in \mathcal{T}_h : \ q|_T \in \mathcal{P}^1(T)\}, \\
X_h &:= \{\mathbf{G} \in C(\overline{\Omega}; \mathbb{R}^{2\times 2}); \ \forall T \in \mathcal{T}_h : \ \mathbf{G}|_T \in \mathcal{P}^1(T)^{2\times 2}\}, \\
Z_h &:= \{\mathbf{G} \in L^2(\Omega; \mathbb{R}^{2\times 2}); \ \forall T \in \mathcal{T}_h : \ \mathbf{G}|_T \in \mathcal{P}^0(T)\}.
\end{aligned}$$

Let e be an interior edge shared by elements T_1 and T_2. Define the unit normal vectors $\boldsymbol{n}^1$ and $\boldsymbol{n}^2$ on e pointing exterior to T_1 and T_2, respectively. For a function φ, piecewise smooth on $\mathcal{T}_h$, with $\varphi^i = \varphi_{|T_i}$ we define the average $\{\varphi\}$ and the jump $[\varphi]$:

$$\{\varphi\} = \frac{1}{2}(\varphi^1 + \varphi^2), \quad [\varphi] = \varphi^1 \boldsymbol{n}^1 + \varphi^2 \boldsymbol{n}^2 \quad \text{on } e \in \mathcal{E}_h^0,$$

where $\mathcal{E}_h^0$ is the set of all interior edges. For a vector-valued function $\boldsymbol{\phi}$, piecewise smooth on $\mathcal{T}_h$, we define the average and the jump analogously

$$\{\boldsymbol{\phi}\} = \frac{1}{2}(\boldsymbol{\phi}^1 + \boldsymbol{\phi}^2), \quad [\boldsymbol{\phi}] = \boldsymbol{\phi}^1 \cdot \boldsymbol{n}^1 + \boldsymbol{\phi}^2 \cdot \boldsymbol{n}^2 \quad \text{on } e \in \mathcal{E}_h^0.$$

Let $\boldsymbol{\beta}$ be a vector-valued function, continuous across e. The upwind value of a quantity $\boldsymbol{\beta}\varphi$ is defined as follows:

$$\{\boldsymbol{\beta}\varphi\}_u = \begin{cases} \boldsymbol{\beta}\varphi^1 & \text{if } \boldsymbol{\beta} \cdot \boldsymbol{n}^1 > 0, \\ \boldsymbol{\beta}\varphi^2 & \text{if } \boldsymbol{\beta} \cdot \boldsymbol{n}^1 < 0, \\ \boldsymbol{\beta}\{\varphi\} & \text{if } \boldsymbol{\beta} \cdot \boldsymbol{n}^1 = 0. \end{cases}$$

We introduce the following space semi-discretizations of (4.1).

Finite element-finite volume approximation. Find $(\boldsymbol{u}_h, p_h, \mathbf{F}_h) \in C^1([0,T]; W_h) \times C([0,T]; L_h) \times C^1([0,T]; Z_h)$ such that

- for all $(\mathbf{v}_h, q_h, \mathbf{G}_h) \in W_h \times L_h \times Z_h$ and $t \in (0,T)$ the following integral identities hold:

$$(\partial_t \boldsymbol{u}_h(t), \mathbf{v}_h) - (\boldsymbol{u}_h(t) \otimes \boldsymbol{u}_h(t), \nabla\mathbf{v}_h) + (\nabla\boldsymbol{u}_h(t), \nabla\mathbf{v}_h)$$
$$- (p_h(t), \operatorname{div} \mathbf{v}_h) + (\mathbf{F}_h(t)\mathbf{F}_h^\top(t), \nabla\mathbf{v}_h) = 0, \quad (4.7a)$$

$$(q_h, \operatorname{div} \boldsymbol{u}_h(t)) = 0, \quad (4.7b)$$

$$(\partial_t \mathbf{F}_h(t), \mathbf{G}_h) + \sum_{e \in \mathcal{E}_h^0} (\{\boldsymbol{u}_h(t)\mathbf{F}_h(t)\}_u, [\mathbf{G}_h])_e - \frac{1}{2}(\operatorname{div} \boldsymbol{u}_h(t)\mathbf{F}_h(t), \mathbf{G}_h)$$
$$- (\nabla\boldsymbol{u}_h(t)\mathbf{F}_h(t), \mathbf{G}_h) = 0; \quad (4.7c)$$

- $\boldsymbol{u}_h$ and $\mathbf{F}_h$ satisfy the initial conditions: for all $\boldsymbol{v} \in W_h$ and $\mathbf{G} \in Z_h$

$$(\boldsymbol{u}_h(0, \cdot), \boldsymbol{v}) = (\boldsymbol{u}_0, \boldsymbol{v}), \qquad (\mathbf{F}_h(0, \cdot), \mathbf{G}) = (\mathbf{F}_0, \mathbf{G}). \quad (4.8)$$

For the approximate problem (4.7) we assume that the existence of a unique global in time solution satisfies the inequality

$$\sup_{\tau \in (0,T)} \|\boldsymbol{u}_h(\tau, \cdot)\|_2^2 + \sup_{\tau \in (0,T)} \|\mathbf{F}_h(\tau, \cdot)\|_2^2 + \int_0^T \|\nabla\boldsymbol{u}_h\|_2^2 \le C, \quad (4.9)$$

where $C > 0$ depends on the data $(\Omega, \boldsymbol{u}_0, \mathbf{F}_0)$, but is independent of $h > 0$.

Some preliminary properties. For the regular triangular family $\mathcal{T}_h$, the discrete spaces W_h, L_h, X_h and Z_h enjoy the following properties:

- (inf-sup condition) There exists a constant $C > 0$ independent of $h > 0$ such that for all $q_h \in L_h$

$$\sup_{\mathbf{v}_h \in W_h,\ \mathbf{v}_h \neq \mathbf{0}} \frac{(q_h, \operatorname{div} \mathbf{v}_h)}{\|\mathbf{v}_h\|_{1,2}} \geq C\|q_h\|_2; \tag{4.10}$$

- (interpolation into W_h) There exists an operator $\Pi_h^u : W_0^{1,2}(\Omega; \mathbb{R}^2) \to W_h$ such that

  – for all $\boldsymbol{v} \in W_0^{1,2}(\Omega; \mathbb{R}^2) \cap W^{k,q}(\Omega; \mathbb{R}^2)$, $1 \leq q \leq \infty$, $k \in \{1, 2, 3\}$, $r \in \{0, \dots, k\}$:

$$\|\Pi_h^u \boldsymbol{v} - \boldsymbol{v}\|_{r,q} \leq Ch^{k-r}\|\boldsymbol{v}\|_{k,q}, \tag{4.11}$$

  where $C > 0$ is independent of $h > 0$;

  – for all $\boldsymbol{v} \in W_0^{1,2}(\Omega; \mathbb{R}^2)$ and $q_h \in L_h$:

$$(q_h, \operatorname{div} \Pi_h^u \boldsymbol{v}) = (q_h, \operatorname{div} \boldsymbol{v}); \tag{4.12}$$

- (interpolation into L_h) There exists an operator $\Pi_h^p : L_0^2(\Omega) \to L_h$ and a constant $C > 0$ independent of $h > 0$, such that

$$\|\Pi_h^p s - s\|_{r,q} \leq Ch^{2-r}\|s\|_{2,q} \tag{4.13}$$

for all $s \in L_0^2(\Omega) \cap W^{2,q}(\Omega)$, $1 \leq q \leq \infty$, $r \in \{0, 1\}$;

- (interpolation into X_h) There exists an operator $\Pi_h^F : L^2(\Omega; \mathbb{R}^{2 \times 2}) \to X_h$ and a constant $C > 0$ independent of $h > 0$, such that

$$\|\Pi_h^F \mathbf{G} - \mathbf{G}\|_{r,q} \leq Ch^{2-r}\|\mathbf{G}\|_{2,q}, \tag{4.14}$$

for all $\mathbf{G} \in W^{2,q}(\Omega; \mathbb{R}^{2 \times 2})$, $1 \leq q \leq \infty$, $r \in \{0, 1\}$.

- (interpolation into Z_h) There exists an operator $\Pi_h^0 : L^2(\Omega; \mathbb{R}^{2 \times 2}) \to Z_h$ and a constant $C > 0$ independent of $h > 0$, such that

$$\|\Pi_h^0 \mathbf{G} - \mathbf{G}\|_q \leq Ch\|\mathbf{G}\|_{1,q}, \tag{4.15}$$

for all $\mathbf{G} \in W^{1,q}(\Omega; \mathbb{R}^{2 \times 2})$, $1 \leq q \leq \infty$.

4.2 Error estimates

The aim of this section is to show the error estimates for the combined FE-FV approximation. Before presenting the main result we first introduce a similar result of a standard finite element approximation from [62].

4.2.1 Error estimates for a standard finite element approximation

Finite element approximation. Find $(\boldsymbol{u}_h, p_h, \mathbf{F}_h) \in C^1([0, T]; W_h) \times C([0, T]; L_h) \times C^1([0, T]; X_h)$ such that

- for all $(\mathbf{v}_h, q_h, \mathbf{G}_h) \in W_h \times L_h \times X_h$ and $t \in (0,T)$ the integral identities (4.7a), (4.7b) and the following equality hold true

$$(\partial_t \mathbf{F}_h(t), \mathbf{G}_h) - (\boldsymbol{u}_h(t) \cdot \nabla \mathbf{G}_h, \mathbf{F}_h(t)) - \frac{1}{2}((\operatorname{div} \boldsymbol{u}_h(t)) \mathbf{F}_h(t), \mathbf{G}_h)$$
$$- (\nabla \boldsymbol{u}_h(t) \mathbf{F}_h(t), \mathbf{G}_h) = 0; \quad (4.16)$$

- $\boldsymbol{u}_h$ and $\mathbf{F}_h$ satisfy the initial conditions: for all $\boldsymbol{v} \in W_h$ and $\mathbf{G} \in X_h$

$$(\boldsymbol{u}_h(0, \cdot), \boldsymbol{v}) = (\boldsymbol{u}_0, \boldsymbol{v}), \qquad (\mathbf{F}_h(0, \cdot), \mathbf{G}) = (\mathbf{F}_0, \mathbf{G}). \qquad (4.17)$$

For the finite element approximation we have the following lemma.

Lemma 4.2.1. *Let the family $\{\mathcal{T}_h\}_{h>0}$ be regular, the initial data $(\boldsymbol{u}_0, \nabla \times \boldsymbol{\Phi}_0)$ satisfy $\boldsymbol{u}_0, \nabla \boldsymbol{\Phi}_0 \in W^{2,2}(\Omega)$ and $[0, T]$ be the maximal time interval in which the strong solution $(\boldsymbol{u}, p, \mathbf{F})$ to (4.1) exists. Then there exist constants $h_0 > 0$ and $C > 0$ such that for all $h \in (0, h_0)$ it holds*

$$\|\boldsymbol{u} - \boldsymbol{u}_h\|_{L^\infty(0,T;L^2(\Omega))} + \|\nabla(\boldsymbol{u} - \boldsymbol{u}_h)\|_{L^2(0,T;L^2(\Omega))}$$
$$+ \|\mathbf{F} - \mathbf{F}_h\|_{L^\infty(0,T;L^2(\Omega))} \leq Ch, \quad (4.18)$$

where $(\boldsymbol{u}_h, p_h, \mathbf{F}_h)$ is the solution to (4.7a), (4.7b), (4.16) and (4.17).

Proof. Lemma 4.2.1 is a part of the Theorem 1 in [62], we refer the readers to this paper for the details of the proof. In what follows we will sketch the proof for the sake of consistency. Let us denote the errors $e_u := \boldsymbol{u} - \boldsymbol{u}_h$, $e_p := p - p_h$ and $e_F := \mathbf{F} - \mathbf{F}_h$. In order to derive estimates of these errors in suitable norms we make the following decomposition

$$e_u = (\boldsymbol{u} - \Pi_h^u \boldsymbol{u}) + (\Pi_h^u \boldsymbol{u} - \boldsymbol{u}_h) =: \eta_u + \delta_u.$$

Similarly, we introduce $e_p = \eta_p + \delta_p$, $e_F = \eta_F + \delta_F$ and

$$\eta_p := p - \Pi_h^p p, \quad \delta_p := \Pi_h^p p - p_h, \quad \eta_F := \mathbf{F} - \Pi_h^F \mathbf{F}, \quad \delta_F := \Pi_h^F \mathbf{F} - \mathbf{F}_h.$$

The first part of the errors is the interpolation error, which is already estimated using the property of the interpolation operators, cf. the preliminary results introduced in the last section.

$$\sup_{\tau \in (0,T)} \|\eta_u(\tau, \cdot)\|_2^2 \leq Ch^4 \sup_{\tau \in (0,T)} \|\boldsymbol{u}(\tau, \cdot)\|_{2,2}^2,$$

$$\int_0^T \|\nabla \eta_u\|_2^2 \leq Ch^4 \int_0^T \|\boldsymbol{u}\|_{3,2}^2,$$

$$\sup_{\tau \in (0,T)} \|\eta_F(\tau, \cdot)\|_2^2 \leq Ch^4 \sup_{\tau \in (0,T)} \|\mathbf{F}(\tau, \cdot)\|_{2,2}^2.$$

Hence, with the help of (4.5) we obtain

$$\sup_{\tau \in (0,T)} \left(\|e_u(\tau, \cdot)\|_2^2 + \|e_F(\tau, \cdot)\|_2^2 \right) + \int_0^T \|\nabla e_u\|_2^2 \leq Ch^4$$

$$+ \sup_{\tau \in (0,T)} \left(\|\delta_u(\tau, \cdot)\|_2^2 + \|\delta_F(\tau, \cdot)\|_2^2 \right) + \int_0^T \|\nabla \delta_u\|_2^2. \quad (4.19)$$

Thus the proof of (4.18) is deduced to control the second part(δ-terms) in the previous inequality by Ch^2.

Due to the initial conditions (4.17) it holds that $\|\delta_u(0)\|_2 = \|\delta_F(0)\|_2 = 0$. Hence, for any $\tau \in (0, T)$ we have

$$\frac{1}{2} \left(\|\delta_u(\tau, \cdot)\|_2^2 + \|\delta_F(\tau, \cdot)\|_2^2 \right) + \int_0^\tau \|\nabla \delta_u\|_2^2$$

$$= \frac{1}{2} \left(\|\delta_u(\tau, \cdot)\|_2^2 - \|\delta_u(0, \cdot)\|_2^2 + \|\delta_F(\tau, \cdot)\|_2^2 - \|\delta_F(0, \cdot)\|_2^2 \right) + \int_0^\tau \|\nabla \delta_u\|_2^2$$

$$= \int_0^\tau \left[(\partial_t \delta_u, \delta_u) + (\partial_t \delta_F, \delta_F) + (\nabla \delta_u, \nabla \delta_u) \right]$$

$$= \int_0^\tau \left[(\partial_t e_u, \delta_u) + (\partial_t e_F, \delta_F) + (\nabla e_u, \nabla \delta_u) \right]$$

$$- \int_0^\tau \left[(\partial_t \eta_u, \delta_u) + (\partial_t \eta_F, \delta_F) + (\nabla \eta_u, \nabla \delta_u) \right] = J_1 + J_2. \quad (4.20)$$

The last integral can be estimated using the Hölder and the Young inequality and (4.11)–(4.14)

$$J_2 \leq \left(\int_0^T \|\partial_t \eta_u\|_2^2 \right)^{1/2} \left(\int_0^\tau \|\delta_u\|_2^2 \right)^{1/2} + \left(\int_0^T \|\partial_t \eta_F\|_2^2 \right)^{1/2} \left(\int_0^\tau \|\delta_F\|_2^2 \right)^{1/2}$$

$$+ \left(\int_0^T \|\nabla \eta_u\|_2^2 \right)^{1/2} \left(\int_0^\tau \|\nabla \delta_u\|_2^2 \right)^{1/2}$$

$$\leq \frac{1}{2} \int_0^\tau \|\delta_u\|_2^2 + \frac{1}{2} \int_0^T \|\partial_t \eta_u\|_2^2 + \frac{1}{2} \int_0^\tau \|\delta_F\|_2^2 + \frac{1}{2} \int_0^T \|\partial_t \eta_F\|_2^2$$

$$+ \alpha \int_0^\tau \|\nabla \delta_u\|_2^2 + \frac{C}{\alpha} \int_0^T \|\nabla \eta_u\|_2^2$$

$$\leq \frac{1}{2} \int_0^\tau \|\delta_u\|_2^2 + Ch^2 \int_0^T \|\partial_t \boldsymbol{u}\|_{1,2}^2 + \frac{1}{2} \int_0^\tau \|\delta_F\|_2^2 + Ch^2 \int_0^T \|\partial_t \mathbf{F}\|_{1,2}^2$$

$$+ \alpha \int_0^\tau \|\nabla \delta_u\|_2^2 + \frac{Ch^4}{\alpha} \int_0^T \|\boldsymbol{u}\|_{3,2}^2. \quad (4.21)$$

Here $\alpha > 0$ is a sufficiently small coefficient to be specified later. The regularity of the solution (4.5), (4.6) implies that

$$J_2 \leq \frac{1}{2} \int_0^\tau \|\delta_u\|_2^2 + \frac{1}{2} \int_0^\tau \|\delta_F\|_2^2 + \alpha \int_0^\tau \|\nabla \delta_u\|_2^2 + Ch^2 + \frac{Ch^4}{\alpha}. \quad (4.22)$$

For the estimates of the first integral J_1 on the r.h.s. of (4.20) we need to use the

82

control equations of the errors.

Equations satisfied by the errors. Multiplying (4.1) with $\mathbf{v}_h \in W_h$, $q_h \in L_h$ and $\mathbf{G}_h \in X_h$, respectively, and integrating over Ω, we obtain for a.a. $t \in (0, T)$ the following identities

$$(\partial_t \boldsymbol{u}(t), \mathbf{v}_h) - (\boldsymbol{u}(t) \otimes \boldsymbol{u}_h(t), \nabla \mathbf{v}_h) + (\nabla \boldsymbol{u}(t), \nabla \mathbf{v}_h)$$
$$- (p(t), \operatorname{div} \mathbf{v}_h) + (\mathbf{F}(t)\mathbf{F}^\top(t), \nabla \mathbf{v}_h) = 0, \quad (4.23a)$$

$$(q_h, \operatorname{div} \boldsymbol{u}(t)) = 0, \quad (4.23b)$$

$$(\partial_t \mathbf{F}(t), \mathbf{G}_h) - (\boldsymbol{u}(t) \cdot \nabla \mathbf{G}_h, \mathbf{F}(t)) - (\nabla \boldsymbol{u}(t)\mathbf{F}(t), \mathbf{G}_h) = 0. \quad (4.23c)$$

Taking the difference of (4.23) and the finite element approximation (4.7a), (4.7b) and (4.16) we obtain

$$\int_0^T \Big[(\partial_t e_u, \mathbf{v}_h) - (e_u \otimes \boldsymbol{u} + \boldsymbol{u} \otimes e_u, \nabla \mathbf{v}_h) + (\nabla e_u, \nabla \mathbf{v}_h) - (e_p, \operatorname{div} \mathbf{v}_h)$$
$$+ (\mathbf{F}\mathbf{F}^\top - \mathbf{F}_h \mathbf{F}_h^\top, \nabla \mathbf{v}_h) \Big] = 0, \quad (4.24a)$$

$$\int_0^T (q_h, \operatorname{div} e_u) = 0, \quad (4.24b)$$

$$\int_0^T (\partial_t e_F, \mathbf{G}_h) - (u_i \mathbf{F} - u_{hi} \mathbf{F}_h, \partial_i \mathbf{G}_h) + \frac{1}{2}((\operatorname{div} \boldsymbol{u}_h)\mathbf{F}_h, \mathbf{G}_h)$$
$$- (\nabla \boldsymbol{u}\mathbf{F} - \nabla \boldsymbol{u}_h \mathbf{F}_h, \mathbf{G}_h) = 0 \quad (4.24c)$$

for any $(\mathbf{v}_h, q_h, \mathbf{G}_h) \in L^2(0, T; W_h) \times L^2(0, T; L_h) \times L^2(0, T; X_h)$.

Now the J_1 term can be substituted from (4.24) as follows

$$J_1 = \int_0^\tau \Big[(e_u \otimes \boldsymbol{u} + \boldsymbol{u}_h \otimes e_u, \nabla \delta_u) + (e_p, \operatorname{div} \delta_u) - (\mathbf{F}\mathbf{F}^\top - \mathbf{F}_h \mathbf{F}_h^\top, \nabla \delta_u)$$
$$+ (u_i \mathbf{F} - u_{hi} \mathbf{F}_h, \partial_i \delta_F) + \frac{1}{2}((\operatorname{div} \boldsymbol{u}_h)\mathbf{F}_h, \delta_F) + (\nabla \boldsymbol{u}\mathbf{F} - \nabla \boldsymbol{u}_h \mathbf{F}_h, \delta_F) \Big]$$
$$=: \int_0^\tau \sum_{j=1}^6 T_j,$$

where the estimates of the terms $T_1, \ldots, T_6$ are, cf. [62],

$$\int_0^\tau T_1 \leq 3\alpha \int_0^\tau \|\nabla \delta_u\|_2^2 + \frac{C}{\alpha^3} \int_0^\tau \|\boldsymbol{u}_h\|_{1,2}^2 \|\delta_u\|_2^2 + \frac{Ch^4}{\alpha}. \quad (4.25)$$

$$\int_0^\tau T_2 \leq \alpha \int_0^\tau \|\nabla \delta_u\|_2^2 + \frac{Ch^2}{\alpha}. \quad (4.26)$$

$$\int_0^\tau T_3 + T_6 \leq 3\alpha \int_0^\tau \|\nabla \delta_u\|_2^2 + C \int_0^\tau \left(\frac{1}{\alpha} + \|\boldsymbol{u}\|_{3,2} \right) \|\delta_F\|_2^2 + Ch^2 + \frac{Ch^4}{\alpha}. \quad (4.27)$$

$$\int_0^\tau T_4 + T_5 \leq 2\alpha \int_0^\tau \|\nabla \delta_u\|_2^2 + \frac{C}{\alpha} \int_0^\tau \|\delta_F\|_2^2 + Ch^2 + Ch^4. \tag{4.28}$$

Gronwall's inequality for the errors and the end of the proof. Collecting (4.22), (4.25), (4.26), (4.27), (4.28) and inserting the result to (4.20), we obtain

$$\frac{1}{2}\left(\|\delta_u(\tau)\|_2^2 + \|\delta_F(\tau)\|_2^2\right) + (1 - C\alpha)\int_0^\tau \|\nabla \delta_u\|_2^2$$
$$\leq C \int_0^\tau \left(1 + \frac{\|\boldsymbol{u}_h\|_{1,2}^2}{\alpha^3}\right)\|\delta_u\|_2^2 + C\int_0^\tau \left(\frac{1}{\alpha} + \|\boldsymbol{u}\|_{3,2}\right)\|\delta_F\|_2^2 + \frac{C}{\alpha}\left(h^2 + h^4\right).$$

Choosing α sufficiently small and using the Gronwall inequality we obtain for $h \in (0, h_0)$

$$\sup_{(0,T)}\|\delta_u\|_2^2 + \sup_{(0,T)}\|\delta_F\|_2^2 + \int_0^T \|\delta_u\|_{1,2}^2 \leq Ch^2.$$

This in accordance with (4.19) completes the proof of Lemma 4.2.1. $\qquad\square$

4.2.2 Error estimates of the combined finite element - finite volume approximation

The aim of this subsection is to present the error estimates for the FE-FV approximation proposed in Section 4.1.2. In advance of that let us introduce the following lemma on the multiplicative trace inequality, which will be useful in the proof of Theorem 4.2.4.

Multiplicative trace inequality In the error analysis of the finite element-finite volume scheme we will need the following variant of *multiplicative trace inequality*.

Lemma 4.2.2. *Let $F \in W^{2,2}(\Omega)$. Then there exists a constant $c > 0$ independent of h such that*

$$\sum_{e \in \mathcal{E}_h^0} \|F - \Pi_h^0 F\|_{4,e} \leq ch^{3/4}\|F\|_{2,2}. \tag{4.29}$$

Before the proof of this statement, we first state the following auxiliary result.

Lemma 4.2.3. *There exists a constant $c > 0$ independent of h and T, such that for $T \in \mathcal{T}_h$, $v \in H^1(T)$, $h \in (0, h_0)$ we have*

$$\|v\|_{L^4(\partial T)}^4 \leq c\left[4\|v\|_{L^6(T)}^3|v|_{H^1(T)} + \frac{d}{h_T}\|v\|_{L^4(T)}^4\right]. \tag{4.30}$$

We refer the proof of Lemma 4.2.3 to [29, Lemma 3.1], see also [62, Lemma 3]. Holding the property (4.30), we can prove Lemma 4.2.2.

Proof of Lemma 4.2.2. Set $v = F - \Pi_h^0 F$, where $F \in W^{2,2}(\Omega)$. Then it holds

$$\|F - \Pi_h^0 F\|_{L^4(\partial T)}^4 = \|\eta_F\|_{L^4(\partial T)}^4 \leq c_1 \left[4h^3 \|F\|_{W^{1,6}(T)}^3 |F|_{H^1(T)} + \frac{2}{h} h^4 \|F\|_{W^{1,4}(T)}^4 \right] \leq$$

$$\leq c_2 \left[h^3 \|F\|_{W^{2,2}(T)}^4 + h^3 \|F\|_{W^{2,2}(T)}^4 \right] \leq$$

$$\leq c_3 h^3 \|F\|_{W^{2,2}(T)}^4.$$

This implies

$$\sum_{e \in \mathcal{E}_h^0} \|F - \Pi_h^0 F\|_{4,e} \leq c h^{3/4} \|F\|_{2,2}.$$

$\square$

Now let us state the main result on the error rates.

Theorem 4.2.4. *Let the family* $\{\mathcal{T}_h\}_{h>0}$ *be regular, the initial data* $(\boldsymbol{u}_0, \nabla \times \boldsymbol{\Phi}_0)$ *satisfy* $\boldsymbol{u}_0, \nabla \boldsymbol{\Phi}_0 \in W^{2,2}(\Omega)$ *and* $[0, T]$ *be the maximal time interval in which the strong solution* $(\boldsymbol{u}, p, \mathbf{F})$ *to (4.1) exists. Then there exist constants* $h_0 > 0$ *and* $C > 0$ *such that for all* $h \in (0, h_0)$ *it holds*

$$\|\boldsymbol{u} - \bar{\boldsymbol{u}}_h\|_{L^\infty(0,T;L^2(\Omega))} + \|\nabla(\boldsymbol{u} - \bar{\boldsymbol{u}}_h)\|_{L^2(0,T;L^2(\Omega))}$$

$$+ \|\mathbf{F} - \bar{\mathbf{F}}_h\|_{L^\infty(0,T;L^2(\Omega))} \leq C h^{3/4}, \quad (4.31)$$

where $(\bar{\boldsymbol{u}}_h, \bar{p}_h, \bar{\mathbf{F}}_h)$ *is the solution to (4.7)–(4.8).*

The essential difference in the proof of error estimates for the solution of problem (4.7)–(4.8) is in the term $\boldsymbol{u} \cdot \nabla \mathbf{F}$. It is therefore sufficient to estimate the error of

$$\int_0^T \left((\boldsymbol{u} \cdot \nabla \mathbf{F}, \delta_F) - \sum_{e \in \mathcal{E}_h^0} (\{\boldsymbol{u}_h \mathbf{F}_h\}_u, [\delta_F])_e + \frac{1}{2} (\operatorname{div} \boldsymbol{u}_h \mathbf{F}_h, \delta_F) \right). \quad (4.32)$$

Proof. (Error estimate for term $\boldsymbol{u} \cdot \nabla \mathbf{F}$)
Let us first denote by F one component of the tensor $\mathbf{F}$, similarly by G_h one component of $\mathbf{G}_h$. Then we can write

$$(\boldsymbol{u} \cdot \nabla F, G_h) = \sum_{T \in \mathcal{T}_h} \int_T \operatorname{div}(\boldsymbol{u} F) G_h \, d\boldsymbol{x} = \sum_{T \in \mathcal{T}_h} \int_{\partial T} (\boldsymbol{u} \cdot \boldsymbol{n}) F \, [G_h] \, dS$$

$$= \sum_{e \in \mathcal{E}_h^0} \int_e \{\boldsymbol{u} F\} [G_h] \, dS.$$

For the approximate solution it holds

$$\int_e \{\boldsymbol{u}_h F_h\}_u \, [G_h] \, dS = \int_e \{\boldsymbol{u}_h F_h\}[G_h] \, dS + \int_e \frac{|\boldsymbol{u}_h \cdot \boldsymbol{n}|}{2} [F_h][G_h] \, dS \quad \forall \, G_h \in Z_h.$$

Thus, we can rewrite (4.32) as follows

$$\dots = \int_0^T \sum_{e \in \mathcal{E}_h^0} \int_e \{(\boldsymbol{u} - \boldsymbol{u}_h)\mathrm{F}\}[\delta_F]\ dS\ dt + \int_0^T \sum_{e \in \mathcal{E}_h^0} \int_e \{\boldsymbol{u}_h(\mathrm{F} - \mathrm{F}_h)\}[\delta_F]\ dS\ dt +$$

$$+ \int_0^T \sum_{e \in \mathcal{E}_h^0} \int_e \frac{|\boldsymbol{u}_h \cdot \boldsymbol{n}|}{2}[\mathrm{F} - \mathrm{F}_h][\delta_F]\ dS\ dt + \frac{1}{2}\int_0^T \int_\Omega \operatorname{div} \boldsymbol{u}_h \mathrm{F}_h \delta_F =$$

$$= \sum_{i=1}^4 I_i.$$

In what follows, we will estimate these terms separately.
Term I_1.

$$I_1 = \int_0^T \sum_{e \in \mathcal{E}_h^0} \int_e \{(\boldsymbol{u} - \boldsymbol{u}_h)\mathrm{F}\}[\delta_F]\ dS\ dt = \int_0^T \sum_{T \in \mathcal{T}_h} \int_{\partial T} (\boldsymbol{u} - \boldsymbol{u}_h) \cdot \boldsymbol{n}\ \mathrm{F}\ \delta_F\ dS\ dt =$$

$$= \int_0^T \sum_{T \in \mathcal{T}_h} \int_T \operatorname{div}\Big((\boldsymbol{u} - \boldsymbol{u}_h)\mathrm{F}\Big)\delta_F\ d\boldsymbol{x}\ dt =$$

$$= \int_0^T \int_\Omega \operatorname{div} \delta_u\ \mathrm{F}\delta_F\ d\boldsymbol{x}\ dt + \int_0^T \int_\Omega \operatorname{div} \eta_u\ \mathrm{F}\delta_F\ d\boldsymbol{x}\ dt +$$

$$+ \int_0^T \int_\Omega \delta_u \cdot \nabla \mathrm{F}\ \delta_F\ d\boldsymbol{x}\ dt + \int_0^T \int_\Omega \eta_u \cdot \nabla \mathrm{F}\ \delta_F\ d\boldsymbol{x}\ dt \le$$

$$\le \int_0^T c_1\|\nabla \delta_u\|_{2,\Omega}\|\mathrm{F}\|_{2,2,\Omega}\|\delta_F\|_{2,\Omega} + c_2\|\nabla \eta_u\|_{2,\Omega}\|\mathrm{F}\|_{2,2,\Omega}\|\delta_F\|_{2,\Omega} +$$

$$+ \int_0^T c_3\|\delta_u\|_{4,\Omega}\|\nabla \mathrm{F}\|_{4,\Omega}\|\delta_F\|_{2,\Omega} + c_4\|\eta_u\|_{4,\Omega}\|\nabla \mathrm{F}\|_{4,\Omega}\|\delta_F\|_{2,\Omega} \le$$

$$\le \alpha \int_0^T \|\nabla \delta_u\|_2^2 + \frac{C}{\alpha}\Big(\sup_{(0,T)} \|\mathrm{F}\|_{2,2}\Big)^2 \int_0^T \|\delta_F\|_2^2 +$$

$$+ C \int_0^T \|\delta_F\|_2^2 + Ch^4\Big(\sup_{(0,T)} \|\mathrm{F}\|_{2,2}\Big)^2 \int_0^T \|\boldsymbol{u}\|_{3,2}^2.$$

Terms $I_2 + I_4$.

$$I_2 = \int_0^T \sum_{e \in \mathcal{E}_h^0} \int_e \{\boldsymbol{u}_h(\mathrm{F} - \mathrm{F}_h)\}[\delta_F]\ dS\ dt =$$

$$= \int_0^T \sum_{e \in \mathcal{E}_h^0} \int_e \{\boldsymbol{u}_h \delta_F\}[\delta_F]\ dS\ dt + \int_0^T \sum_{e \in \mathcal{E}_h^0} \int_e \{\boldsymbol{u}_h \eta_F\}[\delta_F]\ dS\ dt = A_1 + A_2$$

$$A_1 = \int_0^T \int_\Omega \frac{1}{2} \operatorname{div} \boldsymbol{u}_h \delta_F^2 \; d\boldsymbol{x} \; dt = -\int_0^T \int_\Omega \frac{1}{2} \operatorname{div} e_u \Pi_h^0 \mathrm{F} \delta_F \; d\boldsymbol{x} \; dt - I_4$$

$$= -\int_0^T \int_\Omega \frac{1}{2} \operatorname{div} \eta_u \Pi_h^0 \mathrm{F} \delta_F \; d\boldsymbol{x} \; dt - \int_0^T \int_\Omega \frac{1}{2} \operatorname{div} \delta_u \Pi_h^0 \mathrm{F} \delta_F \; d\boldsymbol{x} \; dt - I_4$$

$$\leq C \int_0^T \|\eta_u\|_{1,2}\|\delta_F\|_2 + C \int_0^T \|\nabla \delta_u\|_2 \|\delta_F\|_2 - I_4$$

$$\leq Ch^2 + \alpha \int_0^T \|\nabla \delta_u\|_2^2 + \frac{C}{\alpha} \int_0^T \|\delta_F\|_2^2 - I_4.$$

$$A_2 \leq \int_0^T \sum_{e \in \mathcal{E}_h^0} \int_e \frac{|\boldsymbol{u}_h \cdot \boldsymbol{n}|}{2} \{|\eta_F|\}|[\delta_F]| \; dS \; dt$$

$$\leq \int_0^T \sum_{e \in \mathcal{E}_h^0} \|c_e^{1/2}[\delta_F]\|_{2,e}\|c_e^{1/2}\|_{4,e}\|\{|\eta_F|\}\|_{4,e}$$

$$\leq \alpha \int_0^T \sum_{e \in \mathcal{E}_h^0} \|c_e^{1/2}[\delta_F]\|_{2,e}^2 + \frac{C}{\alpha} h^{3/2} \left(\sup_{(0,T)} \|\mathbf{F}\|_{2,2} \right)^2 \int_0^T \|\nabla \boldsymbol{u}_h\|_2^2 \; dt,$$

where the trace inequalities for η_F and c_e were used and $c_e = \frac{|\boldsymbol{u}_h \cdot \boldsymbol{n}|}{2}$. Further, we have

$$I_3 = \int_0^T \sum_{e \in \mathcal{E}_h^0} \int_e \frac{|\boldsymbol{u}_h \cdot \boldsymbol{n}|}{2}[\eta_F][\delta_F] \; dS \; dt + \int_0^T \sum_{e \in \mathcal{E}_h^0} \int_e \frac{|\boldsymbol{u}_h \cdot \boldsymbol{n}|}{2}[\delta_F][\delta_F] \; dS \; dt =$$

$$= B_1 + B_2,$$

where B_1 can be estimated in the same way as A_2 and

$$B_2 = \int_0^T \sum_{e \in \mathcal{E}_h^0} \|c_e^{1/2}[\delta_F]\|_{2,e}^2.$$

Finally, we can derive

$$(1-\alpha) \int_0^T \sum_{e \in \mathcal{E}_h^0} \|c_e^{1/2}[\delta_F]\|_{2,e}^2 \leq C\alpha \int_0^T \|\nabla \delta_u\|_2^2 + \frac{C}{\alpha} \int_0^T \|\delta_F\|_2^2 + Ch^{3/2} + Ch^2 + Ch^4, \tag{4.33}$$

this concludes the proof. $\qquad\square$

4.3 Numerical experiments

In order to demonstrate validity of our theoretical error estimates we perform experimental error analysis. Let us consider the flow in a rectangular domain $\Omega = (0,1)^2$ driven by the boundary condition

$$\boldsymbol{u} = \begin{cases} (4x(x-1), 0) & \text{if } y = 1, \\ (0,0) & \text{otherwise,} \end{cases}$$

	e_u		∇e_u		e_p		e_F	
h	$L^\infty(L^2)$	EOC	$L^2(L^2)$	EOC	$L^2(L^2)$	EOC	$L^\infty(L^2)$	EOC
1/8	2.08e-02	2.11	1.77e+02	1.00	4.19e+02	0.96	1.37e-01	0.73
1/16	4.80e-03	2.02	8.85e+01	1.00	2.14e+02	0.99	8.21e-02	0.89
1/32	1.18e-03	2.00	4.42e+01	0.99	1.07e+02	1.00	4.41e-02	0.94
1/64	2.95e-04	2.00	2.21e+01	0.99	5.36e+01	1.00	2.29e-02	0.95
1/128	7.37e-05		1.10e+01		2.68e+01		1.17e-02	

(a) FEM

	e_u		∇e_u		e_p		e_F	
h	$L^\infty(L^2)$	EOC	$L^2(L^2)$	EOC	$L^2(L^2)$	EOC	$L^\infty(L^2)$	EOC
1/8	2.07e-02	2.00	1.77e+02	1.00	4.73e+02	0.88	1.94e-01	0.73
1/16	5.16e-03	1.40	8.87e+01	0.98	2.55e+02	0.94	1.16e-01	0.88
1/32	1.94e-03	1.34	4.47e+01	0.98	1.33e+02	0.96	6.33e-02	0.90
1/64	7.67e-04	1.35	2.25e+01	0.98	6.83e+01	0.97	3.37e-02	0.91
1/128	3.00e-04		1.13e+01		3.47e+01		1.78e-02	

(b) FEM-dual FVM

	e_u		∇e_u		e_p		e_F	
h	$L^\infty(L^2)$	EOC	$L^2(L^2)$	EOC	$L^2(L^2)$	EOC	$L^\infty(L^2)$	EOC
1/8	4.22e-02	0.86	3.61e-01	0.86	2.94e-01	1.27	1.58e-01	0.88
1/16	2.32e-02	1.25	1.98e-01	1.04	1.22e-01	1.54	8.56e-02	1.07
1/32	9.73e-03	1.82	9.62e-02	1.22	4.22e-02	1.76	4.09e-02	1.23
1/64	2.77e-03	2.25	4.14e-02	1.59	1.25e-02	2.03	1.75e-02	1.59
1/128	5.81e-04		1.38e-02		3.06e-03		5.80e-03	

(c) FDM-FVM

Table 4.1: Error norms and experimental order of convergence for driven cavity problem.

with the initial conditions $\boldsymbol{u}_0 = (0,0)$, $\mathbf{F}_0 = \mathbf{I}$. We have compared the following three methods:

a) finite element method (FEM) for velocity, pressure and viscoelastic stress,

b) FEM for velocity and pressure, dual finite volume method (FVM) for viscoelastic stress,

c) finite difference method (FDM) for velocity and pressure, FVM for viscoelastic stress.

The case a) is a standard finite element method based on the Taylor-Hood finite elements of the fluid part (piecewise quadratic velocity and piecewise linear pressure) combined with the piecewise linear approximation of the deformation gradient $\mathbf{F}$. In the case b) the deformation gradient was approximated by piecewise constants on dual elements, that arise by connecting the barycenters of primary elements with the edge midpoints. In the case c) we have combined the finite difference approximation of the fluid equations with the finite volume approximation of the deformation gradient $\mathbf{F}$, cf.

Section 2.5. Setting $\boldsymbol{\sigma} = \mathbf{F}\mathbf{F}^T$ and replacing (2.58) by

$$\mathbf{F}_i^{k+1} = \mathbf{F}_i^k - \frac{\Delta t}{|T_i|} \sum_{j \in S(i)} H_{ij}(\mathbf{F}_i^k, \mathbf{F}_j^k) + (\nabla_h \boldsymbol{u}^k)_i \mathbf{F}_i^k, \tag{4.34}$$

we can follow Algorithm 3 in Section 2.5 for the simulation.

In order to compute experimental error orders we use a series of regular triangular meshes consisting of 8 to 256 elements in each direction (methods a) and b)) as well as regular rectangular meshes with 4 to 128 elements (method c)). Calculations were run for the time interval $(0, 0.2)$ with a fixed time step 0.001 that satisfies the CFL stability condition for the finest mesh. Our experimental error analysis, that is presented in Table 4.1, yields the results comparable with the theoretical results, cf. Theorem 4.2.4. Indeed, simulations using the standard finite element method a) confirm the first order error for $\nabla \boldsymbol{u}$ in $L^2(0, T; L^2(\Omega))$ and for $\mathbf{F}$ in $L^\infty(0, T; L^2(\Omega))$. Moreover, we also show that the pressure p is approximated in $L^2(0, T; L^2(\Omega))$ with the first order and the velocity $\boldsymbol{u}$ with the second order error in $L^\infty(0, T; L^2(\Omega))$. The same experimental orders of convergence are obtained by the combined finite element-dual finite volume method b). Note however that the we have a slightly worse convergence for the velocity measured in $L^\infty(0, T; L^2(\Omega))$ than in the finite element method a), though still superlinear. These experimental results also indicate that our theoretical error estimate (4.31) may be suboptimal for $\boldsymbol{u}$. Furthermore, the experimental error analysis of the combined finite difference-finite volume method indicates the second order error for $\boldsymbol{u}$ in $L^\infty(0, T; L^2(\Omega))$ as well as for pressure p in $L^2(0, T; L^2(\Omega))$ and the superlinear convergence for $\nabla \boldsymbol{u}$ in $L^2(0, T; L^2(\Omega))$ and for $\mathbf{F}$ in $L^\infty(0, T; L^2(\Omega))$, see Table 4.1.

In what follows we present graphs of the solution in the final time $T = 0.2$. In Figure 4.1 we plot the streamlines, pressure and velocity components. Figure 4.2 presents all components of the deformation gradient $\mathbf{F}$. Further, Figure 4.3 illustrates time evolution of the kinetic energy $\frac{1}{2}\boldsymbol{u}^2$ and the L^2-norm of the stress tensor $\mathbf{F}$ computed by the combined FD-FV and FE-FV methods, respectively. Although the kinetic energy is non-increasing, we see clearly that L^2-norm of the stress tensor is increasing in time.

In this chapter we have studied a special variant of the Oldroyd-B visocelastic model having the limiting relaxation time going to infinity. Assuming global in time existence of enough regular weak solution we have presented the error estimates of a combined FE-FV method. More precisely, we have combined the lowest order Taylor-Hood finite element discretization of the flow part (piecewise quadratic velocity and piecewise linear pressure) with a piecewise constant finite volume approximation for the deformation gradient. The theoretical result presented in Theorem 4.2.4 shows the errors of order $\mathcal{O}(h^{3/4})$ for the combined FE-FV method. The result is confirmed by numerical experiments, too.

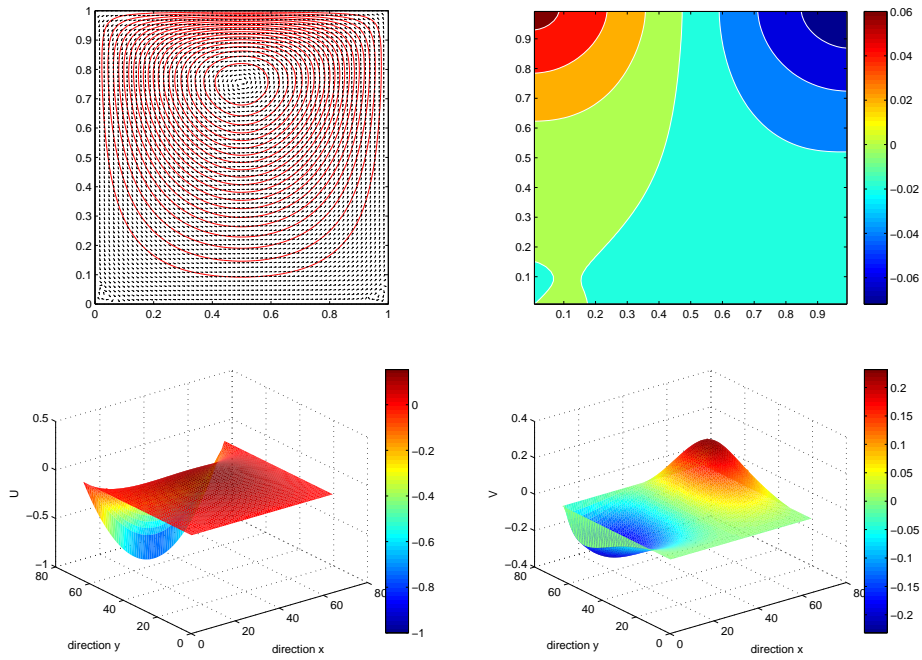Figure 4.1: Graph of the solution at the final time $T = 0.2$: streamline (top left), pressure (top right) and velocity components u_1 and u_2 (bottom), computed by the combined FD-FV method.

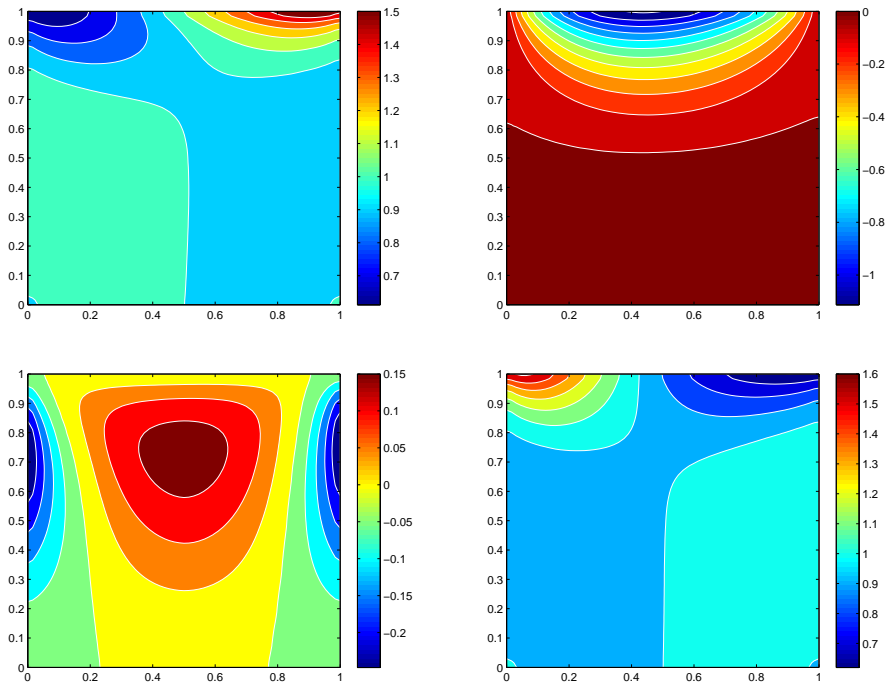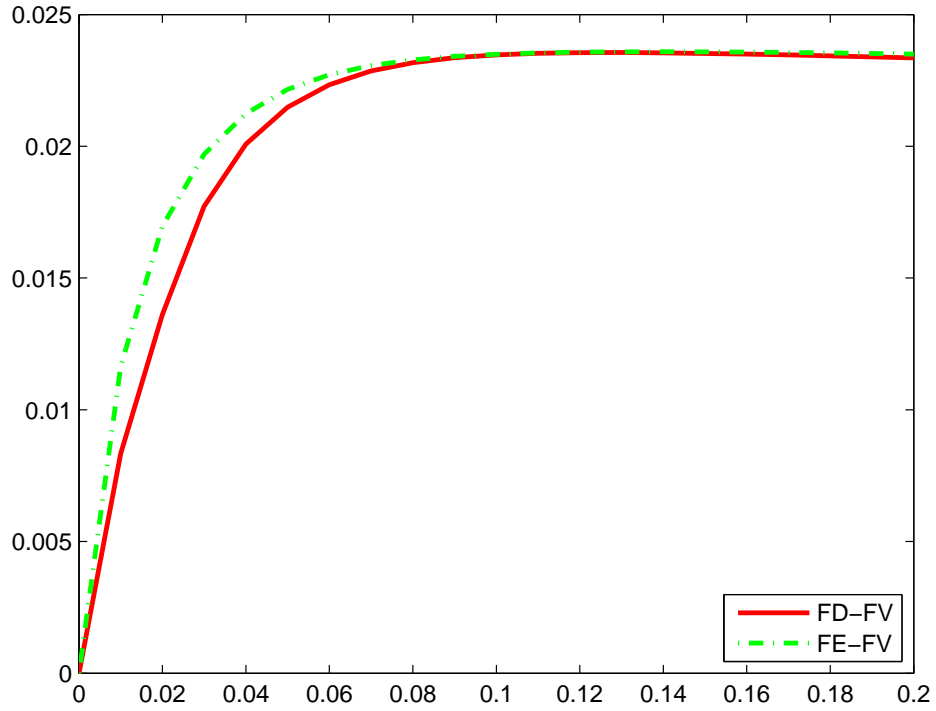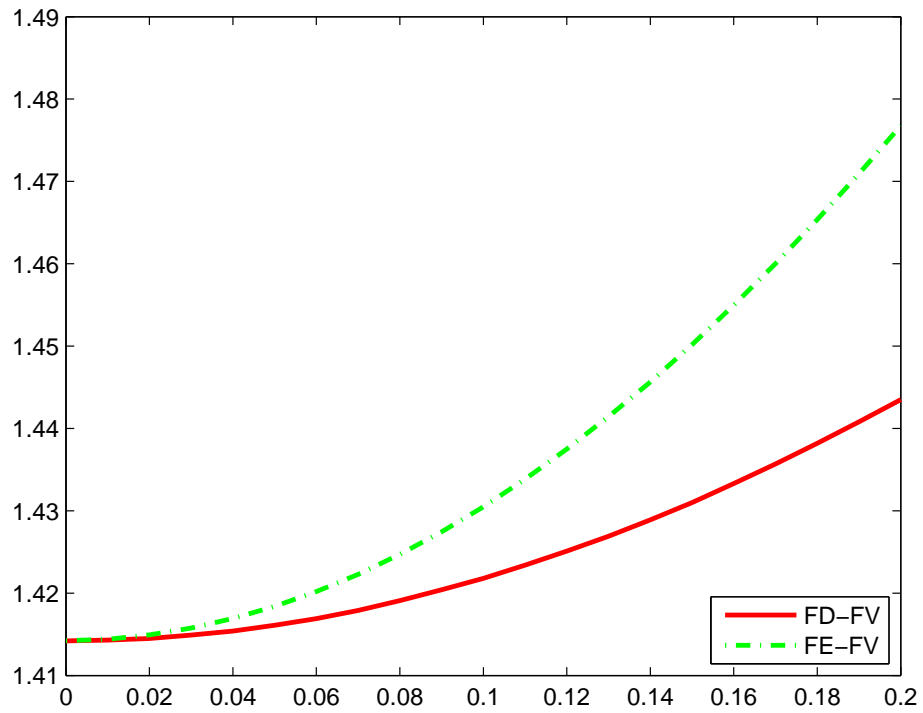Figure 4.2: Graph of the solution at the final time $T = 0.2$; four components of the deformation gradient $\mathbf{F}_{ij}$, $i, j = 1, 2$, from the top left to the bottom right, computed by the combined FD-FV method.

(a) Kinetic energy

(b) L^2-norm of $\mathbf{F}$

Figure 4.3: Time evolution of the kinetic energy and of the L^2-norm of $\mathbf{F}$, computed by the combined FD-FV and FE-FV method, respectively.

5 Summary and outlook

In this thesis we have studied viscoelastic fluids, that are modeled by the Oldroyd-B equations. It is a well-known fact, that this classical Oldroyd-B model yields many open problems both from analytical as well as numerical point of view. We do not have global existence of solutions and can not solve numerically the Oldroyd-B equations for arbitrary Weissenberg numbers. The main part of the thesis is devoted to the stabilization study of the numerical simulations for the Oldroyd-B type viscoelastic models.

In Chapter 1 we have described the fundamental results of the viscoelastic flows and presented an overview of the available literature for the Oldroyd-B viscoelastic model. In Chapter 2 we have firstly described the modelling aspects of the Oldroyd-B system. In particular, we have introduced the diffusive Oldroyd-B model. Further, the so-called logarithm transformation stabilization approach was discussed. We extended the logarithm formulation to the diffusive model. Besides of that, the entropy stability of the both diffusive models, with and without logarithmic transformation, was studied. For the approximation of the Oldroyd-B type models several numerical methods were presented. In particular, we have developed and studied the characteristic finite element, combined finite difference-finite volume and characteristic finite difference methods.

In Chapter 3 the entropy stability of these methods was analyzed. We have proved that the characteristic FEM and characteristic FD method are entropy stable for diffusive models with arbitrary Weissenberg numbers. Except of the entropy stability, which is a suitable tool for nonlinear analysis, we have also presented global linear stability method and apply it to the Oldroyd-B equations, cf. Section 3.1.

At the end of Chapter 3, cf. Section 3.4, we have presented experimental results using the combined FD-FV method, the characteristic finite element scheme and characteristic finite difference scheme. It has been observed that the diffusive models are more stable for high Weissenberg number. One interesting result, that we would like to emphasize is the fact that the mesh convergence was also observed for high Weissenberg numbers using the diffusive Oldroyd-B model with the logarithmic transformation.

Chapter 4 is devoted to the error estimates of a special Oldroyd-B model that covers the limit of Weissenberg number going to infinity. This chapter presents and summarizes the results that have been published in [62]. Based on the assumption of [60, 52] we have achieved a suitable convergence order of the combined finite element - finite volume approximation. Theoretical results have been verified by numerical experiments.

The current numerical study is in two space dimensions. Future goal is to extend these results to three space dimensions.

The question of suitable boundary conditions for viscoelastic fluids is still not completely clear. The boundary effect which plays an important role, is ignored in most of the situations. We would like to study the effects of different boundary conditions in our future research as well.

From the molecular point of view, the complex behavior of the viscoelastic fluids

originates from their micro structures. It is also interesting to study the role of the microscopic effects by using the kinetic models for viscoelastic fluids based on the Fokker-Planck equation.

Bibliography

[1] M. Aboubacar, H. Matallah, and M. F. Webster. Highly elastic solutions for Oldroyd-B and Phan-Thien/Tanner fluids with a finite volume/element method: planar contraction flows. *J. Non-Newton. Fluid Mech.*, 103(1):65–103, 2002.

[2] A. M. Afonso, P. J. Oliveira, F. T. Pinho, and M. A. Alves. The log-conformation tensor approach in the finite-volume method framework. *J. Non-Newton. Fluid Mech.*, 157(1-2):55–65, 2009.

[3] A. M. Afonso, F. T. Pinho, and M. A. Alves. The kernel-conformation constitutive laws. *J. Non-Newton. Fluid Mech.*, 167-168:30–37, 2012.

[4] M. A. Alves, P. J. Oliveira, and Fernando T. Pinho. Benchmark solutions for the flow of Oldroyd-B and PTT fluids in planar contractions. *J. Non-Newton. Fluid Mech.*, 110(1):45–75, 2003.

[5] N. Arada and A. Sequeira. Strong steady solutions for a generalized Oldroyd-B model with shear-dependent viscosity in a bounded domain. *Math. Models Methods Appl. Sci.*, 13(9):1303–1323, 2003.

[6] P. E. Arratia. Complex fluids at work. *Physics*, 4:9, Jan 2011.

[7] N. Balci, B. Thomases, M. Renardy, and C. R. Doering. Symmetric factorization of the conformation tensor in viscoelastic fluid models. *J. Non-Newton. Fluid Mech.*, 166(11):546–553, 2011.

[8] J. W. Barrett and S. Boyaval. Existence and approximation of a (regularized) Oldroyd-B model. *Math. Models Methods Appl. Sci.*, 21(9):1783–1837, 2011.

[9] J. W. Barrett and E. Süli. Existence of global weak solutions to some regularized kinetic models for dilute polymers. *Multiscale Model. Simul.*, 6(2):506–546, 2007.

[10] J. W. Barrett and E. Süli. Existence and equilibration of global weak solutions to kinetic models for dilute polymers. I: Finitely extensible nonlinear bead-spring chains. *Math. Models Methods Appl. Sci.*, 21(6):1211–1289, 2011.

[11] J. W. Barrett and E. Süli. Existence and equilibration of global weak solutions to kinetic models for dilute polymers II: Hookean-type models. *Math. Models Methods Appl. Sci.*, 22(5):1150024, 84, 2012.

[12] J. W. Barrett and E. Süli. Existence of global weak solutions to finitely extensible nonlinear bead-spring chain models for dilute polymers with variable density and viscosity. *J. Differ. Equations*, 253(12):3610–3677, 2012.

[13] M. Bensaada, D. Esselaoui, and P. Saramito. Second-order Galerkin-Lagrange method for the Navier-Stokes equations. *Numer. Methods Partial Differ. Equations*, 21(6):1099–1121, 2005.

[14] R. B. Bird, C.F. Curtiss, R. C. Armstrong, and O. Hassager. *Dynamics of polymeric liquids, kinetic theory.* New York: John Wiley & Sons Inc., 1987.

[15] L. Boltzmamn. Zur Theorie der elastischen Nachwirkung. *Wiedemann Ann.*, pages 624–655, 1875.

[16] K. Boukir, Y. Maday, B. Métivet, and E. Razafindrakoto. A high-order characteristics/finite element method for the incompressible Navier-Stokes equations. *Int. J. Numer. Methods Fluids*, 25(12):1421–1454, 1997.

[17] S. Boyaval. Lid-driven-cavity simulations of Oldroyd-B models using free-energy-dissipative schemes. In *Numerical mathematics and advanced applications 2009. Proceedings of ENUMATH 2009, the 8th European conference on numerical mathematics and advanced applications, Uppsala, Sweden.*, pages 191–198. Springer, 2010.

[18] S. Boyaval, T. Lelièvre, and C. Mangoubi. Free-energy-dissipative schemes for the Oldroyd-B model. *ESAIM, Math. Model. Numer. Anal.*, 43(3):523–561, 2009.

[19] X. Chen, H. Marschall, M. Schäfer, and D. Bothe. A comparison of stabilisation approaches for finite-volume simulation of viscoelastic fluid flow. *Int. J. Comput. Fluid Dyn.*, 27(6-7):229–250, Jul 2013.

[20] Y. Chen and P. Zhang. The global existence of small solutions to the incompressible viscoelastic fluid system in 2 and 3 space dimensions. *Commun. Partial Differ. Equations*, 31(12):1793–1810, 2006.

[21] P. G. Ciarlet. The finite element method for elliptic problems. Studies in Mathematics and its Applications. Vol. 4. Amsterdam - New York - Oxford: North-Holland Publishing Company. XIX, 580 p, 1978.

[22] P. Constantin and M. Kliegl. Note on global regularity for two-dimensional Oldroyd-B fluids with diffusive stress. *Arch. Ration. Mech. Anal.*, 206(3):725–740, 2012.

[23] P. Constantin and W. Sun. Remarks on Oldroyd-B and related complex fluid models. *Commun. Math. Sci.*, 10(1):33–73, 2012.

[24] M. J. Crochet, A. R. Davies, and K. Walters. Numerical Simulation of Non-Newtonian Flow. volume 1 of *Rheology Series*, pages VIII + 352. Elsevier, 1984.

[25] M. J. Crochet and R. Keunings. Finite element analysis of die swell of a highly elastic fluid. *J. Non-Newton. Fluid Mech.*, 10(3):339–356, 1982.

[26] H. Damanik, J. Hron, A. Ouazzi, and S. Turek. A monolithic FEM approach for the log-conformation reformulation (LCR) of viscoelastic flow problems. *J. Non-Newton. Fluid Mech.*, 165(19-20):1105–1113, 2010.

[27] P. Degond and H. Liu. Kinetic models for polymers with inertial effects. *Netw. Heterog. Media*, 4(4):625–647, 2009.

[28] M. Doi and S. F. Edwards. *The Theory of Polymer Dynamics*. Oxford University Press, USA, November 1986.

[29] V. Dolejší, M. Feistauer, and C. Schwab. A finite volume discontinuous Galerkin scheme for nonlinear convection-diffusion problems. *Calcolo*, 39(1):1–40, 2002.

[30] H. Dou and N. Phan-Thien. The flow of an Oldroyd-B fluid past a cylinder in a channel: Adaptive viscosity vorticity (DAVSS-ω) formulation. *J. Non-Newton. Fluid Mech.*, 87(1):47–73, 1999.

[31] J. Jr. Douglas and T. F. Russell. Numerical methods for convection-dominated diffusion problems based on combining the method of characteristics with finite element or finite difference procedures. *SIAM J. Numer. Anal.*, 19:871–885, 1982.

[32] S. S. Edussuriya, A. J. Williams, and C. Bailey. A cell-centred finite volume method for modelling viscoelastic flow. *J. Non-Newton. Fluid Mech.*, 117(1):47–61, 2004.

[33] R. Fattal and R. Kupferman. Constitutive laws for the matrix-logarithm of the conformation tensor. *J. Non-Newton. Fluid Mech.*, 123(2-3):281–285, 2004.

[34] R. Fattal and R. Kupferman. Time-dependent simulation of viscoelastic flows at high Weissenberg number using the log-conformation representation. *J. Non-Newton. Fluid Mech.*, 126(1):23–37, 2005.

[35] E. Fernández-Cara, F. Guillén, and R. R. Ortega. Mathematical modeling and analysis of viscoelastic fluids of the Oldroyd kind. In *Handbook of numerical analysis. Vol. 8: Solution of equations in $\mathbb{R}^n$ (Part 4). Techniques of scientific computing (Part 4). Numerical methods of fluids (Part 2)*, pages 543–661. Amsterdam: North Holland/ Elsevier, 2002.

[36] H. Giesekus. A simple constitutive equation for polymer fluids based on the concept of deformation-dependent tensorial mobility. *J. Non-Newton. Fluid Mech.*, 11(1–2):69–109, 1982.

[37] H. Giesekus. A unified approach to a variety of constitutive models for polymer fluids based on the concept of configuration-dependent molecular mobility. *Rheol. Acta*, 21:366–375, 1982.

[38] C. Guillopé and J. C. Saut. Existence results for the flow of viscoelastic fluids with a differential constitutive law. *Nonlinear Anal. Theory Methods Appl.*, 15(9):849–869, 1990.

[39] R. Guénette and M. Fortin. A new mixed finite element method for computing viscoelastic flows. *J. Non-Newton. Fluid Mech.*, 60(1):27–52, 1995.

[40] J. Hao and T. Pan. Simulation for high Weissenberg number: Viscoelastic flow by a finite element method. *Appl. Math. Lett.*, 20(9):988–993, 2007.

[41] M. Hieber, Y. Naito, and Y. Shibata. Global existence results for Oldroyd-B fluids in exterior domains. *J. Diff. Equations*, 252(3):2617–2629, 2012.

[42] D. Hu and T. Lelièvre. New entropy estimates for the Oldroyd-B model and related models. *Commun. Math. Sci.*, 5(4):909–916, 2007.

[43] M. A. Hulsen. A sufficient condition for a positive definite configuration tensor in differential models. *J. Non-Newton. Fluid Mech.*, 38(1):93–100, 1990.

[44] M. A. Hulsen, R. Fattal, and R. Kupferman. Flow of viscoelastic fluids past a cylinder at high Weissenberg number: stabilized simulations using matrix logarithms. *J. Non-Newton. Fluid Mech.*, 127(1):27–39, 2005.

[45] H. Jia, D. Liu, and K. Li. A characteristic stabilized finite element method for the non-stationary Navier-Stokes equations. *Computing*, 93(1):65–87, 2011.

[46] M. W. Jr. Johnson and D. Segalman. A model for viscoelastic fluid behavior which allows non-affine deformation. *J. Non-Newton. Fluid Mech.*, 2:255–270, 1977.

[47] D. D. Joseph. *Fluid dynamics of viscoelastic liquids.* New York etc.: Springer-Verlag, 1990.

[48] R. Keunings. An algorithm for the simulation of transient viscoelastic flows with free surfaces. *J. Comput. Phys.*, 62(1):199–220, 1986.

[49] R. Keunings. On the high weissenberg number problem. *J. Non-Newton. Fluid Mech.*, 20(0):209–226, 1986.

[50] R. Keunings. A survey of computational rheology. *Proceedings of the XIIIth International Congress on Rheology*, 1:7–14, 2000.

[51] R. Keunings and R. Shipman. Finite element methods for transient viscoelastic free surface flows. *NASA STI/Recon Technical Report N*, 87:13675, 1986.

[52] O. Kreml. Mathematical analysis of models for viscoelastic fluids. PhD thesis, 2010.

[53] O. Kreml and M. Pokorný. On the local strong solutions for a system describing the flow of a viscoelastic fluid. In *Nonlocal and abstract parabolic equations and their applications. Based on the conference, Będlewo, Poland, 2007*, pages 195–206. Warsaw: Polish Academy of Sciences, Institute of Mathematics, 2009.

[54] C. Le Bris and T. Lelièvre. Micro-macro models for viscoelastic fluids: modelling, mathematics and numerics. *Sci. China, Math.*, 55(2):353–384, 2012.

[55] A. Le Hyaric. An integrated environment for FreeFem++.

[56] Y. Lee and J. Xu. New formulations, positivity preserving discretizations and stability analysis for non-Newtonian flow models. *Comput. Meth. Appl. Mech. Eng.*, 195(9–12):1180–1206, 2006.

[57] Y. Lee, J. Xu, and C. Zhang. Global existence, uniqueness and optimal solvers of discretized viscoelastic flow models. *Math. Models Methods Appl. Sci.*, 21(08):1713–1732, 2011.

[58] Y. Lee, J. Xu, and C. Zhang. Stable Finite Element Discretizations for Viscoelastic Flow Models. In R. Glowinski and J. Xu, editors, *Numerical Methods for Non-Newtonian Fluids*, volume 16 of *Handbook of Numerical Analysis*, pages 371–432. Elsevier, 2011.

[59] X. Li, X. Han, and X. Wang. Numerical modeling of viscoelastic flows using equal low-order finite elements. *Comput. Methods Appl. Mech. Eng.*, 199(9-12):570–581, 2010.

[60] F. Lin, C. Liu, and P. Zhang. On hydrodynamics of viscoelastic fluids. *Commun. Pure Appl. Math.*, 58(11):1437–1471, 2005.

[61] P. L. Lions and N. Masmoudi. GLOBAL SOLUTIONS FOR SOME OLDROYD MODELS OF NON-NEWTONIAN FLOWS. *Chinese Annals of Mathematics*, 21(02):131–146, 2000.

[62] M. Lukáčová, H. Mizerová, B. She, and J. Stebel. Error analysis of the finite element and finite volume methods for some viscoelastic fluids. submitted to J. Num. Math., 2014.

[63] J. M. Marchal and M. J. Crochet. A new mixed finite element for calculating viscoelastic flow. *J. Non-Newton. Fluid Mech.*, 26(1):77–114, 1987.

[64] H. Matallah, P. Townsend, and M. F. Webster. Recovery and stress-splitting schemes for viscoelastic flows. *J. Non-Newton. Fluid Mech.*, 75(2-3):139–166, 1998.

[65] L. Nadau and A. Sequeira. Numerical simulations of shear-dependent viscoelastic flows with a combined finite element-finite volume method. *Comput. Math. Appl.*, 53(3-4):547–568, 2007.

[66] H. Notsu. Numerical computations of cavity flow problems by a pressure stabilized characteristic-curve finite element scheme. *Transactions of the Japan Society for Industrial and Applied Mathematics*, 2008.

[67] H. Notsu and M. Tabata. A combined finite element scheme with a pressure stabilization and a characteristic-curve method for the Navier-Stokes equations. *Transactions of the Japan Society for Industrial and Applied Mathematics*, 18(3):427–445, sep 2008.

[68] H. Notsu and M. Tabata. A single-step characteristic-curve finite element scheme of second order in time for the incompressible Navier-Stokes equations. *J. Sci. Comput.*, 38(1):1–14, 2009.

[69] H. C. Öttinger. *Stochastic processes in polymeric fluids.* Springer-Verlag, Berlin, 1996.

[70] A. Ouazzi, H. Damanik, J. Hron, and S. Turek. FEM techniques for the LCR reformulation of viscoelastic flow problems. In *Numerical mathematics and advanced applications 2009. Proceedings of ENUMATH 2009, the 8th European conference on numerical mathematics and advanced applications, Uppsala, Sweden.*, pages 747–754. Springer, 2010.

[71] T. Pan and J. Hao. Numerical simulation of a lid-driven cavity viscoelastic flow at high Weissenberg numbers. *C. R., Math., Acad. Sci. Paris*, 344(4):283–286, 2007.

[72] N. Phan-Thien and R. I. Tanner. A new constitutive equation derived from network theory. *J. Non-Newton. Fluid Mech.*, 2:353–365, 1977.

[73] T. N. Phillips and A. J. Williams. Viscoelastic flow through a planar contraction using a semi-lagrangian finite volume method. *J. Non-Newton. Fluid Mech.*, 87(2–3):215–246, 1999.

[74] O. Pironneau. On the transport-diffusion algorithm and its applications to the Navier-Stokes equations. *Numer. Math.*, 38:309–332, 1982.

[75] O. Pironneau. *Méthodes des éléments finis pour les fluides.* Paris etc.: Masson, 1988.

[76] M. Renardy. Local existence of solutions of the dirichlet initial-boundary value problem for incompressible hypoelastic materials. *SIAM J. Math. Anal.*, 21(6):1369–1385, Sep 1990.

[77] M. Renardy. *Mathematical analysis of viscoelastic flows.* Philadelphia, PA: SIAM, 2000.

[78] H. Rui and M. Tabata. A second order characteristic finite element scheme for convection-diffusion problems. *Numer. Math.*, 92(1):161–177, 2002.

[79] J. D. Schieber. Generalized Brownian configuration fields for Fokker–Planck equations including center-of-mass diffusion . *J. Non-Newton. Fluid Mech.*, 135(2–3):179–181, 2006.

[80] B. Seibold. A compact and fast Matlab code solving the incompressible Navier-Stokes equations on rectangular domains. University Lecture, available at http://math.mit.edu/classes/18.086/2008/, 2008.

[81] E. Süli. Convergence and nonlinear stability of the Lagrange-Galerkin method for the Navier-Stokes equations. *Numer. Math.*, 53(4):459–483, 1988.

[82] A. Tezuka and K. Suzuki. Three-dimensional global linear stability analysis of flow around a spheroid. *AIAA Journal*, 44(8):1697–1708, 2006.

[83] D. Trebotich, P. Colella, and G. H. Miller. A stable and convergent scheme for viscoelastic flow in contraction channels. *J. Comput. Phys.*, 205(1):315–342, 2005.

[84] K. Walters and M. F. Webster. The distinctive CFD challenges of computational rheology. *Int. J. Numer. Methods Fluids*, 43(5):577–596, 2003.

[85] P. Wapperom, R. Keunings, and V. Legat. The backward-tracking lagrangian particle method for transient viscoelastic flows. *J. Non-Newton. Fluid Mech.*, 91(2):273–295, 2000.

[86] P. Wapperom and M. F. Webster. A second-order hybrid finite-element/volume method for viscoelastic flows. *J. Non-Newton. Fluid Mech.*, 79(2–3):405–431, 1998.

[87] P. Wapperom and M. F. Webster. Simulation for viscoelastic flow by a finite volume/element method. *Comput. Meth. Appl. Mech. Eng.*, 180(3–4):281–304, 1999.

[88] S.-C. Xue, N. Phan-Thien, and R. I. Tanner. Three dimensional numerical simulations of viscoelastic flows through planar contractions. *J. Non-Newton. Fluid Mech.*, 74(1–3):195–245, 1998.

[89] O. C. Zienkiewicz and R. L. Taylor. *The finite element method. 1: Basic formulation and linear problems. 4th ed., repr.* London: McGraw-Hill, 4th ed., repr. edition, 1997.

Curriculum Vitae

Personal information
   Name: Bangwei She
   Date of birth: 1987.04.22
   Place of birth: Anhui, China
   Citizenship: Chinese
   Email: bangwei@uni-mainz.de

Education

- 2012.03 – present   PhD candidates
  Institute of Mathematics, Johannes Gutenberg-University Mainz, Mainz, Germany

- 2008.09 – 2011.07   Master of science in Fluid Mechanics
  Institute of Applied Physics and Computational Mathematics, Beijing, China

- 2004.09 – 2008.06   Bachelor of science in Mechanics
  Modern Mechanics, University of Science and Technology of China, Hefei, China

Research

- Numerical simulation of some viscoelastic models, PhD thesis
  The research focuses on the stabilization and simulation of the Oldroyd-B type
  viscoelastic models. Especially, the entropy stability has been studied, as well
  as algorithms based on characteristic approach in both finite element and finite
  difference framework.

- GKS method for non-conservative two-phase flow model, Master thesis
  Based on the Baer-Nunziato two-phase flow model, we propose and establish a
  proper GKS model, numerical simulation with FORTRAN language has also been
  implemented.

- Research of temperature sensor based on micro-cantilever, Bachelor thesis
  Based on the research of micro-cantilever, we design a temperature sensor system,
  which can be applied in oil well. The project includes the design of the mechanical
  structure, as well as analysis of the sensitivity and stability.

Awards

- 2004, Freshman award, 3rd award, USTC

- 2007, Mechanical base award, college award, USTC

- 2008, Graduate recommendation from USTC